

Sources and Processes Affecting the Distribution of Dissolved Sulfate in the Elk Valley Aquifer in Grand Forks County, Eastern North Dakota



By

William M. Schuh, North Dakota State Water Commission, Bismarck, ND

Simon H. Bottrell, Dept. of Earth Sciences, University of Leeds, UK

and

Scott F. Korom: Dept. of Geology and Geological Engineering, University of North Dakota, Grand Forks, ND

Contributing Authors:

John R. Gallagher, Energy and Environmental Resource Center, University of North Dakota, Grand Forks, ND

Jon C. Patch, North Dakota State Water Commission, Bismarck, ND

WATER RESOURCES INVESTIGATION NO. 38
NORTH DAKOTA STATE WATER COMMISSION
BISMARCK, ND

2006

Sources and Processes Affecting
the Distribution of Dissolved Sulfate
in the Elk Valley Aquifer
in Grand Forks County, Eastern North Dakota

By

William M. Schuh, North Dakota State Water Commission, Bismarck, ND

Simon H. Bottrell, Dept. of Earth Sciences, University of Leeds, UK

and

Scott F. Korom: Dept. of Geology and Geological Engineering, University of North Dakota, Grand Forks, ND

Contributing Authors:

John R. Gallagher, Energy and Environmental Resource Center, University of North Dakota, Grand Forks, ND

Jon C. Patch, North Dakota State Water Commission, Bismarck, ND

WATER RESOURCES INVESTIGATION NO. 38
NORTH DAKOTA STATE WATER COMMISSION
BISMARCK, ND

2006

ACKNOWLEDGMENT

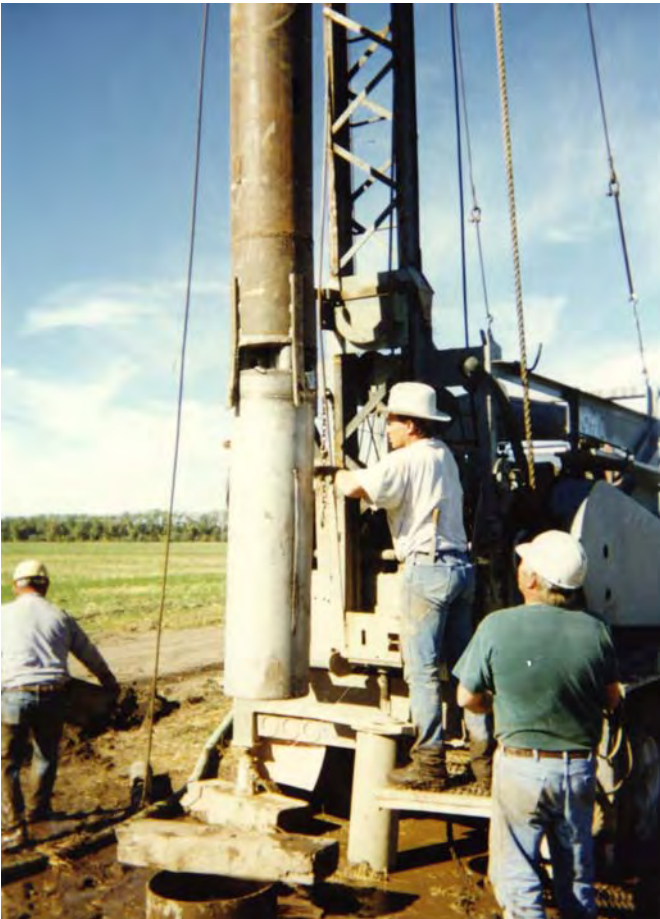
This study was initiated by John Gallagher and Dr. Gale Mayer of the University of North Dakota Energy and Environmental Resource Center (EERC) of the University of North Dakota (UND), Grand Forks, and was undertaken as a cooperative project by the EERC, the School of Earth and Environment at the University of Leeds, Leeds, UK, and the North Dakota State Water Commission (NDSWC), Bismarck, ND. Partial funding for this effort was provided through the EERC's Red River Water Management Consortium (RRWMC). The RRWMC is funded by the United States Department of Agriculture and 15 regional stakeholders. Partial funding was also provided through the University of Leeds by UKNERC grant no. GR9/3492 to SHB, and by the NDSWC. Denitrification work was partially funded by the North Dakota Department of Health, and through a U.S. EPA Section 319 grant.

The authors are grateful to many personnel from all involved institutions who assisted in this effort. These include numerous personnel from the EERC who provided support, through assistance in sampling, analysis, and data interpretation. Their contributions are gratefully acknowledged. We specifically thank Polly Newbery, Dave Hatfield and Rob Newton of the University of Leeds who provided sulfur species and isotopic analysis. We also thank driller Gary Calheim and field technicians Merlyn Skaley and Albert Lachenmeier of the NDSWC for many hours in field measurements and sampling. Finally, we thank John Hoganson of the North Dakota State Geological Survey for field guidance in identifying and obtaining bedrock samples.

This blank page is placed for document
page format control when printing



Field processing of acetate-lined sediment samples from “split-spoon” cores, obtained with a hollow-core auger from the shallow, middle, and deep Elk Valley aquifer on Sites 1 through 6 (June 1997).



Placing an “In Situ Mesocosm” (ISM) in the shallow unoxidized strata of the Elk Valley aquifer for measurement of denitrification and its effects on pore-water chemistry (September 1997).

This blank page is placed for document
page format control when printing

EXECUTIVE SUMMARY

In 1995 rural water associations using water from the south portion of the Elk Valley aquifer (EVA), Grand Forks County, North Dakota (ND) raised concerns over apparent increasing sulfate concentrations in well water. A multi-faceted study was undertaken by the North Dakota State Water Commission in cooperation with researchers from the University of North Dakota (UND) Energy and Environmental Research Center, the School of Earth and Environment of the University of Leeds, UK, and the Department of Geology and Geological Engineering (UND) to determine sources and processes affecting the distribution of sulfate. Previous hypotheses offered to explain elevated sulfate included: 1. Addition through sulfate fertilizer, 2. Gypsum mobilization, 3. Oxidation of pyrite in the vadose zone and leaching to the aquifer, 4. Concentration through long-term evaporative discharge, and 5. Oxidation of pyrite through autotrophic denitrification.

Sources and processes affecting the current distribution of sulfate in the EVA were examined from 1997 through 2002. Long-term and current sources include dissolved sulfate in precipitation, mineralization from organic matter, oxidation of sulfide from pyrite in mineral constituents of the aquifer, the overlying soil and vadose zone, and underlying strata, fertilizer, and runoff from the Pembina Escarpment which feeds recharge waters to the aquifer on its western boundary.

The flow system of the southern EVA consists primarily of a closed or semi-closed recharge-discharge regime near the western boundary at the EVA, and transitions to a more regional flow-through hydrologic regime approaching stream discharge sinks near the eastern boundary.

Findings of the EVA sulfate study include:

- Sulfate concentrations in the south EVA are spatially variable and stratified. With few exceptions, largest concentrations are in the bottom portion of the aquifer and decrease upward in the stratigraphic column. Near the aquifer surface sulfate concentrations are often lowest, but they are variable and can approach 1,500 mg/L in some locations, based on local conditions.
- High sulfate in the lower aquifer is controlled by the underlying silt layer and in some cases, where the silt is thin, by the till aquitard underlying the silt layer. The largest

sulfate pool is in the silt. Sulfate is moving, by diffusion, upward into the overlying EVA and downward into the upper portion of the till aquitard.

- The EVA sand and silt grain matrix contain detrital shale clasts that contain pyrite. Pyrite is mostly depleted in the vadose zone, but small amounts are retained at some locations. A small amount of pyrite is retained in the upper oxidized 1.5 meters (5 feet) of the aquifer. Largest supplies of pyrite in the sand portion of the EVA are at mid aquifer. Pyrite is retained, but somewhat depleted in the lower EVA above the silt layer. The largest overall pyrite concentrations are in the underlying silt layer.
- The EVA was formed from glaciofluvial weathering and elutriation of local Cretaceous bedrock shales of the Carlile, Niobrara and Pierre Formations during the Late Wisconsinan glacial advance and retreat. Comparison of pyrite content and ³⁴S isotope composition of the major shale strata and EVA composition confirm local shale bedrock as a likely parent source for pyrite.
- Local shale bedrock porewater is relatively low in sulfate due to biological sulfate reduction during and following its deposition. Diffusion from bedrock is not the modern proximate source of sulfate for the EVA.
- Other bedrock porewater chemistry is similar to seawater with an approximate 87 to 93% freshwater dilution. Local bedrock underlying the EVA is the main source of chloride in the lower EVA and the underlying silt and unoxidized till strata. Chloride concentrations decrease monotonically with distance above the bedrock source and conform to concentration profiles that can be accounted for almost entirely by upward diffusion from the shale for the period of time following the deposition of the till aquitard (ie. within the last 15,000 to 50,000 years). Chloride in the lower EVA is controlled by stratigraphic distance from bedrock as determined by the thickness of the till aquitard and silt layers.
- Both chemical and isotopic evidence indicates that sulfate in the silt proximate source layer was formed through oxidation of pyrite in the silt layer or in the overlying lower EVA during an oxidizing event (OE).
- The modern EVA has low (< 1 mg/L) dissolved oxygen below the top 1.5 m, except for brief periods following large recharge events. With modern water levels and

dissolved oxygen concentrations, sulfate concentrations in the deep EVA, silt and underlying till could not have been formed or caused by a modern or recent OE. The OE could only have occurred at a time when the water table was much lower.

- Semi-generic advection and dispersion models indicate that the modern sulfate profile in the lower EVA, silt and underlying till likely were formed by an OE that occurred from about 4,000 to 8,000 years ago. A likely time was a period of prolonged drought called the Hypsithermal Interval, which occurred in eastern North Dakota during that same approximate time period. Model simulations indicate that dewatering of the aquifer below the upper boundary of the silt layer during prolonged drought would be unlikely. Model simulations, water chemistry and matrix mineral analysis in the silt layer (which includes depressed pH, low calcite, and presence of iron carbonate minerals as indicators of relic acidification), and a ^{34}S distribution in sulfate disproportionately grouped on the heavy end of the local pyrite range all indicate that the OE most likely occurred in the lower EVA and upper portions of the silt layer several thousand years ago. Since then the silt layer has been serving as a conserving layer, slowly feeding sulfate into the lower EVA through diffusion. The largest single supply of sulfate is in the silt. And the dominant trend affecting the aquifer sulfate balance in the EVA has been the long-term and slow depletion of sulfate from the silt sulfate pool, and this has resulted in more rapid depletion of $^{32}\text{SO}_4$ compared to $^{34}\text{SO}_4$ as a result of mass difference.

- The degree of sulfate depletion from the silt layer is governed by the thickness of the silt layer and the rate of dispersion. In some cases, where the silt layer is thin, sulfate in the silt layer has been depleted and sulfate previously diffused from the silt to the underlying till is now the proximate source, with the till serving as the modern conserving layer and slowly feeding sulfate upward into the silt and the EVA. The rate of sulfate dispersion and subsequent depletion from the silt is governed by the local flow system of the EVA. Rates of depletion are highest under predominant recharge areas. Rates of depletion are lower under quantitatively minor net recharge areas. Depletion rates are slowest under net discharge areas.

- Soils overlying the EVA serve as general indicators of the local flow system. Soils of the Haplaboroll (*now Hapludoll*) Great Group taxa indicate predominant net recharge areas; soils of the Haplaquoll Great Group taxa indicate marginal net recharge areas; and soils of the Calciaquoll Great Group taxa indicate marginal net discharge

areas. By hydrologic proxy, soil Great Group taxa serve as general indicators of deep EVA and silt sulfate concentrations. Deep EVA water samples under Haplaboroll (*now Hapludoll*) soils are usually most depleted of sulfate; deep EVA samples under Haplaquoll soils are somewhat less depleted; and highest concentrations of sulfate in the deep EVA and silt usually underlie the Calciaquoll soils. Significant areas of highly evaporative soils are not indicated over the EVA.

- Gypsum is present as a secondary evaporite mineral in the deep soil profile of Calciaquoll soils overlying parts of the EVA and along drainageways of the Pembina Escarpment. It is not present and does not provide a major modern source of sulfate in the EVA or in any of the underlying strata.
- Sulfate in runoff water from the Pembina Escarpment on the western border of the EVA may affect the shallow and middle EVA sulfate concentrations in areas bordering the Escarpment. Runoff from the Pembina Escarpment is not a major cause of elevated sulfates in the south EVA.
- Pyrite oxidation in the vadose zone and leaching to the upper EVA does occur where pyrite is still retained in the vadose zone. When it occurs it can cause high local sulfate (as high as 1,500 mg/L) in the upper aquifer, and is accompanied by elevated calcium and magnesium concentrations (from acid weathering of carbonate minerals) and elevated sodium from cation exchange. Only one of nine sites monitored exhibited this characteristic.
- Sulfur (^{34}S) and oxygen (^{18}O) isotope analysis and water chemistry indicate that the upper EVA is receiving chloride, sulfate and nitrate from fertilizer. Sulfate from precipitation and ammonium sulfate fertilizer, however, represents a small addition to the overall sulfate pool and generally corresponds to areas of relatively low sulfate concentration in the upper aquifer.
- Nitrate is a significant portion of the anion balance in the upper aquifer, and concentrations from a few to as much as 50 mg/L nitrate-N have been measured. In all cases, however, nitrate is stratified and is non-detectable below the upper two meters of the aquifer.

- Denitrification using pyrite-S, reduced iron and organic carbon as electron donors has been identified in the EVA and has been confirmed through stratigraphic ^{15}N isotope analysis. Denitrification rates of 0.16 ± 0.06 mg/L/d have been measured. The predominant electron donor is pyrite-S. Denitrification using pyrite-S as an electron donor has been identified in the upper EVA using stratified ^{34}S and ^{18}O analysis. At measured nitrate loading rates there is sufficient pyrite-S in the EVA to support autotrophic denitrification for 11,000 to 175,000 years depending on location. These estimates assume non-preferential flow, and the gradual and uniform progression of nitrate.
- Sulfate generated by autotrophic denitrification using pyrite as an electron donor can add sulfate at concentrations of 47 to 246 mg/L/y at measured nitrate-N loading rates in thin upper strata of the aquifer. These additions, combined with dispersion from the lower EVA, may contribute to the intermediate sulfate concentrations at the middle of the aquifer. A long-term buildup of sulfate from denitrification is not, however, reflected in the ambient sulfate concentrations measured in the shallow unoxidized zone, indicating that sulfate is likely being removed through discharge to surface water and evaporative discharge to the overlying soil.
- ^{34}S isotopes can be used to successfully identify and separate sulfate sources from pyrite oxidation and fertilizer, and to some degree from precipitation, which is not clearly separable from fertilizer. Combined with ^{18}O isotope analysis ^{34}S can also be used to discern oxidizing processes and to separate effects of autotrophic denitrification from those of aerated weathering of pyrite.
- On one of nine experimental sites, sulfate depletion through biological sulfate reduction was identified as a cause of low sulfate concentrations in the lower and middle EVA.
- While the EVA has few strongly expressed discharge areas having large sulfate concentrations, high-capacity well fields may cause increased sulfate concentrations in pumped waters by drawing waters from areas of the aquifer having larger sulfate retention in the underlying silt layer. The most likely cause of increasing sulfate in high-capacity well fields is accelerated pyrite oxidation caused by aeration within the cone of depression and the mixing zone affected by the wells themselves. Where pyrite content is high, rapid oxidation of pyrite-S would be expected to occur quickly after the initiation

of pumping, and would be expected to continue for the period of operation of the well, or until pyrite is depleted. High-capacity well fields may indirectly, through aeration and oxidation of pyrite and other shale constituents, cause the local mobilization of other substances of concern, including arsenic, selenium and molybdenum. Some metals released through oxidation may be further mobilized through acidification caused by formation of sulfuric acid, and through reducing conditions re-established after cessation of pumping. Tests in the shallow unoxidized portion of the EVA have indicated increased selenium as a bi-product of autotrophic denitrification. Similar releases may be expected from O₂ weathering.

- One of the greatest potential dangers to the water quality of the EVA would be overabstraction of water causing large depletion of the water table into the pyritic zone. Temporary depletion of the EVA caused by excessive pumping during a prolonged drought could cause large-scale acidification and production of sulfate which could adversely affect aquifer water quality for many years. It would also reduce the denitrifying capacity of the aquifer by removal of pyrite through oxidation with O₂.

TABLE OF CONTENTS

	Page
1. INTRODUCTION	1
1.1 Geological Sources of Sulfate	2
1.2 Geological History of the EVA	5
1.3 Hydrogeology	7
1.3.1 Recharge	9
1.3.2 Discharge	11
1.4 Soil Hydrology of the EVA	12
2. METHODS	15
3. POTENTIAL SULFATE SOURCES IN THE EVA	18
3.1 Bedrock Parent Materials	18
3.2 Precipitation (P)	19
3.3 Pembina Escarpment (PE)	21
3.4 Lower Boundary Source Materials	25
3.5 Authigenic Sulfate	27
3.6 Fertilizer Sulfate	29
3.7 Organic Sulfate	29
4. SUMMARY OF MINERAL SULFUR AND OXYGEN ISOTOPES ($\delta^{34}\text{S}$ AND $\delta^{18}\text{O}$) DATA FOR POTENTIAL EVA SOURCE MATERIALS	31
4.1 A Brief Introduction to the Stable Isotopic Chemistry of Sulfur	38
4.2 The Oxygen Isotopic Chemistry of Sulfate	38
4.3 Potential Bedrock Sulfur Sources	39
4.3.1 Ancient Seawaters and Marine Evaporite Minerals.....	39
4.3.2 Sulfur Geochemistry of Fine-Grained Marine Sediments	39
4.4 Sulfur Geochemistry of the Bedrock Shales	40
4.5 Comparison of North Dakota Cretaceous Bedrock Sources	41
4.5.1 Dakota Group.....	42
4.5.2 Carlile and Niobrara Formations	42
4.5.3 Pierre Formation, Pembina Member.....	42
4.5.4 Pierre Formation, Gregory Member	43
4.5.5 Pierre Formation, DeGrey Member	43
4.6 Sulfur Geochemistry of Tills and Basal Silt	43
4.7 Surface Water (Drainageways) on the Pembina Escarpment	44
4.8 Fertilizer Sulfate	44
4.9 Precipitation	45
4.10 Summary of $\delta^{34}\text{S}$ Characteristics of Potential Sulfur Sources for the EVA	45
5. RESULTS	47
5.1 Transect Hydrology	47
5.2 General Chemistry on Transect A-A'	47
5.3 Dissolved Oxygen (DO) of the EVA	53
5.4 Summary of General Relationships	55
6. ANALYSIS	56
6.1 Major Hypotheses	56

6.1.1 Hypothesis: Gypsum Mobilization	56
6.1.2 Hypothesis: Bedrock Porewater Source.....	57
6.1.3 Hypothesis: Evaporative Concentration	58
6.1.4 Hypothesis: In Situ Pyrite Oxidation	58
6.2 Analysis of EVA Sulfate Sources by Depth	59
6.2.1 Deep Unoxidized EVA.....	59
6.2.1.1 Sulfur Isotope Composition	60
6.2.1.2 Oxidizing Processes	61
6.2.1.3 Hypothesis: Contemporary Oxidizing Event (OE)	62
6.2.1.4 Hypothesis: Historical Oxidation in the Silt Layer.....	64
6.2.1.5 Model Sensitivity.....	68
6.2.1.6 Hypothesis: Historical Oxidation in the Lower EVA.....	69
6.2.1.7 Discussion of Deep EVA Sources	72
6.2.1.8 Climatic Cause of the OE	73
6.2.1.9 Stratigraphic Location of the OE.....	74
6.2.1.10 Impact of Long-Term Diffusion on Sulfate $\delta^{34}\text{S}$ in the Retentive Layer	76
6.2.1.11 Soil Great Group Taxa as Indicators of Hydrologic Conditions in the Deep EVA	76
6.2.2 Middle EVA	79
6.2.3 Shallow EVA.....	79
6.3 Autotrophic Denitrification	80
6.3.1 Denitrification Rates	81
6.3.2 Denitrification Kinetic Models	82
6.3.3 Estimating Long-Term Aquifer Denitrification Potential	85
6.3.4 Summary of Denitrification Effect on the EVA	87
6.4 Isotopic Evidence of Sulfate Sources.....	87
6.4.1 Sulfur Isotopes	87
6.4.2 Oxygen Isotopes.....	88
6.5 Synthesis of Isotopic Composition, Hydrology and Water Chemistry.....	90
6.6 Trace Element Products of Pyrite Oxidation.....	93
6.7 Contemporary Significance of the OE Findings	96
7. CONCLUSIONS	97
8. CITATIONS.....	101
9. APPENDIX.....	114
9.1 Sulfate-Redistribution Model Structure	
9.1.1 Model Structure	114
9.1.1.1 FTM Model Structure	114
9.1.1.2 CDM Model Structure	116
9.1.2 Model Parameters	120
9.1.3 General Model Application.....	121
9.2 Transect B-B' Piezometric Data.....	123
9.2.1 Piezometric Data For Site 7	123
9.2.2 Piezometric Data For Site 8	125
9.2.3 Piezometric Data For Site 9	128
9.3 Transect A-A' (Site 5) Silt-Layer Mineral Analysis.....	131

LIST OF TABLES

		Page
Table 1.	Mean, minimum, and maximum sulfate concentration in precipitation at Icelandic State Park, Pembina County, ND.....	20
Table 2.	Specific conductance of water samples from wells screened in the Pierre shale on the Pembina Escarpment near the study area, reported by Kelly (1970)	23
Table 3.	Statistical parameters for $\delta^{34}\text{S}$ in all source materials. Single samples are identified as non parametric by dashes for SD and SE.....	32
Table 4.	$\delta^{34}\text{S}$ for pyrite- and sulfate-S in grain matrix samples collected from deep bedrock samples.....	33
Table 5.	$\delta^{34}\text{S}$ for pyrite- and sulfate-S in grain-matrix samples collected from the soil, vadose, upper-EVA, mid-EVA, deep-EVA, silt, and till-aquitard layers on Transect A-A'	34
Table 6.	$\delta^{34}\text{S}$ isotope for pyrite- and sulfate-S in grain matrix samples collected from deep EVA, silt, till, and bedrock layers on Transect B-B'	35
Table 7.	$\delta^{34}\text{S}$ and $\delta^{18}\text{O}$ isotope for dissolved sulfate in water samples from Sites 7, 8, and 9 and surface discharge waters (Hazen Brook) of the EVA; from surface water of the Pembina Escarpment and snow samples; from Dakota Group and Pierre shale wells near the EVA; and from supplementary Carlile shale, Niobrara shale, and till wells sampled in southeastern and east central North Dakota	36
Table 8.	Paired Bonferroni tests for all groups having $P_{\text{Bon}} < 0.2$	37
Table 9.	Chemical indicators of recharge-water sources in the shallow oxidized strata of the Elk Valley aquifer (Sites 1-6), and related source materials. The dilution factor is the ratio of sulfate concentration in County Drain #14 abutting the aquifer and the Escarpment (PE) drainage waters - to shallow EVA sulfate concentrations.....	52
Table 10.	Dissolved oxygen (DO) for the shallow oxidized (S), mid unoxidized (M), and deep unoxidized (D) strata of the Elk Valley Aquifer on Transect A-A', Sites 1-6	54
Table 11.	Dissolved oxygen measurements (February 2002) for the B-B' Transect.....	54
Table 12.	Summary of saturation indices (Wateqf, Plummer et al. 1976) for water chemistry samples taken in the Elk Valley aquifer, silt, and shallow till wells on Sites 1-9	57
Table 13.	Summary of well-screen placements for SWC having $\text{SO}_4^{2-} > 400 \text{ mg-L}^{-1}$, and their proximity to the silt layer	61

LIST OF TABLES (cont.)

	Page
Table 14. Simulated sulfate concentration, C_o , in the EVA and silt layer, duration of oxidizing conditions, t_o , and redistribution time, t_r , following the oxidizing event, OE, for the silt-layer source model scenarios, discussed in Section 6.2.1.4	66
Table 15. Simulated initial sulfate concentration, C_o ; or (as indicated) the rate of sulfate formation, dC/dt , through local in-situ oxidation in the deep EVA; duration of oxidizing conditions (t_o); and total final redistribution time (t_r) following the deep EVA oxidizing-event (OE) sulfate source-layer scenario (Section 6.2.1.6).....	72
Table 16. Summary of denitrification rates, $\delta^{15}N$ isotopic enrichment, and % of denitrification attributed to pyrite oxidation	82
Table 17. Nitrate-N concentrations and estimated total pyrite-retention time (t) at current rates of nitrate loading in the EVA from Eq. 7, 8 and 9.....	86
Table 18. Trends of increasing (+), decreasing (-) or non detectable changes in solute species for principle cations and anions, and Fe, Mn and SiO_2 in ISM porewater during tracer tests.....	94
Table 19. Trends of increasing (+), decreasing (-) or non detectable changes in trace elements during four (tests 3 through 6) tracer tests.....	95
Table A.1.1. Hydraulic and solute-transport parameters used for saturated FTM and CDM models.....	116
Table A.1.2. Hydraulic parameters used for unsaturated (Phase 1) CDM models.....	118
Table A.1.3. Hydraulic conductivity values for the EVA and sub strata	120
Table A.1.4. Estimated in-situ diffusion coefficients for chloride and sulfate	121
Table A.2.1. Piezometric data for the Carlile shale, shallow till, silt, and deep EVA on Site 7	124
Table A.2.2a. Piezometric data for the Niobrara shale, shallow till, and deep till, Site 8.....	126
Table A.2.2b. Piezometric data for the silt and EVA on Site 8	127
Table A.2.3a. Piezometric data for the Carlile Shale, shallow till, and deep till, Site 9	129
Table A.2.3b. Piezometric data for the silt and EVA on Site 9	130
Table A.3.1*. Chemical analyses at points 1 through 5	132

** Designates all changes from original report. Modified to fit report format.*

LIST OF FIGURES

	Page
Figure 1.	Location of the Elk Valley aquifer in Grand Forks County, ND.....2
Figure 2.	Piper plot illustrating the ionic composition of ground water from all water samples collected from EVA wells (SWC database).....3
Figure 3.	General stratigraphic column for western Grand Forks County [adapted from Hansen and Kume (1970)]6
Figure 4.	Piezometric map of the Elk Valley aquifer in 19997
Figure 5.	Stratigraphy of the EVA on (A) a north to south transect, and (B) three east to west transects.....8
Figure 6.	Probability distribution of water-table depths for the EVA, 1996-200310
Figure 7.	Generic taxonomic soil map (USDA Great Group taxa) for soils overlying the PE, EVA and neighboring landscape13
Figure 8.	Map of Transect A-A' and B-B' locations in the south EVA.....16
Figure 9.	Pyrite- and sulfate-S composition of Cretaceous shale bedrock samples.....19
Figure 10.	Field specific conductance (EC in $\text{mS}\cdot\text{cm}^{-1}$) of water samples from drainageways on the Pembina Escarpment discharging onto the south EVA. Samples were collected on May 9 and June 27, 2001. Where two values are presented for one location, the lowest value was measured on May 922
Figure 11.	Sulfate vs. EC for surface water from the Pembina Escarpment, from local related EVA, silt, till and bedrock sources (identified as EVA), and other till and bedrock sources in eastern ND24
Figure 12.	Porewater concentrations of (A) chloride and (B) sulfate for deep EVA, silt, till and shale layers on the B-B' Transect sites 7, 8 and 9.....26
Figure 13.	(a) Sulfate to chloride ratios for porewater at all sampled depths, and (b-f) ratios of porewater ion concentrations to seawater chloride-ion concentrations in each strata27
Figure 14.	Pyrite-S % with depth and strata on Transect A-A', Sites 1-628
Figure 15.	Non-pyrite-S % with depth and strata on Transect A-A', Sites 1-628
Figure 16.	Box plots for $\delta^{34}\text{S}$ distribution for grain-matrix pyrite, grain-matrix sulfate, and porewater sulfate from varying sources in eastern North Dakota.....31
Figure 17.	Sulfate and Nitrate-N concentrations for Transect A-A'47

LIST OF FIGURES (cont.)

		Page
Figure 18.	EVA stratigraphy and piezometric profiles for Sites 1-6, Transect A-A'	48
Figure 19.	Water chemistry composition for wells on Transect A-A'	49
Figure 20.	EVA sulfate vs. EC (A), and shallow EVA nitrate vs. EC (B)	50
Figure 21.	SO ₄ ²⁻ /Cl ⁻ vs. SO ₄ ²⁻ for all SWC wells in the EVA (A), and SO ₄ ²⁻ /Cl ⁻ vs. Cl ⁻ for all wells having SO ₄ ²⁻ < 400 mg-L ⁻¹ (B).....	53
Figure 22.	SO ₄ /Cl for EVA wells having SO ₄ concentration > 400 mg-L ⁻¹	60
Figure 23.	Simulated time from the oxidizing event and initial uniform sulfate concentrations in the silt layer required to match the modern sulfate profile in the silt (A through D) and underlying till aquitard (A' through D') using the FTM Model. Simulated values are determined by the matched intersecting lines. Paired simulations D and D' are for the FTM applied to a maximum sulfate concentration in the bottom of the EVA (top axis scale) following an oxidizing event in the lower EVA.....	65
Figure 24.	Temporal changes in simulated sulfate redistribution profiles and comparison with the modern distribution for Sites 7 (A), 8 (B) and 9 (C) on Transect B-B'	67
Figure 25.	Simulated redistribution times (t _r) following the OE and required initial sulfate concentrations (C ₀) in the EVA and silt layer, following the OE, to match the modern sulfate distribution on Site 9 using the CDM model.....	67
Figure 26.	Simulated sulfate concentrations in the silt and shallow till layers vs. simulated redistribution time for varying initial sulfate concentrations in the silt layer. The “crossover” is the time and concentration at which the sulfate concentration in the silt source depletes to that of the till sink, and the till becomes the new source	68
Figure 27.	Estimated maximum possible sulfate concentration in the lower EVA from short-term oxidation of pyrite-S, calculated from sulfide depletion in relation to the underlying silt layer	70
Figure 28.	Simulated water-table depth for a seepage face at the Turtle River with zero net annual recharge	74
Figure 29.	Comparison of observed sulfate δ ³⁴ S in basal silt/till with that predicted from Rayleigh fractionation applied to the diffusional loss model.....	75
Figure 30.	Relationship of sulfate measurement sites on Transect A-A' and B-B' to soil Great Group taxa in the south EVA.....	77
Figure 31.	Map of soil Great Group taxa and sulfate concentrations measured for all EVA wells from the SWC database	78

LIST OF FIGURES (cont.)

	Page
Figure 32. Nitrate-N concentration profiles for water samples collected on 9/17/97, 4/21/98, 12/8/97 and 7/29/98 on Transect A-A'	81
Figure 33. Comparison of zero- and first-order kinetic models for denitrification for in-situ measurements of the EVA (Larimore) and Karlsruhe aquifer ISM sites	84
Figure 34. Stratigraphic distribution of $\delta^{34}\text{S}$ in grain pyrite and porewater sulfate for Transect A-A'. "Arbitrary Depth" is scaled for relative reference to (0) topsoil, (1) the shallow-EVA oxidized zone well, (2) the mid-EVA (unoxidized) wells, and (3) the deep EVA wells.....	88
Figure 35. Stratigraphic distribution of $\delta^{18}\text{O}$ in grain pyrite and porewater sulfate for Transect A-A'. "Arbitrary Depth" is scaled for relative reference to (0) topsoil, (1) the shallow-EVA oxidized zone well, (2) the mid-EVA (unoxidized) wells, and (3) the deep EVA wells.....	89
Figure A.1.1. Schematic description of the FTM model.....	114
Figure A.1.2. Dupuit-Forchheimer approximation for relative piezometric head in the eastern portion of the South EVA.....	115
Figure A.1.3. Schematic description of the CDM model.....	117
Figure A.1.4. Simulated intra-annual distribution of recharge and discharge to the EVA in 1990, used for application in the CDM	119
Figure A.2.1. Piezometric response of the Carlisle shale and shallow till to well evacuation (left), and comparison of long-term piezometric variation in the shallow till, silt and EVA (right)	123
Figure A.2.2. Piezometric response of the Niobrara shale and deep till aquitard to well evacuation (left), and comparison of long-term piezometric variation in the deep till, shallow till, silt and EVA (right)	125
Figure A.2.3. Piezometric response of the Carlisle shale and deep till aquitard to well evacuation (left figure), and comparison of long-term piezometric variation in the deep till, shallow till, silt and EVA (right).....	128
<i>Figure A.3.1.*</i> Figure 1. Ca x-ray map	131
<i>Figure A.3.2.*</i> Figure 2. S x-ray map	131
<i>Figure A.3.3.*</i> Figure 3. Backscattered Image.....	131

** Designates all changes from original report. Modified to fit report format.*

This blank page is placed for document
page format control when printing

1. INTRODUCTION

The Elk Valley Aquifer (EVA) is a regional ground-water source, supplying homes, two local communities, irrigators, and two rural water systems in Grand Forks and Traill Counties, ND (Fig. 1). Water in the EVA is predominantly of the calcium bicarbonate type (Fig. 2). Average sulfate concentrations are low, with a median of about 89 mg-L⁻¹. In some portions of the aquifer, however, sulfate concentrations are relatively high, exceeding 1,000 mg-L⁻¹. Kelly and Paulson (1970), in an early reconnaissance study of the aquifer, observed increased sulfate concentrations in the southern portion. They speculated that increasing fineness, notably increased silt content of the aquifer as it trends southward, increased capillarity and evaporative discharge, leaving residual sulfate salts. Gerla (1992), using a sample set including well screens at varying depths of the EVA, observed that high sulfate was not correlated with decreasing pH and increased iron characteristic of sulfide oxidation, and hypothesized that the source was dissolution of gypsum. Swanson (1992) challenged the gypsum-source hypothesis, noting that lack of correlation with decreasing pH could be accounted for by carbonate-mineral buffering, and that oxidation of iron would likely occur during sulfide oxidation. Swanson further suggested that other potential sulfate sources should be examined, including oxidation of sulfide in the vadose zone and in underlying and bordering shales and tills. Swanson proposed that sulfate sources might be local rather than derived from accumulation along a flow path. He did not, however, provide an analysis of the proposed alternate sources.

In 1995 the Grand Forks Traill Water Users Association (Written Communication, 1/16/95, NDSWC Project File #950) expressed concern over apparent trends of increasing sulfate in 12 supply wells located in the south EVA. They proposed that increasing sulfate was being caused by additions of sulfate fertilizer. Alternately, Korom et al. (2005) have proposed that apparent increases in sulfate may be caused, in some cases, by autotrophic denitrification induced by nitrate loading.

Identification of sources and processes affecting sulfate distributions in the EVA is needed to discern anthropogenic from natural causes of changes in water quality, and to assist in effective management of the water resource. It is also of broader interest in helping to understand the relationships between aquifers, parent materials from which they are derived, and boundary materials with which they interact. These relationships will be increasingly important as hydrologic stress from increased pumpage causes changes in the oxidation-reduction environment of many ground-water systems, and as increasing influx from boundary materials occurs in response to changing gradients caused by pumpage.

Finally, high-organic shale pyrite sources for sulfates are associated with elevated arsenic and selenium (which substitute for S in pyrite), and possibly molybdenum (Schultz et al. 1980 p. B69). Understanding of sulfate sources is therefore important for identification of sources of substances of toxicological concern.

The purpose of this study is: (1) to identify the major sources and processes causing elevated sulfate concentrations in the south EVA, and (2) to examine the use of $\delta^{34}\text{S}$ and $\delta^{18}\text{O}$ isotopes as a means for tracking and identifying those sources and processes.

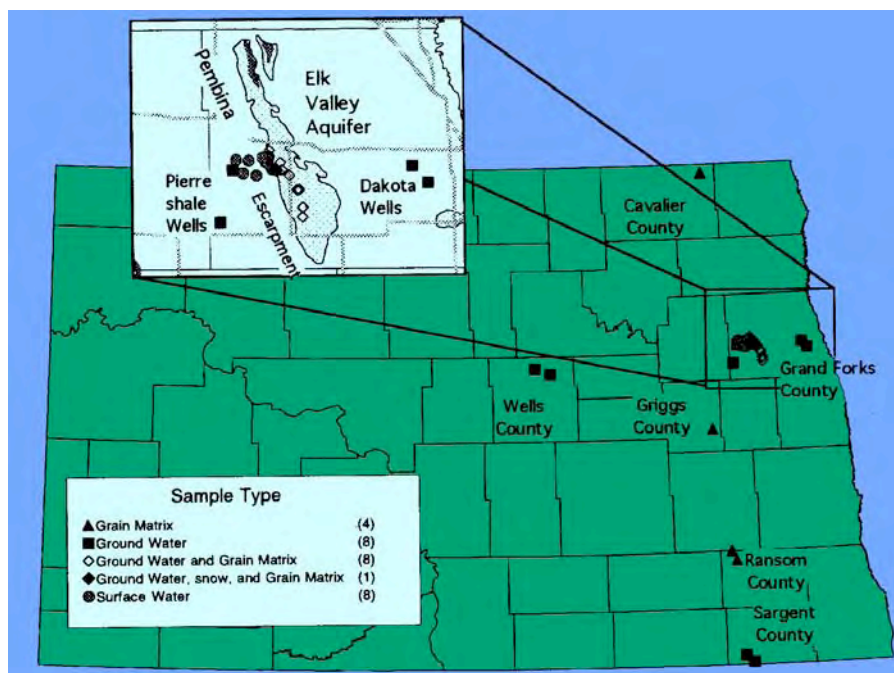


Figure 1. Location of the Elk Valley aquifer in Grand Forks County, ND.

1.1 Geological Sources of Sulfate

High sulfate concentrations in groundwater in the northern Great Plains of North America occur most frequently in lignite, in or above Cretaceous shale deposits, or in matrix materials derived from these deposits. Mineral sulfate sources in the glaciated regions of the northern Great Plains are derived primarily from oxidation of organic matter (Tourtalot 1962, Hendry, Cherry, and Wallick 1986) or reduced pyrite in the underlying bedrock shales (Tourtalot 1962, Gill and Cobban 1965, Schultz et al. 1980, Mermut and Arshad 1985). Weathering of shales may occur either directly at bedrock exposures (Schultz et al. 1980, Mermut and Arshad 1987), at contacts with the overlying

aquifer (McMahon et al., 1999), from ground and highly weathered shale constituents of glacial drift, or from more elutriated and water-worked deltaic or glacial outwash deposits. Because most shales are less resistant to weathering than quartz, they are generally proportionally more abundant in coarse deposits closer to depositional sources, and tend to decrease with distance from the source.

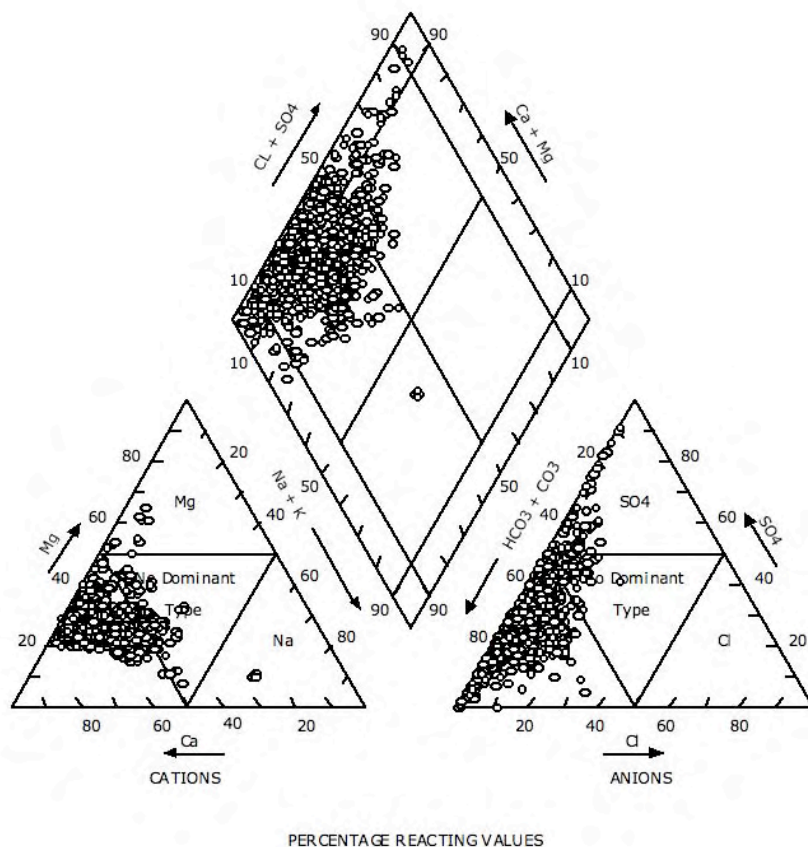


Figure 2. Piper plot illustrating the ionic composition of ground water from all water samples collected from EVA wells (NDSWC database).

One of the most common Cretaceous shale sources in the Upper Great Plains is the Pierre Formation (Tourtalot 1962, Gill and Cobban 1965, Schultz et al. 1980), which extends from the Arctic to the Gulf of Mexico, and from the Rocky Mountains to Eastern Saskatchewan in Canada and Eastern North and South Dakota in the United States. Schultz et al. (1980) have observed that sulfur occurs in the Pierre shale as

pyrite, gypsum and jarosite, but the latter are considered to be weathering products of pyrite. They have also observed that pyrite content varies widely over the expanse of the Pierre Formation, but is most abundant in the "very dark gray to black" organic-rich marine shales near the eastern edge. Tourtalot (1962) states that pyrite-derived sulfate was recognized as early as 1810 by Thomas Nuttall on his trip up the Missouri River.

"He (Nuttall) mentions specifically the pyrite-rich unit (the Sharon Springs Member) at the base of the Pierre just above the Niobrara Formation and speculates that the abundant gypsum throughout the Pierre was formed by the weathering of Pyrite." (Tourtalot, 1962, p.4). "

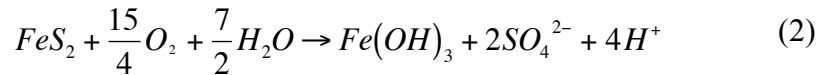
The observed relationship between S and organic carbon in the marine shale was caused by reducing conditions created by accumulating organic carbon in the Cretaceous marine depositional environment. These conditions were favorable for direct reduction of sulfate and for the proliferation of sulfate-reducing bacteria. The reaction, from Strebel et al. (1990) is:



from which H₂S reacts with reduced iron weathered from clay minerals to form pyrite (FeS₂). Tourtalot (1962) reported acid soluble S (as SO₃) at 4.85% with insoluble S (as S) at 1.57% in the Pembina Member compared with 1.31% and 0.01% for the Gregory Member, and even less for overlying Crow Creek and DeGrey Members. In a plains-wide survey of mineral content in the Pierre shale, the highest frequency (80% of eight core samples) and the highest average pyrite content (7.6%) was in the Sharon Springs Member in eastern South Dakota (Schultz et al. 1980). The Pembina Member of eastern North Dakota has been identified with the Sharon Springs Member by Tourtalot (1962), Gill and Cobban (1965), Schultz et al. (1980), and Hansen and Kume (1970).

The Pembina Member in eastern North Dakota directly overlies the Niobrara and Carlile Formations of mid- to late-Cretaceous origin (Tourtalot 1962, Gill and Cobban 1965 p. A9, Hansen and Kume 1970 p. 15-16). The Pembina Member has been described as consisting of unique striated layers of interbedded volcanic ash and sea-bottom muds, containing large concentrations of fish bones and other fossils (Gill and Cobban 1965) which provide sources of calcium and phosphorus. The lower portion of the Gregory Member, directly overlying the Pembina Member, has also been identified as a high organic deposit, containing fossiliferous bones and an abundance of pyrite (Gill and Cobban 1965 p. A.11).

Sulfates of shale origin result from the changing situation of the shale through tectonic uplift, subsequent erosion and the consequent oxidized weathering of the shale. A massive historical example of weathering occurred through glacial action which excavated, ground, and weathered shale in forming glacial till, and through consequent fluvial action causing elutriation and deposition of shale with other minerals in ground-water deposits. Pyrite-S in such weathered materials produces sulfate through oxidation (Kolle et al. 1985, McKibbin and Barnes 1986, Moncaster et al. 2000):



or through microbially mediated autotrophic denitrification:



if nitrate is present under unoxidized conditions. The modern disposition of sulfate can thus be viewed as the product of the historical transport, oxidation, and transformation of sulfide deposited on ancient estuaries.

1.2 Geological History of the EVA

The Elk Valley aquifer (EVA) is a silt, sand and gravel deposit of deltaic and glaciofluvial origin. The site is in the Central Lowlands Physiographic Province, but borders on, and shares many of the bedrock features of the Great Plains Province. It is located on the eastern edge of a landform called the Pembina (or Manitoba) Escarpment (PE) (Fig. 3), which marks the western boundary of large-scale erosive events that carved the current Red River Valley from much deeper deposits of Cretaceous shales and sandstones (deposited > 67 Ma B.P.), mainly during the Pliocene Epoch (*circa* 5 Ma to 1.8 Ma B.P.) (Bluemle 1991, pp. 51, 155). Pliocene erosion and subsequent Pleistocene glacial action exposed Cretaceous deposits which locally dip to the west. According to Bluemle (1991, pp. 51, 155) the Dakota Group, which consists of beds of sandstone, marl, and shale, was exposed in the eastern part of Grand Forks County, west of the Red River, during the Pliocene Epoch. Slumping at the discharge face of the Dakota Group, subsequent fluvial erosion, and later glacial action eroded the overlying shale deposits, cutting them westward to form the current Pembina Escarpment (PE) in western Grand Forks County. The modern-day PE constitutes a relatively steep cut through the Pierre shale and the underlying Niobrara and Carlile shales of Late Cretaceous origin (Fig. 3). Bedrock beneath the EVA consists of Niobrara and Carlile

shale. The Carlile shale has been described as a "spongy shale" that contains "thin interbeds" of "bentonitic clays" (Hansen and Kume, 1970, p. 15).

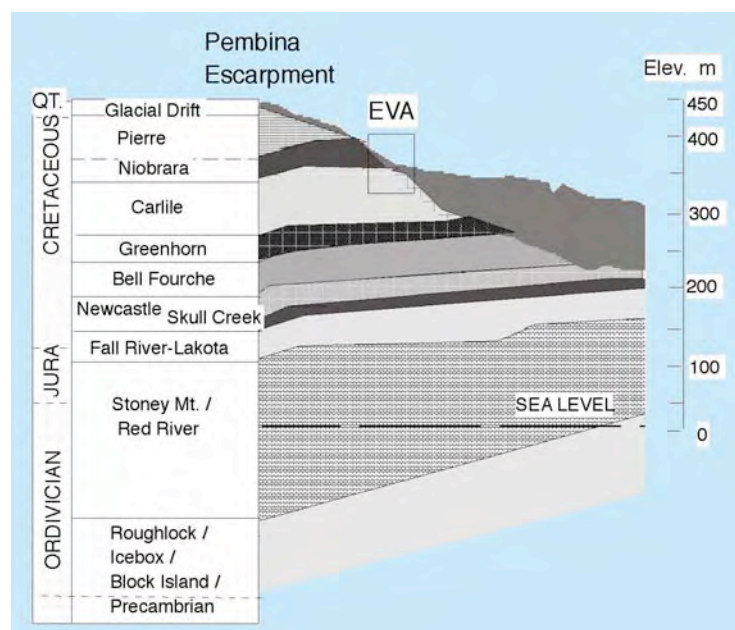


Figure 3. General stratigraphic column for western Grand Forks County [adapted from Hansen and Kume (1970)].

The shale bedrock beneath the middle of the EVA is overlain by 50 to 60 m of argillaceous till, which decreases in thickness approaching the PE, and which comprises a thin cap on the escarpment itself. According to Hansen and Kume (1970, p. 33), the till underlying the EVA would comprise at least three coextensive but separate layers, the deepest of which is dated at "earliest" to the Early-Wisconsinan Age [71 to 28 ka B.P., (Moran et al. 1973)], and the latest of which is dated in the Late Wisconsinan (beginning at about 22 ka B.P.). The retreat of the Late-Wisconsinan glaciation occurred in North Dakota from *circa* 16 to 13 ka B.P., with stagnation ice remaining until about 9 ka B.P. (Bluemle 1991). According to Clayton and Moran (1982), the glaciofluvial and deltaic materials composing the current EVA were deposited by the proglacial Elk River, which flowed southward constrained on the west by the Pembina Escarpment, and on the east by an ice margin of what is locally labeled the Edinburgh Phase (Clayton and Moran 1981, Hansen and Kume 1976), which deposited the current Edinburgh Moraine east of the EVA. The oldest reliable dates (based on ^{14}C measurements) for these melt-related events would be about 12 ka B.P., with some samples dated as late as 10 ka B.P. (Clayton and Moran 1981). Likely constituents of

the EVA are glaciated and elutriated residues from the Pierre shale of the Pembina Member and possibly the Gregory and DeGrey Members (Hansen and Kume 1976, p17), admixed with glacial residues of the underlying Carlile and Niobrara shales. These are the probable original sources of pyrite in the EVA.

1.3 Hydrogeology

The EVA consists of up to 20 m of mostly unconfined or shallow confined sand and gravel. It underlies an area of about 725 km² (Mayer 1992) and stores about 1.22 billion cubic meters of water (Kelly and Paulson 1970). A piezometric map of the EVA in 1999 is shown on Fig. 4. The EVA is composed of quartzose sand, detrital shale sand, and some gravel (Kelly and Paulson 1970). The aquifer has been described as "somewhat lenticular," with some interbedded clay and silt rich materials (Kelly and Paulson 1970). Grain-matrix coarseness varies from north to south, with gravels found predominantly in the north, medium sands predominant in the central areas, near Larimore, and finer sands in the south (Fig. 5). The shaley composition of part of the sand fraction is confirmed by texture disconformities observed when drilling using a

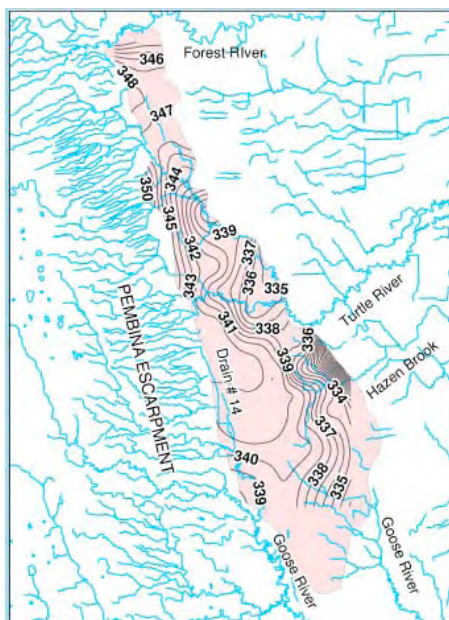
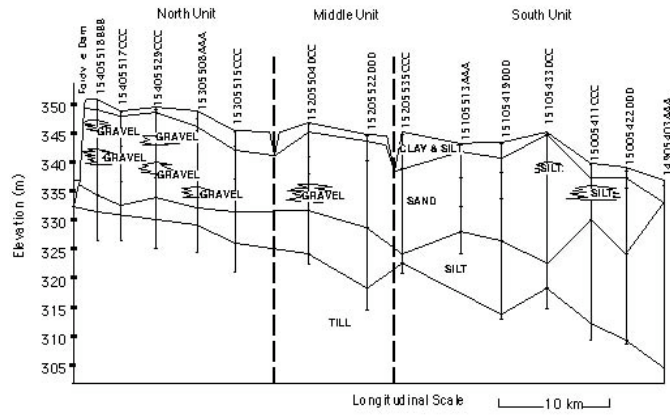


Figure 4. Piezometric map of the Elk Valley aquifer in 1999. Elevations are in meters.

A.



B.

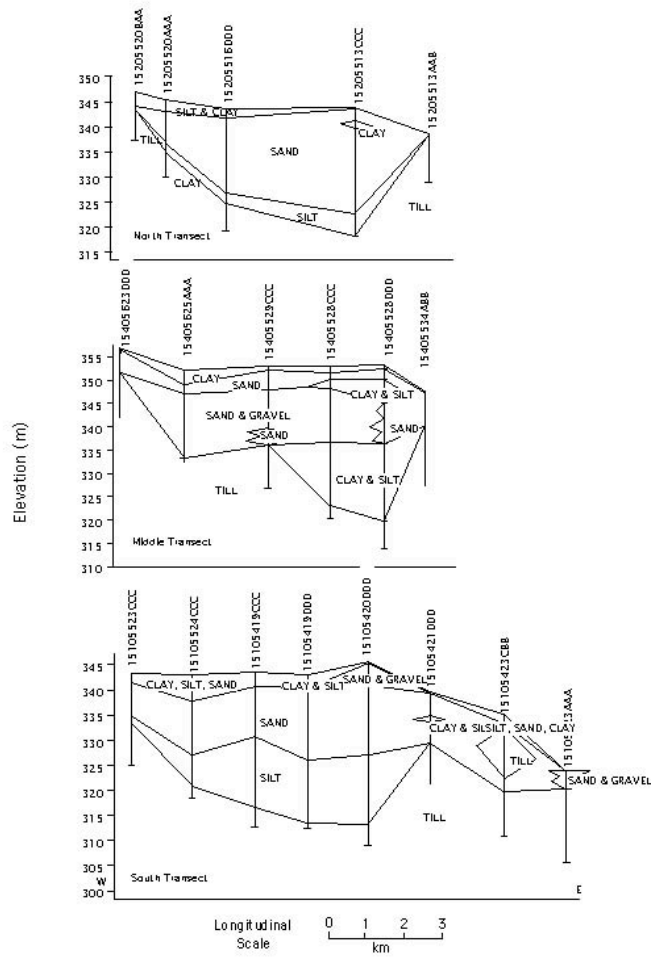


Figure 5. Stratigraphy of the EVA on (A) a north to south transect, and (B) three east to west transects.

hollow-core dry auger. Materials sampled from the hollow core maintain a firm sand- and gravel-grain composition, while spoil reaching the surface from the outside of the auger is sufficiently high in clay content to resemble coarse till. Hydraulic properties of the EVA, underlying till and shale, and other similar materials are summarized on Table A.1.3 in the Appendix. The general stratigraphy of the aquifer overlying the Wisconsinan till consists of a loam to sandy-loam surface layer, overlying EVA sands and gravels from 0 to 13 m thick, and deltaic silt and clay from 0 to 20 m thick. The silt layer thickens from north to south until it comprises the entire thickness from surface to till on the southern boundary (Fig. 5A).

The EVA is well-integrated with local rivers and streams, all of which are gaining water from the aquifer. Ground water in the northern and middle portions of the EVA flows northward, discharging to the Forest River, and eastward and southward, discharging to the deeply incised (20 to 30 m) North and South Branches of the Turtle River, (Fig. 4) creating relatively steep horizontal gradients between the PE and the Rivers. The south portion of the EVA, however, is not directly and deeply incised except on its northern boundary at the Turtle River. Most waters in the eastern half of the south EVA discharge through intermittent surface seeps fed by high water tables, which then drain eastward through small streams, like Hazen Brook, into either the Turtle or Goose Rivers (Fig. 4). The western half of the south EVA is poorly integrated with surface drainage. Local precipitation and runoff from the PE infiltrate, and following large runoff events fill and are rejected by the aquifer, flooding lands adjacent to the PE. Poorly integrated natural drainage results in a relatively high water table, subsequent evapotranspiration from the water table, and a flow system which is predominantly composed of closed depressions. This is reflected in the flat piezometric gradients in the south EVA adjacent to the PE (Fig. 4).

1.3.1 Recharge

Recharge sources are percolation from precipitation (P) and infiltration of runoff waters from the PE. Average precipitation is approx. 486 mm-y⁻¹, of which an average of 30% (95% CI 25 to 35%), or 150 mm-y⁻¹, would be expected to drain below the root zone in non-coupled areas (based on lysimeter data from 1990 to 2001 at Oakes, ND from Nathan Derby, NDSU, written communication, 8/15/02). About 340 mm remains for soil storage and transpiration. This compares with an estimated range of 330 mm to 432 mm P required for a wheat crop (Schlehuber and Tucker, 1967), the most common non-forage dryland crop historically grown over the EVA. Uncoupled conditions, however, predominate only in the central and northern EVA. Considerably less net

recharge would be expected to occur in the southern EVA, where water tables are closer to the surface and evapotranspiration (ET) losses are higher. Benz et al. (1981) have demonstrated that water tables within 1.5 m of land surface are strongly coupled with respect to root withdrawal on sandy soils in ND. About 40% of all water levels measured (in 53 locations) between 1996 and 2001 in the Elk Valley aquifer were within this depth (Fig. 6).

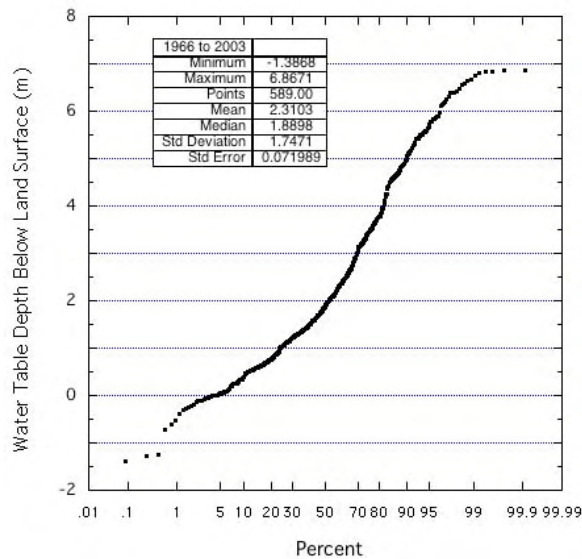


Figure 6. Probability distribution of water-table depths for the EVA, 1996-2003.

Runoff from the PE is most important in the western half of the south EVA where drainage from the PE is less well integrated with major streams, and where waters flow from the west more directly onto the aquifer. This can be seen in a flat piezometric surface near the PE (Fig. 5). Computations for a 10-km portion of the western PE boundary near County Drain #14 using estimated annual runoff at 50% probability (USDA-SCS 1980) indicate about $1.08 \times 10^5 \text{ m}^3\text{-km}^{-1}\text{y}^{-1}$ or $108 \text{ m}^2\text{-y}^{-1}$ of average surficial influx occurs along the aquifer boundary. This compares with a maximum aquifer cross-sectional flux capacity of about 20 to 25 $\text{m}^2\text{-y}^{-1}$ in the adjoining EVA.

Local combinations and variations of recharge and discharge sources, sinks and processes have major ramifications for the long-term flow system, the soil hydrology of the aquifer, and the distribution of sulfate. These will be discussed later in this report.

1.3.2 Discharge

Discharge occurs through evapotranspiration, discharge to surface water bodies, and pumpage for consumptive use. Evapotranspiration has been described briefly in the discussion of recharge. Its relation to the flow system and sulfate concentrations will be discussed later in this report.

Surface seeps are at two main locations. The first is near the western boundary, where waters from drainageways carrying runoff from the PE enter the aquifer. Total runoff from the PE to the EVA on the western boundary is large and is most hydrologically dominant near County Drain #14 (Fig. 5) where EVA surface drainage is poorly developed. The difference between aquifer cross-sectional flux capacity and runoff from the PE (by a factor of about 5) was described in the previous section. Waters exceeding the aquifer capacity overflow during large recharge events. Overflow waters drain overland to the Turtle River in the north and mid sections of the aquifer, and to the Goose River in the south. Overflow occurs mainly during spring snow melt and during large summer rains. Following large runoff events, aquifer overflows occur until the water table is sufficiently low to cease.

Natural drainageways near County Drain #14 are poorly developed, and the drains were constructed in the 1950s to shorten flooding of agricultural land on the western EVA. Even at the present time, however, substantial flooding occurs following large snow-melt events or storms. During these events local growers have, on occasion, constructed temporary drainageways within their fields to facilitate water movement to the county drains. The significance of this feature for the present study is shown by equipotential lines in its vicinity (Fig. 4), which indicate the spreading of water near a major recharge locus. It may be presumed that flooding and aquifer recharge from the PE was considerably prolonged over historical times preceding construction of the drain.

The second area of predominant discharge is on the eastern half of the EVA. Here ground water discharges into Hazen Brook and other shallow and ephemeral seeps which feed tributaries of the Goose and Turtle Rivers.

Kelly and Paulson (1970) estimated the average increase in base flow through discharge to the Forest River at $0.167 \text{ m}^3 \text{ s}^{-1}$, based on summer data from 1940 to 1967. While stream data for the Turtle River was not available, Kelly stated that it "seems likely that the combined discharge of these streams (combined Turtle, Goose, and other seeps) is at least as much as for the Forest River." Using this rough combined estimate of $0.334 \text{ m}^3 \text{ s}^{-1}$, we estimate a minimum annual stream-flow discharge of 10.5 million $\text{m}^3 \text{ y}^{-1}$. If all of the recharge water were derived from local P, a minimum of about 15 $\text{mm} \text{ y}^{-1}$ of precipitation would be reaching the rivers as through-flow. Based on the

aquifer volume to discharge ratio, the modern mean cycling time for water in the aquifer would be about 117 years.

An average of 8 million $\text{m}^3\text{-y}^{-1}$ were pumped from the EVA in 1990 through 2002 (NDSWC database). Of this 75% was pumped for irrigation, 21% was pumped for rural water systems, and 4% was used for two municipal supplies. Most irrigation and rural water development has occurred in the last 30 years (before 2005). Irrigation water transpires after application, and only a small portion of it can be counted as additional loss to the aquifer. For most of the 20th century pumpage was less than 0.5 million $\text{m}^3\text{-y}^{-1}$. Large consumptive use is thus a recent phenomenon. Consumptive use before 1900 was negligible.

1.4 Soil Hydrology of the EVA

Soils overlying the EVA provide evidence of recharge-discharge regimes (Fig. 7). Soils in the middle and north EVA are mainly Haplaborolls (now Hapludolls) of the Arvilla and Hecla series (USDA-SCS 1981, Patterson and Heidt, 1987) which are coarse and well drained. These have been described by Seelig and Richardson (1994) as hydrologically "neutral" on the landscape, characterized by neither concentrated recharge from runoff nor evaporative discharge, but by summer percolation of precipitation through the root zone. Examples of net recharge measured under Haplaboroll soils are 150 mm for a sandy Haplaboroll at Oakes, ND (see Section 1.3.1 above) and 180 to 200 mm for a loamy Haplaboroll near Carrington, ND (Schuh et al. 1993). They predominantly overlie portions of the EVA that are drained to deeply incised rivers and streams, which tend to deepen the water table.

Over the southern EVA, predominant soils are Calciaquolls of the Arveson, Bearden and Wyndmere series, and associated Haplaquolls of the Perella and Tiffany series, which serve as local recharge areas. Relative areas of Calciaquolls and Haplaquolls have been estimated at about 65% and 30% respectively (USDA-SCS 1980). The Calciaquolls are characterized by seasonal high water tables and sufficient summer evaporation to deposit calcium carbonate (a calcic horizon) in the upper soil profile. Knuteson et al. (1989) have characterized the Bearden calcic horizon as the product of 5 to 6 ky of a hydrologic regime consisting of seasonal local evaporative upflux, resulting in shallow deposition of carbonates in fine (capillary-dominated) pores. Local recharge is sufficient, however, to flush the more soluble gypsum (formed near the surface during evaporation) to a depth below the calcic horizon, while leaving the carbonates in place. The local hydrologic regime is thus fluctuating on an intra-annual scale, but represents a long-term weak net discharge regime.

Arndt and Richardson (1989) have described Calciaquolls as predominantly the product of a "flowthrough" regime. Rare, over the EVA, are soils such as Natriborolls, which signal major long-term evaporative discharge areas (which are limited to borders of drainageways on the PE), or Argiaquolls which are strongly defined concentrated recharge areas (Arndt and Richardson 1989, Seelig and Richardson 1994). The closed-depression recharge regime near the PE in the south EVA, indicated by the flat piezometric surface, combined with the absence of strongly developed discharge soils, indicates that in the EVA landscape the Calciaquolls are functioning primarily as weakly-expressed net discharge areas, accompanying weakly-expressed net recharge areas in the associated Haplaquolls. The EVA landscape is very flat, so that the two soil Great Groups are intermixed and difficult to discern with the naked eye.

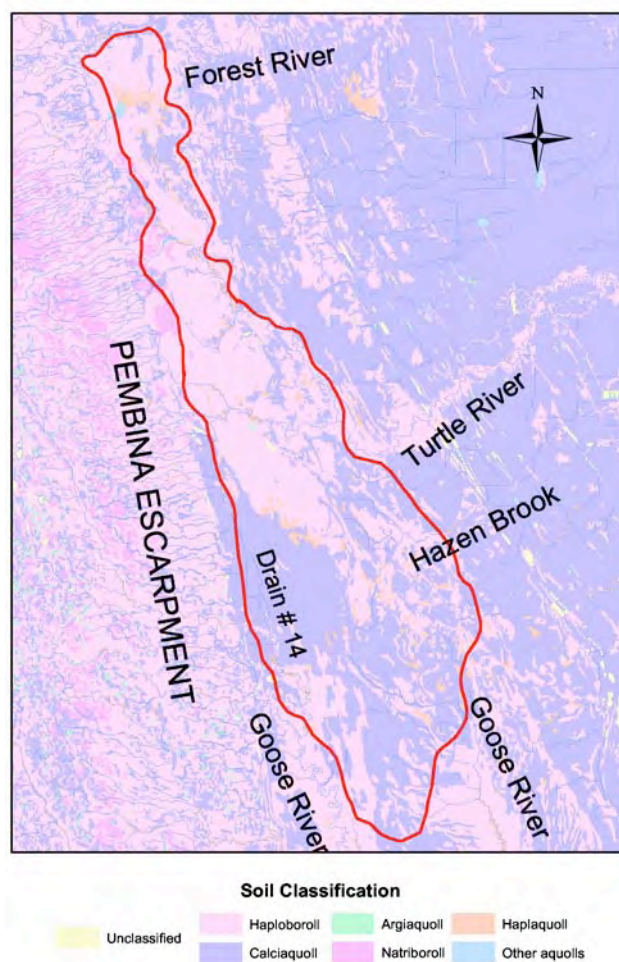


Figure 7. Generic taxonomic soil map (USDA Great Group taxa) for soils overlying the PE, EVA and neighboring landscape.

The recharge-discharge regime, as indicated by soils, can thus be described as moderately dominated by recharge in the northern portions of the EVA with discharge to rivers, and predominantly a closed-depression flow regime in the southern portion of the aquifer with more enhanced seasonal ET than in the north.

2. METHODS

In June of 1997 six nests of wells were placed on a transect (Transect A-A' on Fig. 8) generally oriented in the direction of aquifer flow (northwest to southeast) in the southern third of the Elk Valley aquifer. On each site wells were placed in the shallow oxidized zone (generally within the top meter), in the middle (unoxidized) zone, and in the deep aquifer (near the silt layer). The lithology and well depths are summarized on Fig. 18 (in Section 5.1). All wells were placed using a dry hollow-stem auger. Wells were constructed of rigid 5.1-cm diameter rigid polyvinyl chloride (PVC) casing. During drilling acrylic-cased sediment samples were collected at all levels from the topsoil to the underlying till aquitard. All samples were capped immediately after extraction and transported in a cooler (on ice) to the University of North Dakota Energy and Environmental Research Center (EERC) laboratory where they were frozen within three hours of collection, and transported to an isotope laboratory for determination of pyrite- and non-pyrite S, and $\delta^{34}\text{S}$ and $\delta^{18}\text{O}$ isotopes.

In October of 2001 three nests of observation wells were constructed (Transect B-B', on Fig. 8) for the purpose of examining the relationship between water chemical composition in the lower aquifer, and the underlying silt, clay, till, and shale. Wells were placed using a forward rotary drill. No bentonite or other additives were used during drilling. Drill cuttings were sampled in the silt and shale, and at varying depths in the intervening till. All cuttings were chosen for the largest possible aggregates, and were rinsed using distilled water in a stainless steel strainer to prevent contamination with EVA water used as drilling fluid. Samples were double-bagged in plastic, placed on ice in a cooler, and transported to the North Dakota State Water Commission (NDSWC) soils laboratory where they were dried at 105° C and shipped in vials for determination of pyrite-S concentrations and $\delta^{34}\text{S}$ and $\delta^{18}\text{O}$ isotopes. Wells were developed to remove any added water immediately after drilling, first by air-lifting, and then by bailing repeatedly. Wells were then allowed to recover for two months, and were fully evacuated by bailing again in early December 2002.

All well elevations were measured to within 0.003 m from a standard survey benchmark. Hydraulic conductivities of the shale on Sites 7 and 9, of the deep till above the shale contact on Site 9, and of the deep till, and shallow till (beneath the silt) on Site 8 were measured using the method of Bouwer and Rice (1976). Six weeks of recovery time were measured for the till wells, several months were measured for the shale. Laboratory K measurements were performed using the standing head method of Klute (1986).

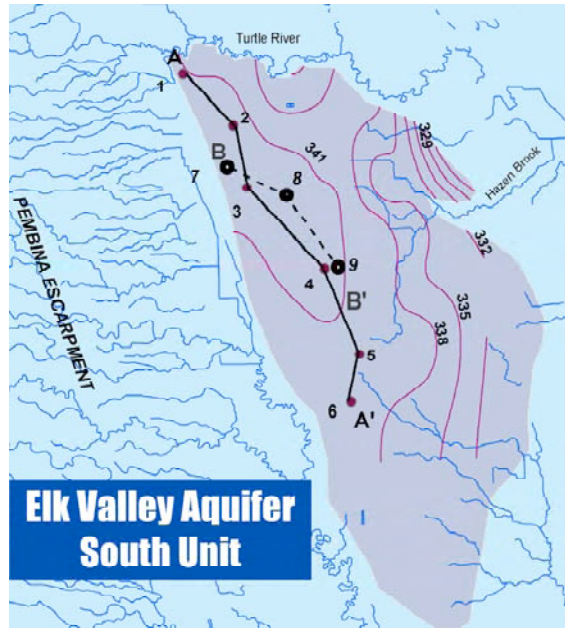


Figure 8. Map of Transect A-A' and B-B' locations in the south EVA. Contours are ground-water piezometric head elevation in meters above mean sea level.

Water samples were taken from the well screen using a PVC point-source bailer after evacuating three well volumes, except in the till and shale wells which were sampled two weeks after a single bailing because of slow recovery. Bicarbonate (HCO_3^-) and electrical conductivity (EC) were determined using the raw-untreated 500-mL sample. Sulfate (SO_4^{2-}), fluoride (F^-), chloride (Cl^-), and dissolved solids (DS) were determined using the filtered ($0.45 \mu\text{m}$) sample. Calcium (Ca^{2+}), magnesium (Mg^{2+}), sodium (Na^+), and potassium (K^+) were determined using the filtered ($0.45 \mu\text{m}$) and acidified (2 mL-nitric acid) sample. A Perkin-Elmer Model 4000 atomic-absorption spectrophotometer was used to measure concentrations of Ca^{2+} , Mg^{2+} , Na^+ , K^+ , Fe^{2+} , Mn^{2+} , Li^+ , and Sr^{2+} . Orion Model 960 and 940 titralyzers were used to measure concentrations of HCO_3^- , CO_3^{2-} and Cl^- . A gravimetric method was used to measure the concentration of SO_4^{2-} . Fluoride (F^-) was measured using a specific iron electrode.

Dissolved oxygen (DO) was measured quarterly from September of 1997 through October 1998 on Transect A-A', and in May 2002 on Transect B-B'. DO was measured in Transect A-A' wells using a YSI Model 5700 DO meter. After July 1998 a YSI Model 85 DO meter was used. The meters were calibrated to the site altitude and ground-water temperature. Measurements were taken at the mid-screen depth and recorded when the meter stabilized for 30 seconds or more. Transect B-B' deep EVA and silt wells were measured within the well screen using a YSI model 51B DO meter.

Deeper wells (in the till aquitard and shale) were measured in water within a 1.8-m long bailer immediately after withdrawal from the well. A comparison of down-hole and bailer methods on nine wells gave a maximum difference range of -0.1 to $+0.3 \text{ mgL}^{-1}$. Sulfate oxygen isotopic composition were determined using the method of McCarthy et al. (1998) and are similarly reported as delta values relative to the V-SMOW standard.

Ground-water sulfate was recovered by precipitation as BaSO_4 for shipment to the University of Leeds. Sulfides were extracted from solid samples by reaction with acidified chromous chloride and the H_2S produced trapped by reaction with a standardized CuCl_2 solution and CuS precipitate recovered for isotopic analysis (Newton et al. 1995). Sulfide concentration was determined by back-titration of unused Cu in the traps. Sulfate and sulfide isotopic analyses were performed following procedures described in Moncaster et al. (2000). Isotopic data are reported in delta (δ) notation as part per thousand (‰) enrichments (+ve values) and depletions (-ve values) of the heavy minor isotope (^{34}S) relative to the V-CDT standard.

All supplementary water chemistry analyses using data from the NDSWC database, were taken from sites having known and recorded lithologies and well construction information. Chemical properties used were measured using the same procedures described above.

3. POTENTIAL SULFATE SOURCES IN THE EVA

3.1 Bedrock Parent Materials

The landscape and stratigraphy of the EVA, as described in Section 1.2, was formed by water erosion during the Pliocene Epoch, and by glacial action during the Pleistocene Epoch. Probable parent materials for the till aquitard, the deltaic silt at the bottom of the EVA, and the EVA itself are ground and elutriated local bedrock. One likely source of sulfate in EVA porewater is pyrite-S oxidized either in place or in bordering materials with subsequent transport to the EVA. Most of the EVA is underlain by shale of the Carlile Formation. The eastern EVA and the border with the PE is underlain by shale of the overlying Niobrara Formation. On the PE and other landforms west of, and within 5 miles of the EVA, probable successive layers (proceeding upward) of Pembina, Gregory, DeGrey and Odonah Members of the Pierre Formation have been identified (Hansen and Kume (1970). These provide likely erosional sources for the EVA and underlying glacio-fluvial deposits.

Published descriptions on pyrite-S sources in Cretaceous shales of the Northern Great Plains were discussed in Section 1.1. Local data for northeastern North Dakota bedrock is sparse. For this study, shale samples and porewater samples from shale strata were obtained from wells and outcrops at several sites in eastern ND, as described in Section 2 (Methods). Sample locations are shown on Fig. 1. Quantitative sulfate- and pyrite-S, and corresponding $\delta^{34}\text{S}$ isotope data are reported in Section 4. A comparison of bedrock pyrite- and sulfate-S for all of the shale strata discussed above and one weathered (identified as "till-s") material above a Niobrara shale contact is shown on Fig. 9 below. These data indicate a substantial pyrite presence in all of the measured Members of the Carlile, Niobrara and Pierre Formations, with the exception of the Odonah Member of the Pierre Formation. The Niobrara Formation and the Pembina Member of the Pierre Formation exhibit a similar range, but lower median pyrite content than other strata. However, data for the Pembina Member, which was specifically cited as "pyrite rich" by other published sources (Section 1.2), is counter balanced by a wider range of sulfate-S values. This indicates that the Pembina Member samples, which were sampled at a road cut in the Pembina Gorge in northeast ND, were likely oxidized prior to sampling.

These results indicate that all of the Cretaceous shale sources underlying and bordering the EVA, with the exception of the Odonah Member, would likely have provided pyrite as parent materials for the EVA and other nearby sources.

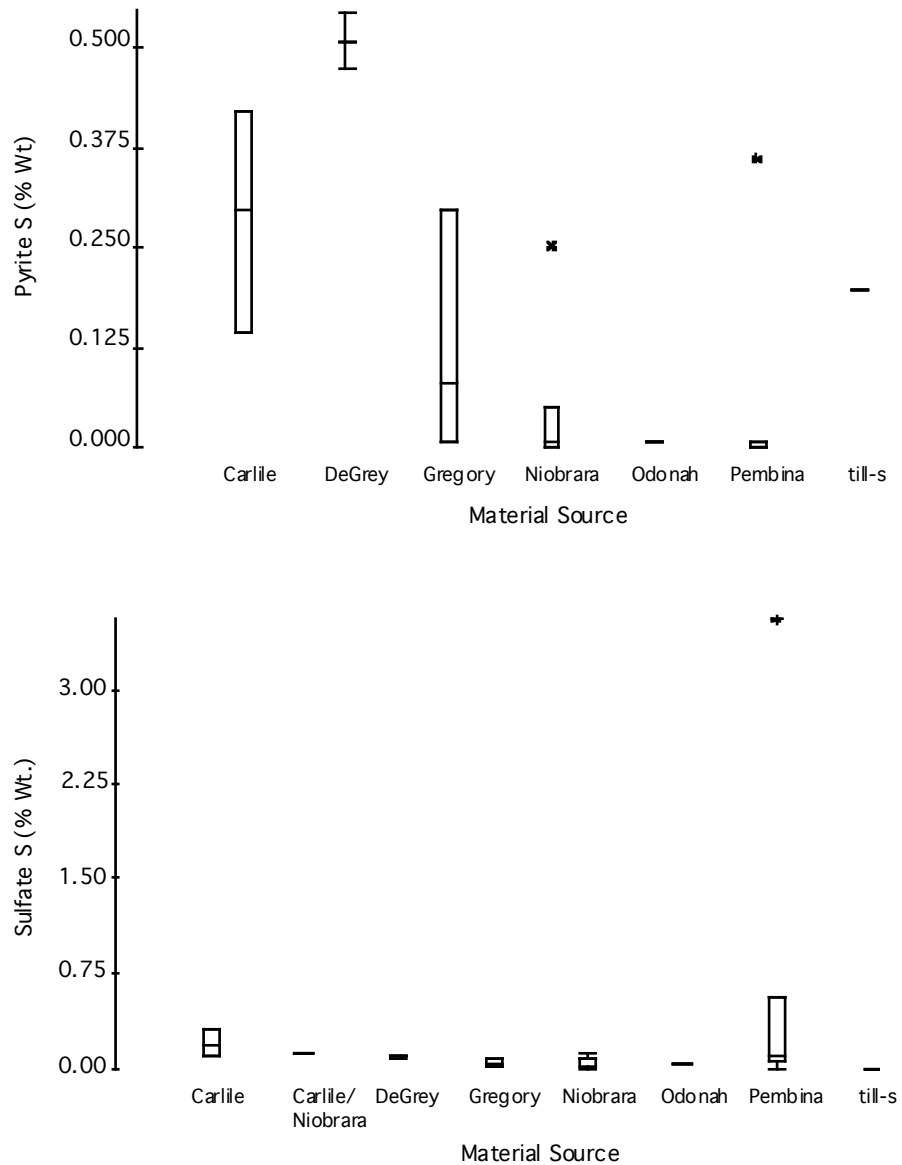


Figure 9. Pyrite- and sulfate-S composition of Cretaceous shale bedrock samples.

3.2 Precipitation (P)

Common sources of sulfate in precipitation are oceanic sea spray, dusts entrained by wind, and residues from combustion of fossil fuels. Sulfate concentrations in precipitation have been measured by the U.S. Geological Survey at Icelandic State Park since 1982 (Harkness et al. 1986, 1990, 1995, 1999). Data for four selected dates are on

Table 1. Annual median values ranged from 0.68 to 0.89 mg-L⁻¹, and individual values varied from 0.03 to 5 mg-L⁻¹. Sulfate-to-chloride ratios (gravimetric) were usually about 10:1 (3.7:1 molar), compared with a ratio of 0.13:1 (0.048:1 molar) for seawater, which indicates that a large proportion of the sulfate is from fossil fuels and dust. Highest values for each year were in October and the April-May period, which indicate that the predominant source is likely wind-eroded dust entrained during months with high winds and bare soil surface. Periods of highest fossil fuel use in North Dakota would be in the winter and summer months. The current source distribution has likely varied over time, with lower fossil fuel and dust contributions prior to settlement of the area *approx.* 100 years ago. Climatic periods characterized by extended drought, like the Hypsithermal Interval (*circa* 8 to 4.5 ka B.P.) (Bluemle 1991) may have accelerated dust contributions for longer periods of the year. However, less precipitation in those times would partially offset higher concentrations in rainfall (although direct additions from wind erosion could have occurred).

Table 1. Mean, minimum, and maximum Sulfate concentration in precipitation at Icelandic State Park, Pembina County, ND.

Year	Median mg-L ⁻¹	Minimum mg-L ⁻¹	Maximum mg-L ⁻¹
1986	0.86	0.3	4.96
1990	0.89	0.03	5
1995	0.85	0.04	4.18
1999	0.68	0.12	3.6

In a single modern average EVA water-cycle (*approx.* 117 y, see Section 1.3), a mean precipitation of 45 cm-y⁻¹ having a mean sulfate concentration of 0.9 mg-L⁻¹ for 518 km² of aquifer would have added about 2.1 x 10⁵ kg of sulfate to the vadose-aquifer system. Sulfate concentrations for six water samples at discharge points in the southern EVA range from 210 to 1,400 mg-L⁻¹, with a logarithmic mean of 473 mg-L⁻¹ and 95% confidence interval of 213 to 1,054 mg-L⁻¹ (see Section 1.3.2). Using the minimum value (210 mg-L⁻¹) for an estimated minimum annual discharge to streams of 1.05 x 10⁷

$\text{m}^3\text{-y}^{-1}$, total sulfate discharged to streams would be estimated at 2.2×10^6 kg, about 10x the estimated addition through precipitation. Precipitation does not appear to have provided the major source for gross sulfate accumulation in the aquifer. Conversely, the aquifer appears to be cleansing itself of sulfate at a net rate of at least 2×10^6 kg-y^{-1} (after subtracting precipitation influx).

In addition, however, sulfate is required for amino-acid formation in plant tissue and is cycled within plant biomass. Precipitation amounts and the mean (0.9 mg-L^{-1}) concentration used above would deliver only $4.05 \text{ kg-ha}^{-1}\text{-y}^{-1}$ ($4.5 \text{ lb.-acre}^{-1}\text{-y}^{-1}$) of sulfate. This amount would be far below most plant community requirements, and would be predominantly removed in crops (in modern times) or cycled within the organic mat prior to cropping. Direct sulfate additions to the EVA through precipitation would thus be expected to be almost negligible.

3.3 Pembina Escarpment (PE)

One of the sources of recharge water for the Elk Valley aquifer is the Pembina Escarpment (PE). In the southwest EVA, between the south branch of the Turtle River and the Goose River, there are seven major drainageways with associated tributaries draining from the PE to the western border of the aquifer (Fig. 10). Much of this water is now carried southward to the Little Goose River in County Drain #14, and north to the Turtle River. A substantial portion of it, however, enters the aquifer and overflows seasonally in surface seeps (See Section 1.3.1). Before construction of the drain, however, most PE water was retained in or over the aquifer for longer periods. Drainage from the PE is an important historical recharge source. Equipotential lines (Fig. 4) indicate that water tables are high near the PE in the south EVA, resulting in evapotranspiration (ET) discharge and a closed-depression recharge-discharge regime (Sections 1.3 and 1.4).

The PE bedrock consists of the Pembina Member of the Pierre Formation, and possibly some of the Gregory and DeGrey Members. These are overlain by a till mantle varying from about 3 to 12 m in thickness. The PE defines the local western limit of the gorge eroded from the Pierre shale (Fig. 3) by Pliocene fluvial events and Pleistocene glaciation. The Pembina Member of the Pierre shale has been shown to be generally high in pyrite (see Section 1.2). Gregory and DeGrey Members as well as the Carlile Formation have also been shown (Section 3.1) to be pyrite-bearing materials. Kelly and Paulson (1970) reported that depths of 12 well screens in the Pierre shale in three townships of the PE west of the study area (150N-56W, 151N-056W, 152N-056W) varied from 4 to 31 m, but more than half were less than 7 m deep. Hansen and Kume (1970) reported that drainage cuts in the PE varied from a maximum of about 30 m for

valleys of the Turtle and Goose Rivers, while lesser drainageways have cut 5 to 16 m. Drainageways that flow into the aquifer in the study area are cut in the range of 5 to 15 m. Basal waters feeding the drainageways are thus draining directly from the Pierre shale and overlying till materials that were likely derived from the Pierre shale, with some possible admixture of Niobrara or Carlile shale.

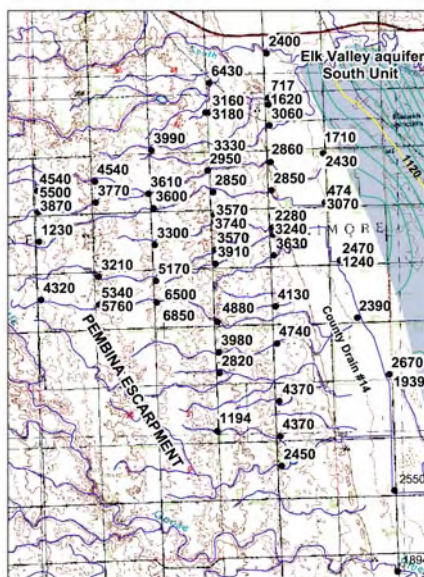


Figure 10. Field specific conductance (EC in $\mu\text{S}\cdot\text{cm}^{-1}$) of water samples from drainageways on the Pembina Escarpment discharging onto the south EVA. Samples were collected on May 9 and June 27, 2001. Where two values are presented for one location, the lowest value was measured on May 9.

Kelly and Paulson (1970) stated that the water chemistry of the Pierre shale in Grand Forks County is highly variable. The TDS is usually greater than $2,000 \text{ mg}\cdot\text{L}^{-1}$ and the principle ions are usually sodium, calcium, and sulfate. This TDS would correspond in North Dakota waters to an approximate EC between 3,000 and 3,500 ($\mu\text{S}\cdot\text{cm}^{-1}$). A summary of published (Kelly and Paulson 1970) EC values for six Pierre shale wells in the PE near the study area is on Table 2. Values of EC range from about 2,855 to $6,800 \mu\text{S}\cdot\text{cm}^{-1}$, $\bar{x} = 4,307 \mu\text{S}\cdot\text{cm}^{-1}$, median = $4,005 \mu\text{S}\cdot\text{cm}^{-1}$, SE = $540 \mu\text{S}\cdot\text{cm}^{-1}$.

To evaluate the potential sulfate sources from PE drainage waters, we measured field EC in surface water at 47 locations in drainageways of the PE. EC was also measured at two locations (one previously measured) on the Turtle River at the North boundary of the south aquifer unit, and at one location in the Little Goose River, which

drains along the southwestern boundary of the aquifer (Fig. 10). Measurements were made so as to track EC values from the source areas in the upper tributaries beginning at the divide in the upper PE, and progressively to the lower main drainage trunks leading to the Turtle River, and through County Drain #14 to the Little Goose River. The measurements were made on June 27, 2001, and were preceded by predominantly dry conditions. Drainageways in the upper PE at the sampling time were mostly static pools representing water-table exposures from the Pierre shale and overlying till. Farther east on the PE some drainageways were flowing slightly. The main drainageways to the Little Goose and Turtle Rivers were also flowing slightly.

Table 2. Specific conductance of water samples from wells screened in the Pierre shale on the Pembina Escarpment near the study area, reported by Kelly (1970).

Location	EC ($\mu\text{S}\cdot\text{cm}^{-1}$)
15005629DCC	2,855
15105612DAD	6,706
15205602BAA	3,810
15205612CCC	4,200
15205630BBB	3,600
15205632ADA	4,676

Variability of EC in the drainageways is high but systematic, with values decreasing downstream, indicating dilution with runoff waters (Fig. 10). The main drainageways on the eastern border of the PE were similar in EC to the rivers into which they flowed ($2,400 \mu\text{S}\cdot\text{cm}^{-1}$ for the Turtle River and $1,894 \mu\text{S}\cdot\text{cm}^{-1}$ for the Little Goose River). EC for the spring samples was from 27% to 60% lower than summer samples. One measurement taken in November of 2001 was only 15% of that taken in summer.

Sulfate versus EC was calibrated for five samples taken June 27 and four samples taken earlier, on May 8, when there was active runoff from spring rains and possibly some residual snowmelt. The summer data yielded a consistent transfer function (Fig. 11) ($r>0.99$), although May data departed somewhat at higher EC values because of increased bicarbonate from runoff. The derived linear transfer function compares well with water samples taken from both oxidized and unoxidized tills on sites elsewhere in eastern ND, and Pierre shale water samples near the EVA (SWC database).

It also agrees with two water samples taken from other bedrock formations described as "Carlile or Niobrara" elsewhere, in southeastern ND (NDSWC database). It differs widely, however, from local samples taken in the deep till and Niobrara and Carlile shale underlying the EVA.

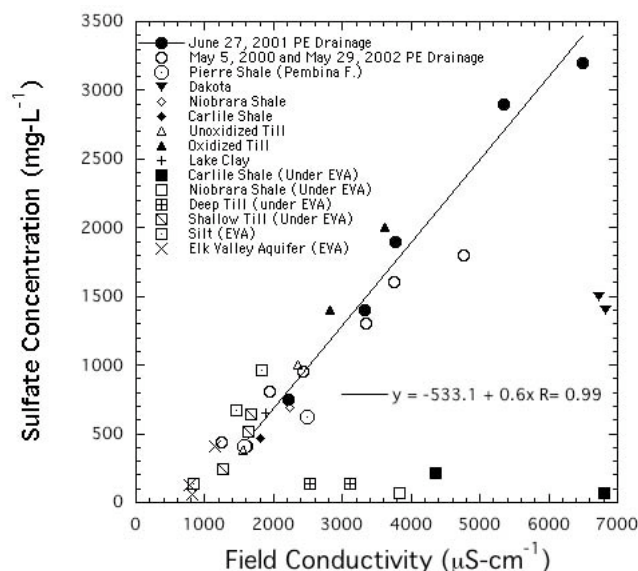


Figure 11. Sulfate vs. EC for surface water from the Pembina Escarpment, from local related EVA, silt, till and bedrock sources (identified as EVA), and other till and bedrock sources in eastern ND.

These data indicate that the sulfate vs. EC relationship is consistent and appears to be widely applicable in shale and till samples in eastern ND. The range of EC values (between 3,000 and 7,000) in the upper (and least diluted) PE drainageways was very close to the measurements in area Pierre wells reported on Table 2, further confirming that drainage waters were consistent with porewater from the Pierre shale and from derived till materials. High EC values and the presence of Natriboroll soils adjacent to drainageways in the upper PE (Fig. 7) indicate that evaporative cycling of sulfate with precipitation and remobilization of evaporite minerals is occurring in the upper basin before entering the drainageways.

The sulfate vs. EC transfer function (Fig. 11) was applied to all measured EC from the PE. Results indicate that estimated sulfate concentrations were as high as 2,789 mg-L⁻¹ in the upper Escarpment. The mean sulfate concentration estimated from 13 EC samples in the upper Escarpment is 2,244 mg-L⁻¹ (median = 2,076 mg-L⁻¹, SE = 199 mg-L⁻¹). However, most sulfate concentrations in waters reaching the border of the aquifer

are about 1,000 mg-L⁻¹ in summer, and about half that in May when diluted with runoff water. It is likely that the dilution may be even greater during the earlier spring periods with heaviest snowmelt.

In summary, one current source of sulfate reaching the western EVA from the PE is the Pierre shale and till derived from it. Some sulfate has also been cycled through evaporite minerals as a secondary process occurring along drainageways. Concentrations downstream are diluted with freshwater from runoff so that modern sulfate concentrations reaching the EVA are usually < 1,000 mg-L⁻¹ during periods of major runoff. This does not prove, however, that concentrations were never higher.

3.4 Lower Boundary Source Materials

Underlying silt (*approx.* 0 to 30 m thick), till (50 to 80 m thick) and Cretaceous shales of the Niobrara and Carlile Formations are possible sulfate sources for the EVA. Possible processes contributing to upflux of sulfate would be upward extrusion of sulfatic bedrock porewater under the weight of glacial ice (Cherry, 1972), advective upflux of sulfatic porewater from bedrock and till into the aquifer, and upward diffusion of sulfate ions. Three nests of wells (Transect B-B', Fig. 8, Sites 7, 8, 9) were placed in the bedrock shale, deep till (except well-site 15105523BBB), shallow till, silt, and the lower EVA in October of 2001, and were sampled in January of 2002. Results indicate that porewater in bedrock and the deep till were chloridic, and contained relatively low sulfate concentrations (Fig. 12).

The sulfate vs. EC relationship on Fig. 11 has indicated that the Carlile and Niobrara shales underlying the aquifer differ from the EVA. Plots of ratios of major cations and anions to chloride in each material layer, versus seawater chloride ratios from Hem (1959, p. 10) indicate that porewater in the shale and the deep till are connate (Fig. 13e,f), with chemical constituents proportionally similar to dilute seawater having a freshwater proportion of 85%. The shales, which were formed by deposition in a shallow marine environment (Hansen and Kume 1970), are proportionally identical in calcium, potassium, and sodium, with elevated bicarbonate and lower magnesium. The sulfate ratio is slightly less than seawater proportion on two sites. This is consistent with reducing conditions common to high organic-matter shallow-marine depositional environments (Schultz et al. 1980, Garrels and Perry 1974, Ohmoto 1993, Claypool et al. 1980, Holser and Kaplan 1966).

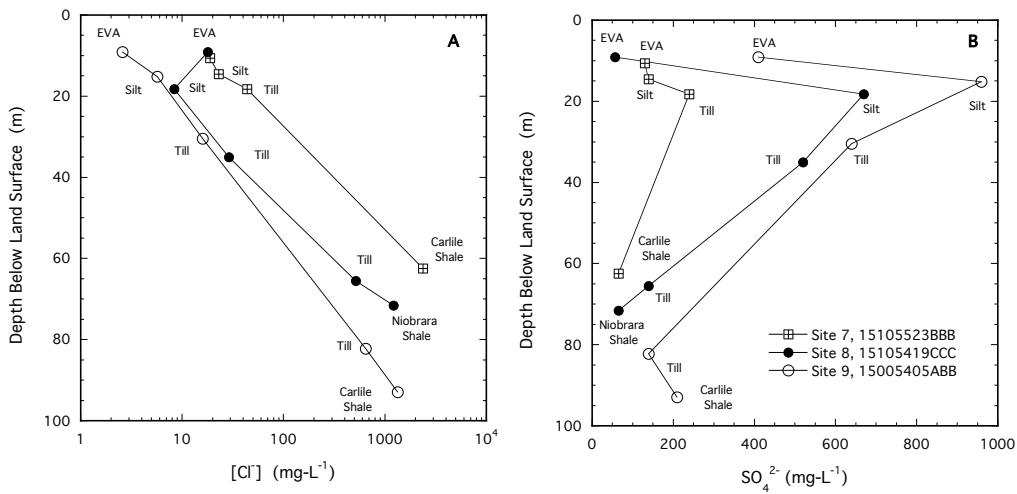


Figure 12. Porewater concentrations of (A) chloride and (B) sulfate for deep EVA, silt, till and shale layers on the B-B' Transect sites 7, 8 and 9.

The deep till bordering the shale is similar to the shale, but with evidence of some minor oxidation and weathering. Slightly elevated sulfate indicates oxidation of sulfide, while increased calcium, magnesium, sodium, and bicarbonate, are consistent with acid weathering of carbonate minerals, and calcium-induced exchange for sodium on clays. All other materials layers comprising the immediate lower boundary of the aquifer, the silt and shallow till, exhibit proportionalities that are dominated by the products of sulfide oxidation, carbonate weathering, and cation exchange.

The separation of the two porewater groups with respect to sulfate is best illustrated on Fig. 13a, which speciates deep waters dominated by connate characteristics from surficial waters with oxidized and weathered characteristics. It seems clear from both concentrations of sulfate (Fig. 12), and characteristics of other chemical constituents (Fig. 13b-d) that porewater from local bedrock and deep unoxidized till cannot be the source of sulfate in the lower aquifer through extrusion, advection, or diffusion. On sites with high sulfate, highest concentrations are in the silt layers with second highest in the shallow underlying till (Fig. 12). On the exceptional site (Site 7, 15105523BBB) sulfate concentrations are highest in the shallow till, and second highest in the silt, but the overall concentrations are relatively low and the silt layer is thin. The silt layer must, therefore, be a modern source for sulfate in the lower EVA.

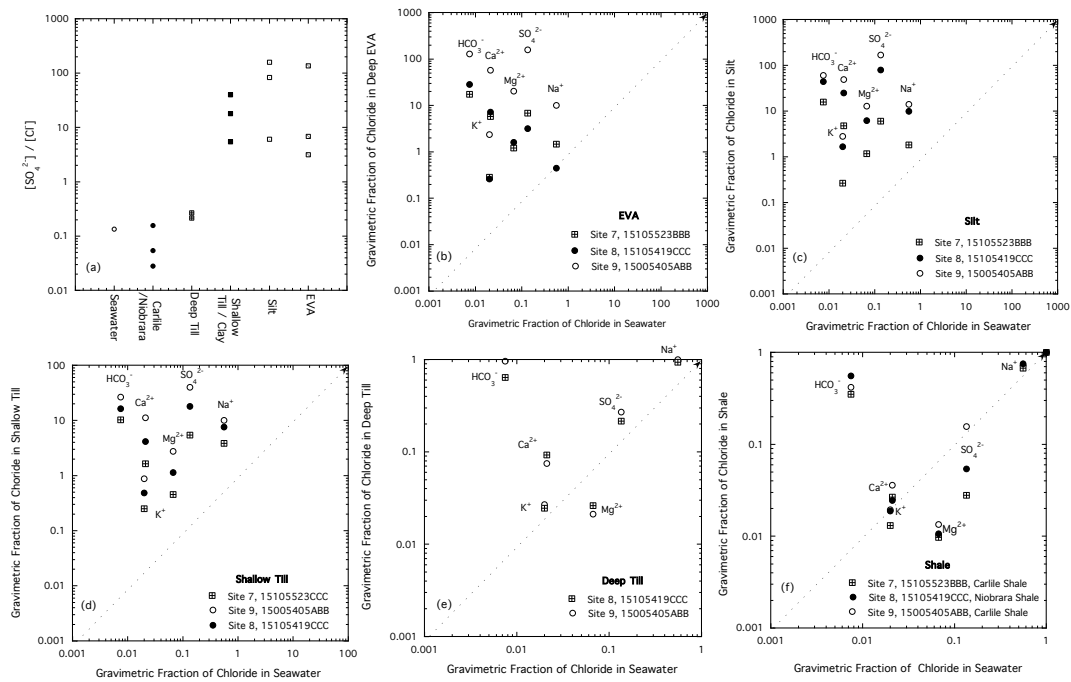


Figure 13. (a) Sulfate to chloride ratios for porewater at all sampled depths, and (b-f) ratios of porewater ion concentrations to seawater chloride-ion concentrations in each strata.

3.5 Authigenic Sulfate

Pyrite-S profiles for Sites 1-6 (Fig. 14) indicate that substantial sulfide is present in the EVA. Generally, sulfide is most depleted in the vadose zone and shallow aquifer, more plentiful in the mid aquifer, somewhat depleted in the lower aquifer, and largest in the underlying silt. Mineral sources for authigenic sulfate by aerated oxidation (Eq. 1) or through autotrophic denitrification (Eq. 2) are thus present. Non-pyrite S is less than pyrite-S in all cases except for the silt layer on Site 5, where the two fractions are similar (Fig. 15).

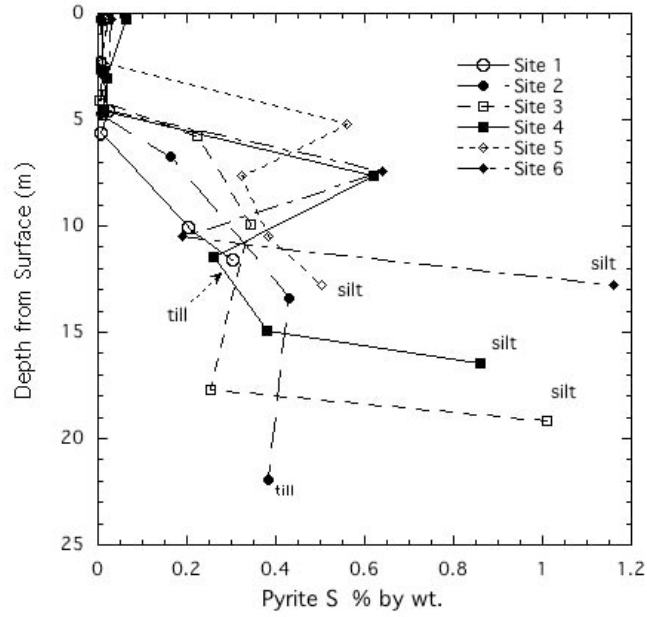


Figure 14. Pyrite-S % with depth and strata on Transect A-A', Sites 1-6.

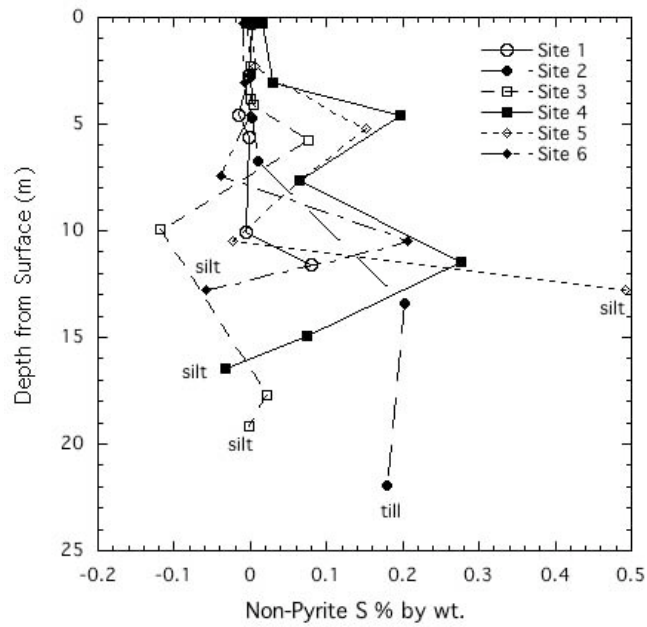


Figure 15. Non-pyrite-S % with depth and strata on Transect A-A', Sites 1-6.

3.6 Fertilizer Sulfate

Little sulfur is applied as fertilizer on the EVA. Ammonium-sulfate (21-0-0-24.2) has been used in some instances, mainly as a nitrogen source when economically feasible. But a recent query of one of the largest producers of irrigated potatoes has indicated that the main nitrate sources are urea and 28% (ammonium-nitrate) solution (Dr. Duane Preston, written communication, 8-5-03). Although some sulfur fertilizer is applied, the main fertilizer effect on sulfur in the aquifer, however, would likely be indirect, through autotrophic denitrification of nitrate fertilizer using pyrite sulfur as an electron donor (Korom et al. 2005).

3.7 Organic Sulfate

Organic matter in soil overlying the EVA is constantly decomposing and being reconstituted. The sulfur composition of organic matter, expressed as carbon to nitrogen to sulfur ratios (C:N:S), as determined in Minnesota mollisols (and elsewhere) is in the general range of 100:10:1.3-1.5 (Tisdale and Nelson 1966, p289-290). While most nutrients were likely cycled within the soil and plant layer over most of the history of the EVA, a large mineralizing event occurred with the introduction of agriculture and the breaking of the prairie sod about 100 years ago. Harker et al. (1997, p47) have cited sources which estimate that as much as 20 % of all of the N in the organic pool was leached beneath the root zone during and following the first turning of the sod.

We are unaware of published data and analyses on early C, N, and S cycling in North Dakota. However, data for well-drained and poorly-drained prairie soils in neighboring Minnesota (published in Buckman and Brady, 1969, p152) indicate that average organic carbon (OC) percent for the 81-cm solum was about 2.4 and 3% respectively. Using an estimated bulk density of 1.3 g-cm³ for a sandy mollisol we calculate about 1.05×10^7 kg-ha⁻¹ of soil, which would contain about 252,720 to 315,000 kg-ha⁻¹ of OC. Using the C:N:S ratio above yields 25,270 to 31,500 kg-ha⁻¹ total N, and 3,285 to 4,095 kg-ha⁻¹ total S. If leaching losses of S and N are proportional, a reasonable assumption for two highly water-soluble anions, S leached to ground-water would have been approximately 657 to 729 kg-ha⁻¹ (1,971 to 2,187 kg-ha⁻¹ as sulfate). Post-cultivation mineralization decreased exponentially over about 50 years, approximately stabilizing thereafter. Over this time period estimated mean sulfur leaching to ground-water would thus have been about 13 to 15 kg-ha⁻¹-y⁻¹ (39 to 44 kg-ha⁻¹-y⁻¹ as sulfate). Most of this, however, would have been lost early in the post-cultivation time period.

Buckman and Brady (1969, p. 441) have estimated that modern rates of organic carbon mineralization probably do not exceed 2-3% of the carbon pool per year. The

mean organic carbon (OC) percent in the top 20-cm acre-furrow slice on six sites (two replicates per site) sampled on two toposequences (crest, mid-slope and swale) on tilled sandy soils near Oakes, ND was 1.4% (Schuh et al. 1991). The weighted (depth) mean bulk density was 1.47 g-cm^3 . Applying these means and the above cited C:N:S ratio to an acre-furrow slice of 20 cm we estimate the soil mass at $2.94 \times 10^6 \text{ kg-ha}^{-1}$, $41,160 \text{ kg-ha}^{-1}$ OC, $4,116 \text{ kg-ha}^{-1}$ N, and 576 kg-ha^{-1} S. Buckman and Brady's approximate 'maximum' organic carbon decomposition rates result in an estimated maximum modern S mineralization rate of 11 to $17 \text{ kg-ha}^{-1}\text{-y}^{-1}$ (33 to $51 \text{ kg-ha}^{-1}\text{-y}^{-1}$ of sulfate). For comparison, on a field in western Minnesota with low fertility and surface biomass (silage) harvested, a recent 13-y mean organic carbon loss of $0.029\%\text{-y}^{-1}$ was measured (Bloom et al. 1982). This constituted $1.1\%\text{-y}^{-1}$ of the measured 2.63% OC pool. The resulting estimated annual S mineralization is $6 \text{ kg-ha}^{-1}\text{-y}^{-1}$ ($18 \text{ kg-ha}^{-1}\text{-y}^{-1}$ as sulfate).

Sulfate mineralization estimates for the early post-cultivation period likely approximate actual loss (leaching) rates. Almost all of this would have reached groundwater. The 18 to $51 \text{ kg-ha}^{-1}\text{-y}^{-1}$ sulfate mineralization rate estimated for the modern period is within the range of crop requirements and would be reassimilated within the crop and soil biomass, and even removed from the system with crop biomass. If all of the annual mineralized sulfate were leached to ground water in 8 cm of recharge, the sulfate concentration in recharge water resulting from organic matter mineralization would be in the range of 2 to 6 mg-L^{-1} . This is similar to the range of modern concentrations (0.03 to 5 mg-L^{-1}) for rainfall. It is unlikely, however, that a large proportion of the mineralized sulfur fraction is currently reaching ground water. Sulfate concentrations of recharge waters resulting from such mineralization rates would thus constitute a minor contribution to the overall sulfur pool in the aquifer.

4. SUMMARY OF MINERAL SULFUR AND OXYGEN ISOTOPES ($\delta^{34}\text{S}$ AND $\delta^{18}\text{O}$) DATA FOR POTENTIAL EVA SOURCE MATERIALS

Sulfur ($\delta^{34}\text{S}$) isotopes were determined for grain matrix samples from a broad range of potential bedrock source materials (Table 4); for incremental depths from topsoil through the EVA and underlying silt and till on Transect A-A' (Table 5); and from the deep EVA, silt, shallow-, mid- and deep-level till aquitard and underlying shale on Transect B-B' (Table 6). It was also determined for porewater from the EVA on A-A' and B-B' Transects, from bedrock (Pierre Fm. and Dakota Fm.) wells near the EVA, from bedrock (Carlile Fm. and Niobrara Fm.) wells in southeastern ND, from deep till wells in east-central ND; from snow samples on the EVA, and from ammonium-sulfate fertilizer samples collected from local suppliers (Table 7). In addition, $\delta^{18}\text{O}$ were determined for Transect A-A'. Statistical distributions are described on Figure 16 and on Table 3. Bonferroni comparisons for all paired comparisons having $P < 0.2$ are on Table 8. *For statistical summary and comparison mineral sulfate determinations by barium precipitation (Tables 4, 5 and 7) and mineral non-pyrite S (Table 8) determined by the difference between total and pyrite S are combined.*

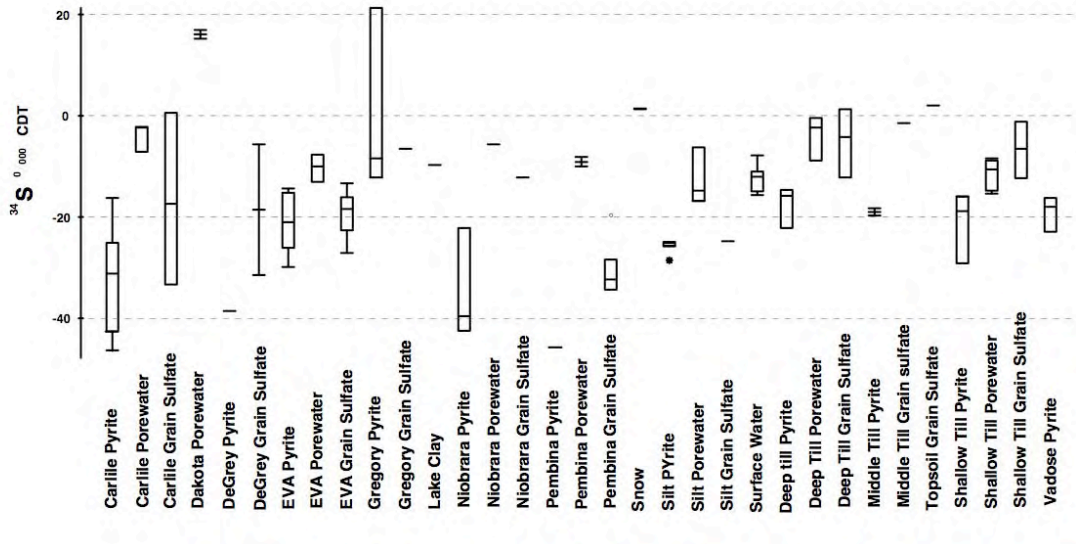


Figure 16. Box plots for $\delta^{34}\text{S}$ distribution for grain-matrix pyrite, grain-matrix sulfate, and porewater sulfate from varying sources in eastern North Dakota.

Table 3. Statistical parameters for $\delta^{34}S$ in all source materials. Single samples are identified as non parametric by dashes for SD and SE.

Source	N	\bar{X}	Median	SD	Min.	Max.	Range	SE
Carlile pyrite	5	-32.1600	-31.1000	12.3723	-46.2000	-16.1000	30.1000	5.53305
Carlile porewater	3	-3.76667	-2.20000	2.80060	-7	-2.10000	4.90000	1.61692
Carlile grain sulfate	4	-16.7500	-17.2500	13.8834	-33.2000	0.700000	33.9000	6.94172
Dakota porewater	2	16.2000	16.2000	1.27279	15.3000	17.1000	1.80000	0.900000
DeGrey pyrite	1	-38.5000	-38.5000	•	-38.5000	-38.5000	0	•
Degrey grain pyrite	2	-18.5000	-18.5000	18.2434	-31.4000	-5.60000	25.8000	12.9000
EVA pyrite	1	-20.5273	-20.9000	5.93483	-29.8000	-14.3000	15.5000	1.78942
EVA porewater	3	-10.1667	-10	2.65393	-12.9000	-7.60000	5.30000	1.53225
EVA grain sulfate	7	-18.9829	-18.3000	4.60522	-27	-13.3000	13.7000	1.74061
Gregory pyrite	3	0.333333	-8.30000	18.3429	-12.1000	21.4000	33.5000	10.5903
Gregory grain sulfate	1	-6.40000	-6.40000	•	-6.40000	-6.40000	0	•
Lake Clay porewater	1	-9.60000	-9.60000	•	-9.60000	-9.60000	0	•
Niobrara pyrite	4	-35.9000	-39.4500	9.32988	-42.6000	-22.1000	20.5000	4.66494
Niobrara porewater	1	-5.60000	-5.60000	•	-5.60000	-5.60000	0	•
Niobrara grain sulfate	1	-12.1000	-12.1000	•	-12.1000	-12.1000	0	•
Pembina pyrite	1	-47	-47	•	-47	-47	0	•
Pembina porewater	2	-9	-9	1.27279	-9.90000	-8.10000	1.80000	0.900000
Pembina grain sulfate	6	-30.1833	-32.3000	5.66548	-34.3000	-19.5000	14.8000	2.31292
SNOW sulfate	3	1.46667	1.50000	0.057735	1.40000	1.50000	0.100000	0.033333
Silt pyrite	7	-25.8429	-25.6000	1.22591	-28.5000	-24.8000	3.70000	0.463351
Silt porewater	3	-12.5333	-14.7000	5.57524	-16.7000	-6.20000	10.5000	3.21887
Silt grain sulfate	1	-24.7000	-24.7000	•	-24.7000	-24.7000	0	•
Surface Water*	9	-12.4667	-12	2.70601	-15.6000	-7.80000	7.80000	0.902004
Deep till pyrite	3	-17.4333	-15.7000	4.08575	-22.1000	-14.5000	7.60000	2.35891
Deep till porewater	3	-3.73333	-2.20000	4.40492	-8.70000	-0.300000	8.40000	2.54318
Deep till grain sulfate	3	-4.96667	-4.20000	6.78258	-12.1000	1.40000	13.5000	3.91592
Middle till pyrite	2	-18.9500	-18.9500	1.06066	-19.7000	-18.2000	1.50000	0.750000
Middle till grain sulfate	1	-1.40000	-1.40000	•	-1.40000	-1.40000	0	•
TOPSOIL grain sulfate	1	2.10000	2.10000	•	2.10000	2.10000	0	•
Shallow Till pyrite	4	-20.5750	-18.7000	5.85228	-29	-15.9000	13.1000	2.92614
Shallow Till porewater	6	-11.3667	-10.5000	3.04478	-15.3000	-8.40000	6.90000	1.24302
Shallow Till grain sulfate	4	-6.55000	-6.40000	5.07904	-12.3000	-1.10000	11.2000	2.53952
Vadose pyrite	3	-18.9667	-17.9000	3.42685	-22.8000	-16.2000	6.60000	1.97850

Table 4. $\delta^{34}\text{S}$ for pyrite- and sulfate-S in grain matrix samples collected from deep bedrock samples.

Lab code	Sample ID	Site Name	USBLM location	Formation	Member	Wt used for pyrite extraction (g) *	Wt % pyrite-depth S	pyrite $\delta^{34}\text{S}$ †/ † _{oo,CDT}	Wt. used for SO_4^{2-} extraction (g)	Wt.% SO_4^{2-} -S	SO_4^{2-} $\delta^{34}\text{S}$ †/ † _{oo,CDT}	Sample Date	Description
32	070119	Pembina Gorge	16305813AAD	Carlisle	-	-	0.144	-42.4	13.62	0.288	-33.2	7/19/01	gray, fresh, blocky shale, depth 0.6m, 3m above water Pembina River water line
33	070120	Pembina Gorge	16305813AAD	Carlisle/Niobrara	-	-	saturated	-31.1	13.59	0.113	-18.4	7/19/01	gray, more laminar than sample 20, possible Niobrara
15	070101	Preston Church	13605719DDDBB	Niobrara	-	-	0.000	-38.9	15.15	0.067		7/9/01	unweathered, gray, highly lithified, naturally exposed
16	070103	Preston Church	13605719DDDBB	Niobrara	-	-	0.050		24.28	0.010		7/9/01	weathered, yellow and orange, highly lithified
18	070105	Preston Church	13605719DDDBB	Niobrara	-	-	0.008		15.19	0.000		7/9/01	weathered sample, just below till contact
34	070121	Pembina Gorge	16305813AAD	Niobrara	-	13.57	0.251	-40	13.85	0.119	-37.8	7/19/01	same as site 1, lithified, laminar, gray, no volcanic ash, unweathered
19	070106	Pembina Gorge	13705731CC	Pierre	Pembina	-	0.006		20.26	0.132	-19.5	7/9/01	dark gray, non lithified, iron concretions, > 40% clay, massive structure
26	070113	Pembina Gorge	16305813AAD	Pierre	Pembina	-	0.005		12.54	0.007	-28.4	7/19/01	top volcanic ash layer, unweathered
27	070114	Pembina Gorge	16305813AAD	Pierre	Pembina	-	0.000		12.21	0.052	-32.7	7/19/01	upper sedimentary layer, unweathered
28	070115	Pembina Gorge	16305813AAD	Pierre	Pembina	-	0.000		13.58	0.096	-31.9	7/19/01	second volcanic ash layer, unweathered
29	070116	Pembina Gorge	16305813AAD	Pierre	Pembina	-	0.000		12.38	0.048	-34.3	7/19/01	lower sedimentary layer, unweathered
30	070117	Pembina Gorge	16305813AAD	Pierre	Pembina	-	0.000		1.13	3.552	-34.3	7/19/01	gypsum evaporite/ in pressure faces
31	070118	Pembina Gorge	16305813AAD	Pierre	Pembina	-	0.361	-47	14.47	0.556		7/19/01	iron and gypsum interlayer- above and below bentonite layer
20	070107	Little Yellowstone Park	13705836CC	Pierre	Gregory	-	0.007		22.91	0.056		7/9/01	gray, red and brown striations on pressure faces, salt on faces (likely gypsum) somewhat weathered
21	070108	Ft. Ransom	13705731CC	Pierre	Gregory	-	0.296	-12.1	21.90	0.035	-6.4	7/9/01	< weathered than #7, @ 0.2 m below surface, laminar, horizontal primary fractures, blocky structure, w/ pressure faces, gray, brown, and red, @ 30% clay
24	070111	Cooperstown	14505816ACC	Pierre	Gregory	-	0.037	-8.3	18.16	0.010		7/9/01	gray, yellow, brown and red in bedding planes, laminar bedding planes, no secondary structure, from active cut bank of Sheyenne R.
25	070112	Cooperstown	14505816ACC	Pierre	Gregory	-	0.126	21.4	12.21	0.018		7/9/01	same as 11#f, slightly deeper in bank (0.2 m) - from active cut bank of Sheyenne River
22	070109	Cooperstown	14505816ACC	Pierre	DeGrey	-	0.544	-38.5	17.45	0.081	-31.4	7/9/01	gray, fine flakey, popcorn weathering, @25-30% clay / residual nob from former channel of Sheyenne R.
23	070110	Cooperstown	14505816ACC	Pierre	DeGrey	-	0.475		15.80	0.062	-5.6	7/9/01	same as 9#f, slightly deeper (0.2 to 0.3 m)
35	070122	Pembina Gorge	16305813AAD	Pierre	Odameh	12.94	0.007		12.90	0.032		7/19/01	highly lithified, poss. silicious, unweathered.
17	070104	Ft. Ransom	13605719DDDBB	Till	-	-	0.199	-42.6	15.97	0.000		7/9/01	till, some mn and iron, gray, just above Niobrara contact

Table 5. $\delta^{34}\text{S}$ for pyrite- and sulfate-S in grain-matrix samples collected from the soil, vadose, upper-EVA, mid-EVA, deep-EVA, silt, and till-aquitard layers on Transect A-A'.

lab code ND-	Site Name	Site #	USBLM Location	Formation	Sample Depth	Wt % total S	Wt % pyrite S	pyrite- $\delta^{34}\text{S}$ ‰ CDT	SO ₄ ²⁻ - $\delta^{34}\text{S}$ ‰ CDT
1-1	Larimore	1	15105533BBB	topsoil	0.00-0.305	0.011	0.009	nd	2.1
1-2	Larimore	1	15105533BBB	vadose	1.52-2.74	0.008	0.009	-17.9	nd
1-3B	Larimore	1	15105533BBB	brown sand	3.05-4.57	0.01	0.025	nd	nd
1-4	Larimore	1	15105533BBB	gray sand	4.88-5.64	0.005	0.006	-26	nd
1-9	Larimore	1	15105533BBB	gray sand	9.30-10.1	0.196	0.202	-14.3	nd
1-10	Larimore	1	15105533BBB	till	10.8-11.6	0.384	0.303		
2-1	Larimore	2	15105511DCD	topsoil	0.00-0.30	0.009	0.006	nd	-1.1
2-2	Larimore	2	15105511DCD	vadose	2.13-2.74	0.01	0.01	nd	nd
2-4	Larimore	2	15105511DCD	brown sand	3.66-4.73	0.009	0.006	nd	nd
2-7	Larimore	2	15105511DCD	gray sand	5.94-6.71	0.175	0.164	-15.3	nd
2-9	Larimore	2	15105511DCD	gray sand	12.7-13.4	0.631	0.429	-25	nd
2-12	Larimore	2	15105511DCD	till	21.2-21.9	0.562	0.382	-19.9	nd
3-1B	Larimore	3	15105523DAA	topsoil	0.00-0.30	0.017	0.023	nd	nd
3-2	Larimore	3	15105523DAA	vadose	1.52-2.29	0.008	0.008	-16.2	nd
3-3	Larimore	3	15105523DAA	brown sand	3.05-3.81	0.009	0.009	nd	-16.1
3-4	Larimore	3	15105523DAA	brown sand	3.81-4.12	0.009	0.004	nd	-15.9
3-6	Larimore	3	15105523DAA	gray sand	5.03-5.79	0.302	0.225	nd	-22.5
3-7	Larimore	3	15105523DAA	gray sand	9.15-9.91	0.226	0.345	-20.9	nd
3-14	Larimore	3	15105523DAA	gray sand	16.9-17.7	0.276	0.255	-15.2	nd
3-16	Larimore	3	15105523DAA	silt	18.4-19.2	1.009	1.01	-25.7	nd
4-1	Larimore	4	15005405BBA	topsoil	0.00-0.30	0.077	0.062	nd	nd
4-3	Larimore	4	15005405BBA	vadose	2.29-3.05	0.051	0.021	nd	nd
4-4	Larimore	4	15005405BBA	brown sand	3.05-4.57	0.21	0.013	nd	-18.3
4-6	Larimore	4	15005405BBA	gray sand	6.86-7.62	0.684	0.62	-29.8	nd
4-7	Larimore	4	15005405BBA	gray sand	10.7-11.4	0.537	0.26	nd	-19.7
4-10	Larimore	4	15005405BBA	gray sand	14.2-14.9	0.455	0.38	-21.2	nd
4-12	Larimore	4	15005405BBA	silt	15.7-16.5	0.828	0.86	-28.5	nd
5-1	Larimore	5	15005416CBC	topsoil	0.00-0.30	0.017	0.016	nd	nd
5-2	Larimore	5	15005416CBC	vadose	1.52-2.29	0.017	0.01	-22.8	nd
5-5	Larimore	5	15005416CBC	brown sand	4.42-5.18	0.714	0.561	-28.2	-27
5-7	Larimore	5	15005416CBC	gray sand	6.86-7.62	0.388	0.323	-14.7	-13.3
5-8	Larimore	5	15005416CBC	gray sand	9.76-10.5	0.363	0.385	-15.2	nd
5-11	Larimore	5	15005416CBC	silt	11.9-12.8	0.997	0.505	-25	-24.7
6-1	Larimore	6	15005429AAAD	topsoil	0.00-0.30	0.022	0.031	nd	nd
6-4A	Larimore	6	15005429AAAD	vadose	2.29-3.05	0.013	0.02	nd	nd
6-6	Larimore	6	15005429AAAD	brown sand	3.81-4.57	0.017	0.016	nd	nd
6-7	Larimore	6	15005429AAAD	gray sand	6.71-7.47	0.602	0.64	nd	nd
6-9	Larimore	6	15005429AAAD	gray sand	9.76-10.5	0.398	0.191	nd	nd
6-12	Larimore	6	15005429AAAD	silt	12.0-12.	1.102	1.16	-25.8	nd

Table 6. $\delta^{34}\text{S}$ isotope for pyrite- and sulfate-S in grain matrix samples collected from deep EVA, silt, till, and bedrock layers on Transect B-B'.

Lab Code	Site Name	Site #	USBM Location	Sample ID	Formation	Sample Depth	Wt used for pyrite extraction (g) *	Wt % pyrite-depth S	pyrite $\delta^{34}\text{S}$ ‰/∞ CDT	Wt used for SO_4^{2-} extraction (g)	Wt % SO_4^{2-} -S	SO_4^{2-} $\delta^{34}\text{S}$ ‰/∞ CDT	Description
40	Larimore	7	15115423BBB	100105	Silt		21.82	0.000	-24.8	6.16	0.038		unweathered, dark gray
41	Larimore	7	15115423BBB	100106	Till	18.29-24.39	17.24	0.089	-17.5	5.73	0.021	-3.7	unweathered, dark gray, just below silt
42	Larimore	7	15115423BBB	100107	Till	42.68-48.78	18.67	0.114	-16.7	5.73	0.016	-1.4	unweathered, gray, mid depth in till
43	Larimore	7	15115423BBB	100108	Till	< 57.92	20.74	0.082	-15.7	5.10	0.010	1.4	unweathered, just above Carfile shale
44	Larimore	7	15115423BBB	100109	Carfile	57.92-64.02	16.95	0.422	-2.5	6.43	0.079	-16.1	unweathered, very dark gray, cuttings about 1 inch.
36	Larimore	8	15105419CCC	100101	Silt	13.72-32.01	5.20	1.320	-25.6	12.84	0.015		unweathered, gray silt between aquifer and till
37	Larimore	8	15105419CCC	100102	Shallow	33.54-36.58	14.36	12.300	-15.9	7.81	0.016	-9.1	unweathered gray till, just below silt
39	Larimore	8	15105419CCC	100104	Deep	54.88-62.80	13.75	0	-14.5	7.34	0.019	-1.2	unweathered, dark gray, just above Niobrara shale
38	Larimore	8	15105419CCC	100103	Niobrara	89.32-	11.06	0.000	-22.1	6.96	0.056	-12.1	unweathered, dark gray, less fine and slick than clarfile
45	Larimore	9	15005405ABBB	100110	Till	33.84-33.97	16.75	0.105	-29	6.24	0.038	-12.3	unweathered, gray, sampled just below the silt layer
46	Larimore	9	15005405ABBB	100111	Till	48.78-	22.56	0.154	-18.2	6.67	0.095		unweathered, gray, sampled / between silt and carfile
47	Larimore	9	15005405ABBB	100112	Till	65.55-	19.68	0.091	-14.5	5.35	0.032	-4.2	deep sample, near the carfile
48	Larimore	9	15005405ABBB	100113	Carfile	89.32-97.56	19.07	0.296	-16.1	5.43	0.169	0.7	Carfile shale, very dark, slick, oily feel, very small cuttings

Table 7. $\delta^{34}\text{S}$ and $\delta^{18}\text{O}$ isotope for dissolved sulfate in water samples from Sites 7, 8, and 9 and surface discharge waters (Hazen Brook) of the EVA; from surface water of the Pembina Escarpment and snow samples; from Dakota Group and Pierre shale wells near the EVA; and from supplementary Carlile shale, Niobrara shale, and till wells sampled in southeastern and east central North Dakota.

Lab code	Site Name	USBM Location	Source	Sample Type	Well SI / Water Body	SO_4^{2-}	
						$\delta^{34}\text{S}$ ‰ / ‰ CDT	$\delta^{18}\text{O}$ ‰ / ‰ MSW
Site 7							
1	Larimore	15105523 BBB	EVA	Well	10.67-12.19	-7.6	9.3
2	Larimore	15105523 BBB4	Silt	Well	14.63-16.16	-6.2	8.7
3	Larimore	15105523 BBB3	Shallow Unoxidized Till	Well	18.29-21.34	-11.7	6.5
4	Larimore	15105523 BBB2	Carlile	Well	62.5-65.55	-2.2	1.8
Site 8							
5	Larimore	15105419 CCC	EVA	Well	9.146-10.67	-10	-0.2
6	Larimore	15105419 CCC5	Silt	Well	14.63-16.16	-16.7	0.6
7	Larimore	15105419 CCC4	Shallow Unoxidized Till	Well	35.06-36.58	-14.7	1.1
8	Larimore	15105419 CCC3	Deep Unoxidized till	Well	65.55-67.07	-0.3	11.5
9	Larimore	15105419 CCC2	Niobrara	Well	71.64-73.17	cont	cont
Site 9							
10	Larimore	1500545 ABB5	EVA	Well	9.15-10.67	-12.9	cont
11	Larimore	1500545 ABB4	Silt	Well	15.24-16.77	-14.7	cont
12	Larimore	1500545 ABB3	Shallow Unoxidized Till	Well	30.49-32.01	-15.3	cont
13	Larimore	1500545 ABB2	Deep Unoxidized till	Well	82.31-83.84	-2.2	cont
14	Larimore	1500545 ABB1	Carlile	Well	92.98-96.03	-2.1	cont
27	Larimore	15105509 DDD	EVA discharge	Surface	Hazen Brook	-7.8	4.2
28	Larimore	15105611 CBB	EVA discharge	Surface	Hazen Brook	-15.6	-4.3
.	Larimore	15105523 BBB	snow	Surface			
A	Larimore	15105523 BBB	snow	Surface		1.5	tba
B	Larimore	15105523 BBB	snow	Surface		1.5	tba
C	Larimore	15105523 BBB	snow	Surface		1.4	tba
26	Larimore	15105509 AAA2	Pembina Escarpment / EVA	Surface	Cty Drain # 14	-12	0.9
PE-1	Larimore	15105611CBB	Pembina Escarpment (2)	Surface	Drainageway	-14.8	-2.4
PE-2	Larimore	15105624CBB	Pembina Escarpment (14)	Surface	Drainageway	-15.4	-1.9
PE-3	Larimore	15105612DAD	Pembina Escarpment (16)	Surface	Drainageway	-14.3	3.5
PE-4	Larimore	15105520CCC	Pembina Escarpment (33)	Surface	Drainageway	-11.2	1.7
PE-5	Larimore	15105509BBC7	Pembina Escarpment (37)	Surface	Drainageway	-10.1	2.2
PE-6	Larimore	15105515CDD	Pembina Escarpment (51)	Surface	Drainageway	-11	nd
27	Larimore	15105509 DDD	EVA discharge	Surface	Hazen Brook	-7.8	4.2
28	Larimore	15105611 CBB	EVA discharge	Surface	Hazen Brook	-15.6	-4.3
21	Larimore	15105622 ABB	Pierre (Pembina Member)		0-4.18	-8.1	5.5
22	Larimore	15005629 DCC1	Pierre (Pembina Member)		0-33.55	-9.9	1.1
19	Larimore	15105133 AAA	Dakota	Flowing Well	0.0000-38.12	17.1	11.1
20	Larimore	15105118 DB	Dakota	Flowing Well	0.0000-54.88	15.3	12.3
15	Hamburg	14906909 CBB2	unoxidized till	Well	21.95-23.47	-9.3	1.5
16	Hamburg	14906909 CBB3	unoxidized till	Well	14.63-16.16	-8.8	-0.1
17	Hamburg	14906909 CBB4	oxidized till	Well	8.54-10.06	-8.4	-3.6
18	Hamburg	15007032 ABB4	lake sediment clay	Well	26.22-27.74	-9.6	4.4
23	Cogswell	14905717 AAA1	Carlile	Well	67.68-69.20	-7	3.4
24	Cogswell	12905736 BAA1	Carlile/Niobrara	Well	64.33-65.85	-5.6	5
25	Cogswell	12905736 BAA3	unoxidized till	Well	46.03-47.56	-8.7	5.4

Table 8. Paired Bonferroni tests for all groups having $P_{Bon} < 0.2$.

Source 1	Source 2	$\Delta \bar{x}$	SE	P_{bon}
Carlisle Porewater	Carlisle Grain PYrite	28.393	5.013	0.000125
Carlisle Porewater	Dakota Grain PYrite	34.733	7.926	0.018957
Dakota Porewater	Carlisle Grain PYrite	48.360	5.743	0
Dakota Porewater	Carlisle Grain Sulfate	32.950	5.945	0.000206
Dakota Porewater	Degrav Grain PYrite	54.700	8.407	4e-06
Dakota Porewater	Degrav Grain Sulfate	34.700	6.865	0.001465
Dakota Porewater	EVA Grain PYrite	-36.727	5.277	0
EVA porewater	Carlisle Grain PYrite	21.993	5.013	0.018602
EVA porewater	Dakota Porewater	-26.367	6.266	0.035467
EVA Grain Sulfate	Dakota Porewater	-35.183	5.504	6e-06
Gregory Grain PYrite	Carlisle Grain PYrite	32.493	5.013	4e-06
Gregory Grain PYrite	Gregory Grain PYrite	38.833	7.926	0.002694
Gregory Grain PYrite	EVA Grain PYrite	20.861	4.471	0.006601
Gregory Grain PYrite	EVA Grain Sulfate	19.316	4.737	0.055804
Niobrara Grain PYrite	Carlisle Porewater	-32.133	5.243	1.8e-05
Niobrara Grain PYrite	Carlisle Grain Sulfate	-19.150	4.854	0.087354
Niobrara Grain PYrite	Dakota Porewater	-52.100	5.945	0
Niobrara Grain PYrite	EVA Grain PYrite	-15.373	4.008	0.12493
Niobrara Grain PYrite	EVA porewater	25.733	5.243	0.002601
Niobrara Grain PYrite	EVA Grain Sulfate	-16.917	4.303	0.091309
Niobrara Grain PYrite	Gregory Grain PYrite	-36.233	5.243	1e-06
Niobrara Grain PYrite	Gregory Grain Sulfate	-29.500	7.675	0.12166
Pembina Grain PYrite	Carlisle Porewater	-43.233	7.926	0.000296
Pembina Grain PYrite	Dakota Porewater	-63.200	8.407	0
Pembina Grain PYrite	EVA porewater	-36.833	7.926	0.007086
Pembina Grain PYrite	Gregory Grain PYrite	-47.333	7.926	3.5e-05
Pembina Grain PYrite	Gregory Grain Sulfate	-40.600	9.708	0.0388
Pembina Grain PYrite	Lake Clay	-37.400	9.708	0.11828
Pembina Grain PYrite	Niobrara Porewater	-41.400	9.708	0.028964
Pembina Porewater	Carlisle Grain PYrite	23.160	5.743	0.065138
Pembina Porewater	Dakota Porewater	-25.200	6.865	0.20748
Pembina Porewater	Niobrara Grain PYrite	26.900	5.945	0.011195
Pembina Porewater	Pembina Grain PYrite	38.000	8.407	0.011407
Pembina Grain Sulfate	Carlisle Porewater	-26.417	4.854	0.00031
Pembina Grain Sulfate	Dakota Porewater	-46.383	5.605	0
Pembina Grain Sulfate	EVA porewater	-20.017	4.854	0.04739
Pembina Grain Sulfate	Gregory Grain PYrite	-30.517	4.854	9e-06
Pembina Grain Sulfate	Pembina Porewater	-21.183	5.605	0.14914
Snow	Carlisle Grain PYrite	33.627	5.013	1e-06
Snow	Gregory Grain PYrite	39.967	7.926	0.001541
Snow	EVA Grain PYrite	21.994	4.471	0.002494
Snow	EVA Grain Sulfate	20.449	4.737	0.023992
Snow	Niobrara Grain PYrite	37.367	5.243	0
Snow	Pembina Grain PYrite	48.467	7.926	1.9e-05
Snow	Pembina Grain Sulfate	31.650	4.854	3e-06
Silt Grain PYrite	Carlisle Porewater	-22.076	4.737	0.006733
Silt Grain PYrite	Dakota Porewater	-42.043	5.504	0
Silt Grain PYrite	Gregory Grain PYrite	-26.176	4.737	0.000221
Silt Grain PYrite	Snow	-27.309	4.737	8.2e-05
Silt Porewater	Carlisle Grain PYrite	19.627	5.013	0.096517

Source 1	Source 2	$\Delta \bar{x}$	SE	P_{bon}
Silt Porewater	Pembina Grain PYrite	34.467	7.926	0.021424
Silt Grain Sulfate	Dakota Porewater	-40.900	8.407	0.003079
Surface Water	Carlisle Grain PYrite	19.693	3.829	0.001032
Surface Water	Dakota Porewater	-28.667	5.366	0.000466
Surface Water	Niobrara Grain PYrite	23.433	4.125	0.000117
Surface Water	Pembina Grain PYrite	34.533	7.236	0.004392
Surface Water	Pembina Grain Sulfate	17.717	3.618	0.002718
Surface Water	Silt Grain PYrite	13.376	3.459	0.11303
Deep Till Grain PYrite	Dakota Porewater	-33.633	6.266	0.000421
Deep Till Grain PYrite	Pembina Grain PYrite	29.567	7.926	0.1737
Deep Till Porewater	Carlisle Grain PYrite	28.427	5.013	0.000122
Deep Till Porewater	Niobrara Grain PYrite	32.167	5.243	1.7e-05
Deep Till Porewater	Pembina Grain PYrite	43.267	7.926	0.000291
Deep Till Porewater	Pembina Grain Sulfate	26.450	4.854	0.000302
Deep Till Porewater	Silt Grain PYrite	22.110	4.737	0.006556
Deep Till Grain Sulfate	Carlisle Grain PYrite	27.193	5.013	0.000334
Deep Till Grain Sulfate	Gregory Grain PYrite	33.533	7.926	0.032697
Deep Till Grain Sulfate	Niobrara Grain PYrite	30.933	5.243	4.7e-05
Deep Till Grain Sulfate	Pembina Grain PYrite	42.033	7.926	0.000546
Deep Till Grain Sulfate	Pembina Grain Sulfate	25.217	4.854	0.00084
Deep Till Grain Sulfate	Silt Grain PYrite	20.876	4.737	0.017295
Medium Till Grain PYrite	Dakota Porewater	-35.150	6.865	0.00113
Medium Till Grain Sulfate	Carlisle Grain PYrite	30.760	7.52	0.053391
Medium Till Grain Sulfate	Gregory Grain PYrite	37.100	9.708	0.13057
Medium Till Grain Sulfate	Niobrara Grain PYrite	34.500	7.675	0.012499
Medium Till Grain Sulfate	Pembina Grain PYrite	45.600	9.708	0.005856
Medium Till Grain Sulfate	Pembina Grain Sulfate	28.783	7.415	0.10752
Topsoil Grain Sulfate	Carlisle Grain PYrite	34.260	7.52	0.009969
Topsoil Grain Sulfate	Gregory Grain PYrite	40.600	9.708	0.0388
Topsoil Grain Sulfate	Niobrara Grain PYrite	38.000	7.675	0.0022
Topsoil Grain Sulfate	Pembina Grain PYrite	49.100	9.708	0.001449
Topsoil Grain Sulfate	Pembina Grain Sulfate	32.283	7.415	0.020981
Topsoil Grain Sulfate	Silt Grain PYrite	27.943	7.338	0.13646
Shallow Till Grain PYrite	Dakota Porewater	-36.775	5.945	1.4e-05
Shallow Till Grain PYrite	Gregory Grain PYrite	-20.908	5.243	0.075737
Shallow Till Grain PYrite	Snow	-22.042	5.243	0.035907
Shallow Till Porewater	Carlisle Grain PYrite	20.793	4.157	0.001801
Shallow Till Porewater	Dakota Porewater	-27.567	5.605	0.002501
Shallow Till Porewater	Niobrara Grain PYrite	24.533	4.431	0.000211
Shallow Till Porewater	Pembina Grain PYrite	35.633	7.415	0.003865
Shallow Till Porewater	Pembina Grain Sulfate	18.817	3.963	0.004829
Shallow Till Porewater	Silt Grain PYrite	14.476	3.819	0.14407
Shallow Till Grain Sulfate	Carlisle Grain PYrite	25.610	4.605	0.000191
Shallow Till Grain Sulfate	Dakota Porewater	-22.750	5.945	0.12843
Shallow Till Grain Sulfate	Gregory Grain PYrite	31.950	7.675	0.041503
Shallow Till Grain Sulfate	Niobrara Grain PYrite	29.350	4.854	2.5e-05
Shallow Till Grain Sulfate	Pembina Grain PYrite	40.450	7.675	0.000621
Shallow Till Grain Sulfate	Pembina Grain Sulfate	23.633	4.431	0.000482
Shallow Till Grain Sulfate	Silt Grain PYrite	19.293	4.303	0.013029
Vadose Grain PYrite	Dakota Porewater	-35.167	6.266	0.000155

4.1 A brief introduction to the stable isotopic chemistry of sulfur

The element sulfur is composed of four naturally occurring stable isotopes with masses 32 (95%), 33 (0.75%), 34 (4.2%) and 36 (0.017%) (MacNamara and Thode 1950). A number of natural processes are selective among these isotopes, thus sulfur from different sources is characterized by different ratios of the heavy (mass 34) isotope to the major isotope, ^{32}S , which are measurable by mass spectrometry. The fractionation is generally proportional to the square root of the mass difference, and for this reason, coupled with the very low abundance of ^{36}S , sulfur isotopic variations are usually measured as ratios of $^{34}\text{S}/^{32}\text{S}$. Since isotopic effects are relatively small, it is convenient to express isotopic compositions as fractional differences in the isotopic ratios in parts per thousand (or “per mil”) on a delta (δ) scale, defined as:

$$\delta^{34}\text{S} (\text{‰}) = \left\{ \left[\left(\frac{^{34}\text{S}/^{32}\text{S}}{\text{sample}} \right) / \left(\frac{^{34}\text{S}/^{32}\text{S}}{\text{standard}} \right) - 1 \right] \times 1,000 \right\} \quad (4)$$

The standard used is the internationally recognized Cañon Diablo Troilite (CDT). Note that samples enriched in ^{34}S compared to the standard will have positive values of $\delta^{34}\text{S}$, while samples more depleted in ^{34}S than the standard will have negative values. Most natural materials have sulfur isotopic compositions in the range -40‰ to $+40\text{‰}_{\text{CDT}}$ and analytical uncertainty is generally $\pm 0.2\text{‰}$.

4.2 The oxygen isotopic chemistry of sulfate

Oxygen is composed of three stable isotopes, ^{16}O (99.76%), ^{17}O (0.0375%) and ^{18}O (0.1995%) (Garlick and Eugster 1969) and oxygen isotopic compositions are expressed on a similar δ scale defined on the basis of $^{18}\text{O}/^{16}\text{O}$, with the international reference standard Standard Mean Ocean Water (SMOW). Again the range of natural variability in the abundance of the ^{18}O isotope is far greater than analytical uncertainty. Variation in the oxygen isotopic composition of sulfate molecules primarily reflects two factors:

- i) the source(s) of oxygen atoms used in the formation of the sulfate molecule;
- ii) the effects of processes which have subsequently transformed the original isotopic composition.

Where one of these factors dominates, the sulfate isotopic composition may be used to gain useful information. Where sulfate is formed by oxidation of sulfide the resulting oxygen isotopic composition is dependent on the source of the oxygen atoms, e.g. oxygen derived from water molecules tends to be isotopically “light” (^{18}O -depleted), with generally negative $\delta^{18}\text{O}$ values on the SMOW scale, while atmospheric O_2 is ^{18}O -

enriched at +23‰_{SMOW}. There may, however, be some isotopic selectivity in the incorporation of the O atoms, which must be accounted for. The sulfate molecule is very resistant to exchange of oxygen atoms with the water in which it is dissolved (a process that would normally enrich sulfate in ¹⁸O, as ¹⁸O atoms are relatively more stable when bonded in a sulfate molecule than a water molecule). This exchange only takes place on timescales of ~10⁵ years at the near-neutral pH of many natural waters (Lloyd 1967). However, the process is catalysed during bacterial sulfate reduction (BSR, which may also exert a kinetic effect, whereby sulfate containing ¹⁸O atoms is discriminated against during reduction). Both of these processes lead to enrichment of ¹⁸O in the residual sulfate during BSR.

4.3 Potential Bedrock Sulfur Sources

Bedrock sulfur sources are highly variable with respect to $\delta^{34}\text{S}$, but can be broadly characterized into two groups: (1) sulfate-bearing evaporite mineral deposits (which also indicate the isotopic composition of contemporaneous seawater), and (2) organic-rich shales [which contain pyrite (FeS_2)].

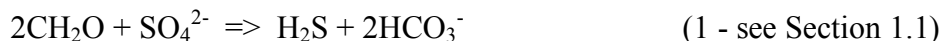
4.3.1 Ancient Seawaters and Marine Evaporite Minerals

Marine evaporite minerals are usually enriched with respect to ³⁴S. Claypool et al (1980) charted the isotope geochemistry of sedimentary sulfates with geological age. Evaporite minerals show large changes in $\delta^{34}\text{S}$ over geological time that reflect changes in the composition of contemporaneous seawater sulfate. Their general characterization of evaporite $\delta^{34}\text{S}$ was: a rise in the late PreCambrian to maximum values above +30‰ (around 550 Ma ago); Cambrian and Ordovician, high values around +30‰ Gilkeson et al. (1981) stated that average values for marine evaporites of North America are approximately 30‰ in Cambrian and Ordovician systems]; a fall in the Silurian/Early Devonian (around 400 Ma ago) to values around +17‰, followed by a more gradual fall to +11‰ in the Late Permian (240 Ma ago); a marked positive excursion occurred in the early Triassic, followed by a long period when $\delta^{34}\text{S}$ remained close to +16‰ during the Jurassic and Lower Cretaceous (around 100 Ma ago); over the last 100 Ma $\delta^{34}\text{S}$ gradually rose to a maximum of +21‰ around 12 Ma ago and has since declined to around +20.1‰ at the present day.

4.3.2 Sulfur Geochemistry of Fine-Grained Marine Sediments

Bacterial sulfate reduction (BSR) is one of the most important processes characterizing the early chemical diagenesis of marine muds and their pore-waters. In

anaerobic environments (typically found at depths of 0.1 to 1 m in marine muds), sulfate-reducing bacteria use dissolved sulfate as an electron acceptor for respiration, oxidizing organic matter by a reaction that can be summarized by:



The ultimate fate of sulfide reacting with iron-bearing minerals in the sediment is to form pyrite (FeS_2) (e.g. Berner 1974). This process carries a kinetic isotopic fractionation for sulfur, whereby $^{32}\text{SO}_4^{2-}$ molecules are preferentially converted into the sulfide product (e.g. Chambers and Trudinger, 1978). Thus in an open system, where sulfate is constantly re-supplied from the overlying ocean, sulfide and pyrite which are depleted in ^{34}S can form. In a closed system, with no re-supply of sulfate, the sulfate concentration of the pore-water will fall and, if all sulfate is converted, the final pyrite product must have the same isotopic composition as the initial seawater sulfate that constituted the sediment pore-water. In fact, such marine sediments commonly exhibit a range of pyrite sulfur isotopic compositions, dependent primarily on the amount of pyrite that formed under open vs. closed system conditions (with progressive burial all sediment pore-waters become isolated from exchange with the ocean), though other factors, such as the amount of any sulfide reoxidation which takes place, can also play a role (see review by Bottrell and Raiswell, 2000). Since burial will isolate pore-waters from re-supply of sulfate, deep sediment pore-waters are typically highly depleted in sulfate relative to seawater as a result of BSR. Note that the isotopic fractionation associated with BSR will mean that any residual pore-water sulfate will be significantly enriched in ^{34}S as a result of the preferential removal of $^{32}\text{SO}_4^{2-}$.

4.4 Sulfur geochemistry of the bedrock shales

The foregoing discussion provides a framework in which to interpret the analyzed sulfur abundance and isotopic composition of the shales forming the bedrock to the EVA and surrounding area. Table 4 gives the analyses of pyritic and sulfatic sulfur in the shales and their sulfur isotopic compositions at non-EVA locations (Fig. 1), while Table 6 provides the analysis for bedrock locations underlying the EVA. Table 9 contains the data for porewater dissolved sulfate in bedrock underlying the EVA.

Pyrite contents are variable (between <0.005 and 1.13 Wt% pyrite-S), a result of both differences in original depositional/diagenetic conditions and likely differing degrees of recent weathering. Pyrite isotopic compositions are also variable but always have negative $\delta^{34}\text{S}$. This will have resulted from differences in original

depositional/diagenetic conditions; pyrite with more negative $\delta^{34}\text{S}$ having originated from reduction under more open-system conditions.

The sulfate leached from these shales may be derived from one of two sources:

- i) Sulfate remaining after sulfate reduction, present as either sulfate in pore-water or substituted in soluble diagenetic minerals [e.g. carbonate – Burdett et al. (1989); or phosphate – Poulton et al. (1998)]. This would have an isotopic composition of ancient seawater or a more ^{34}S -enriched value (i.e. a strongly positive $\delta^{34}\text{S}$).
- ii) Sulfate added to pore-water by recent weathering of pyrite. This would have a $\delta^{34}\text{S}$ close to the pyrite in the rock as there is minimal isotopic fractionation during oxidation of solid-phase sulfides (Toran and Harris 1989).

Many of the shale sulfates have highly negative $\delta^{34}\text{S}$ (around -30% or more negative), similar to the majority of analyzed pyrite compositions. In these samples the shale sulfate is clearly dominated by pyrite weathering. In deeply-buried shales, where little or no O_2 is available for pyrite oxidation, a small degree of oxidation may still occur driven by oxidized iron (Fe(III)) from mineral sources (see e.g. Bottrell et al. 2000; Brown and Schoonen 2004). However other shales have sulfate $\delta^{34}\text{S}$ far more positive than the pyrite composition. This could indicate the presence of a component of original “connate” pore-water sulfate. However, since sulfate is typically nearly totally removed from marine pore-waters by BSR it is highly unlikely that sufficient ^{34}S -enriched “connate” sulfate could remain to generate the more positive shale sulfate $\delta^{34}\text{S}$ values observed. It is considered more likely that either:

- i) this sulfate is secondary, generated via pyrite oxidation, but in some instances has been subsequently modified by in-situ BSR (and removal of ^{34}S -depleted sulfide produced by Fe-sulfide formation) to produce the more positive sulfate $\delta^{34}\text{S}$ values (see e.g. Bottrell et al. 1996); or
- ii) this sulfate originates from dissolution of soluble diagenetic minerals.

The above possibilities are not mutually exclusive and may both contribute sulfate to pore-water.

4.5 Comparison of North Dakota Cretaceous Bedrock Sources

The following is a disaggregated comparison of sulfur chemistry in individual Cretaceous bedrock formations and members from the lowest to highest relative stratigraphic position (Fig. 3).

4.5.1 Dakota Group

Two water samples were collected in Grand Forks County from wells placed in the Dakota Group (Fall-River Lakota F.) of the lower Cretaceous Period. Their $\delta^{34}\text{S}$ exhibited a range of +15.3 to +17.1‰ (Fig. 17, Table 3, Table 7). These are less than modern seawater [20 (±2)‰_{CDT} (Holser and Kaplan 1966, Rightmire et al. 1974, Claypool et al. 1980, Strauss 2001)] but match well with measurements for the Lower Cretaceous Period (approx. 15 to 17‰) reported by Paytan et al. (2004). Lighter $\delta^{34}\text{S}$ during the Lower Cretaceous Period were attributed to increased volcanic and hydrothermal activity (Paytan et al. 2004.) Intrusion of Dakota Group water to overlying strata would be indicated by substantially heavier isotope composition as shown by the measured range or appropriate mixed effects.

4.5.2 Carlile and Niobrara Formations

Carlile F. and Niobrara F. grain matrix samples were collected from under the EVA (Table 6); and from road and river cuts in the Sheyenne River valley, and river cuts in the Pembina Gorge (Fig. 1, Table 4). All pyrite $\delta^{34}\text{S}$ values (Fig. 17) are in the BSR range (-16 to -46‰). Samples from under the EVA have a minimum of -25‰ (Table 9). All grain sulfate $\delta^{34}\text{S}$ from the Pembina Gorge are in the pyrite range, indicating predominant local and likely recent oxidation. Mineral sulfate-S under the EVA varies from one (Site 7) in the pyrite range indicating some likely local oxidation, with the other (Site 9 on Table 9) sufficiently heavy to indicate other sources and processes (Section 4.4). Heavier Carlile and Niobrara porewater sulfate (Table 7) may have been caused by a combination of sources and processes including $\delta^{34}\text{S}$ exclusion through BSR during initial pyrite formation and/or dissolution of diagenetic minerals as described under Section 4.3.2.

4.5.3 Pierre Formation, Pembina Member

$\delta^{34}\text{S}$ for the single Pembina pyrite sample was on the light extreme of the Carlile and Niobrara sample range (Fig. 17, Tables 3, 4). The Pembina grain-matrix sulfate was also in the BSR range (<-15‰), which is consistent with oxidation caused by proximity to an exposed face in the road cut from which the samples were taken (Table 4). The lightest $\delta^{34}\text{S}$ ratio was from a sample collected in a thin layer of gypsum crystals between a thin band of volcanic ash and fine sediment layer. Light $\delta^{34}\text{S}$ composition indicates that the gypsum sulfur was a product of pyrite oxidation.

4.5.4 Pierre Formation, Gregory Member

$\delta^{34}\text{S}$ for three pyrite samples of the Gregory Member (Fig. 17, Tables 3 and 4) collected at three different and widely separated locations were all heavier than the normal BSR range ($<-15\%$) suggested by Goldhaber and Kaplan (1974), and were significantly different ($P < 0.2$ Bonferroni, Table 11) from all other bedrock source groups. A likely cause was BSR under rapid burial in which sulfate substrate could not be replenished from seawater (Vinogradov et al. 1962, Bottrell et al. 2000b, and Section 4.3 above). The single grain sulfate sample is within the local pyrite $\delta^{34}\text{S}$ range, and given the sample source (a cutbank of the Sheyenne River) is likely a product of recent local oxidation from pyrite.

4.5.5 Pierre Formation, DeGrey Member

$\delta^{34}\text{S}$ for two pyrite samples of the DeGrey Member (Fig. 17, Tables 3 and 4) are on the light extreme of the pyrite range for the Carlile and Niobrara samples. The two grain-matrix sulfate samples varied from one nearly as light as the local pyrite to a much heavier sample with $\delta^{34}\text{S}$ composition similar to that of the Carlile, Niobrara and Pembina samples. The two samples were taken at the same surface location (a non eroded mound), and the heavier sample was more distant from the surface (Table 4). This indicates that sulfate from the lightest sample was likely a recent oxidation product from the local pyrite, and the deeper heavier sample similar to other bedrock samples.

4.6 Sulfur Geochemistry of Tills and Basal Silt

Table 5 gives analyses of pyritic and sulfatic sulfur in till samples and their isotopic compositions. Like the shales, till and silt pyrite concentrations are very variable and pyrite always has negative $\delta^{34}\text{S}$. This is consistent with an origin of pyrite in the tills from glacial erosion of shale bedrock, which contains pyrite with similar $\delta^{34}\text{S}$. Sulfate in the till is always enriched in ^{34}S (i.e. has less negative $\delta^{34}\text{S}$ than) the pyrite in the same sample. Thus sulfate in the tills cannot be simply derived by local pyrite oxidation (which would generate sulfate with $\delta^{34}\text{S}$ closely similar to the pyrite; Toran and Harris 1989) – either the sulfate isotopic composition has been subsequently modified or an additional component of sulfate more enriched in ^{34}S is also required. In the tills and silts this additional sulfate cannot be derived from shale connate water, since these materials were emplaced in glacial/glacio-fluvial environments and would thus have included glacial melt-water as pore-water, which would have had only very low sulfate concentrations. Hendry et al. (1986) ascribed the origin of ^{34}S -enriched sulfate in pore-water and

groundwater in deep unweathered tills of southern Alberta, Canada, to dissolution of gypsum contained within the tills. However, in their case there were significant differences in sulfate $\delta^{34}\text{S}$ between deep till and underlying bedrock shale. Their bedrock shale ground-water sulfate had $\delta^{34}\text{S}$ in the range -2 to $+2\%$, closely similar to the shale and deep till groundwaters reported here. Since the bedrock shales are not gypsiferous, the source of ^{34}S -enriched sulfate in shale and till below the EVA cannot be gypsum dissolution. An alternative scenario in which some pore-waters in shale and deep till could develop more ^{34}S -enriched sulfate isotopic compositions would be initial production of sulfate in all cases by pyrite oxidation, followed by partial BSR (and removal of ^{34}S -depleted sulfide produced by Fe-sulfide formation) to leave a more ^{34}S -enriched residual sulfate in some cases only. Alternately, local sulfate ^{34}S enrichment could be caused by removal of ^{34}S -depleted sulfate through diffusion to adjacent materials following local pyrite oxidation. This will be discussed further in a later section.

4.7 Surface Water (Drainageways) on the Pembina Escarpment

Drainageways on the PE were sampled during a static period, without substantial runoff. Waters were predominantly porewater draining from the local till and in some cases likely the Pierre shale. The range of PE $\delta^{34}\text{S}$ (-10.1 to -15.4% on Table 7) is consistent with a mixture of a locally oxidized portion of bedrock-derived biogenic pyrite in the till and heavier surface water, which would periodically seep into till porewater during precipitation, and increased runoff contribution downstream on the drainageways. The rainwater contribution is further confirmed by gradation of isotopic composition from lightest upstream to heaviest near the outlets at County Drain #14. These values are also similar to measurements (Table 7) on porewaters of unoxidized and oxidized tills at Hamburg in east central North Dakota (Fig. 1).

4.8 Fertilizer Sulfate

Sulfate in ammonium-sulfate fertilizer is produced from sulfuric acid generated during the coking of coal and its $\delta^{34}\text{S}$ composition therefore varies with the sulfur source used in producing sulfuric acid. Three fertilizer ammonium-sulfate samples from three different suppliers in Grand Forks County had $\delta^{34}\text{S}$ composition between -0.4 and $+9.9$ (Table 7).

4.9 Precipitation

Snow samples collected near Larimore, ND, and overlying the EVA have $\delta^{34}\text{S}$ composition of +1.4 to +1.5‰. Rightmire et al. (1974) described sulfate in precipitation as derived from "gaseous SO_2 from oxidation of natural H_2S , volcanic emanations, burning fossil fuels, and inclusion of sulfates in sea-spray aerosols" (p 192). They described from the literature a mean of +8.1‰ and a range of -1.5 to + 19.4‰ for $\delta^{34}\text{S}$ in precipitation (Table 1) (Fig. 17, Table 6). Low sulfate rainfall over non industrial rural areas was attributed $\delta^{34}\text{S}$ in the range of + 3.2 to +15.6‰, while industrial areas were attributed more depleted $\delta^{34}\text{S}$ because of SO_2 from fossil fuels. Krouse and Mayer (2000) reported a range of -5‰ to 25‰ for atmospheric sulfur. They reported a range of -3‰ to +9‰ for anthropogenic atmospheric sulfur in the northern hemisphere, and about + 5‰ for volcanic sulfur. Gilkeson et al. (1981) reported an average $\delta^{34}\text{S}$ composition of +0.7‰ in precipitation. Bottrell et al. (1996) reported from +0.7‰ in summer to +4.4‰ in winter measured in the United Kingdom. They attributed the isotopically light summer measurement to effects of fossil fuel and heavier winter measurements to seawater aerosol (+ 20‰) caused by heavier winds and choppy seas. The relatively light isotopic composition of EVA snow is consistent with sulfate to chloride ratios which indicate a predominant source in fossil fuel and dust (Section 3.2).

4.10. Summary of $\delta^{34}\text{S}$ Characteristics of Potential Sulfur Sources for the EVA

Atmospheric $\delta^{34}\text{S}$ is likely to be between -3 and 9‰, and has been measured locally at the EVA in winter at about +1.5‰. Ammonium sulfate fertilizers used on the EVA have $\delta^{34}\text{S}$ of -0.4 to 9.9‰. Local Dakota F. pore-water sulfate is *approx.* +15 to + 17‰. Pyrite in bedrock shales of Carlile F. and Niobrara F. and Pembina and DeGrey Members of the Pierre F. have a similar light range (-47 to -16.1‰). Of this range, local Carlile and Niobrara samples from beneath the EVA are of the heavier (-25 to -16.1‰) portion. Sulfate-containing minerals from these shales vary widely in $\delta^{34}\text{S}$, from -32 to + 0.7‰, depending on fractionation at the time of formation, recent oxidative history, non pyrite mineral sources, and in some cases possible atmospheric input. Their mean value (-22.86‰) is significantly different from the mean pyrite value (-35.45‰) at $P_{\text{Bon}} < 0.017$. Local values underlying the EVA are at the heavier end of the range (from -16.1 to 0.7‰), likely reflecting a smaller pyrite oxidation component. Porewater sulfate from these shales have a reasonably tight range (from -2 to -10‰). The mean porewater $\delta^{34}\text{S}$

(-5.8‰) is different from both pyrite at $P_{\text{Bon}} < 1.4 \times 10^{-5}$, and from grain-matrix sulfate at $P_{\text{Bon}} < 0.007$. Local (EVA) Carlile porewater is on the heavy end (approx. -0.2‰) of this range. Shale bedrock porewaters were likely diluted by freshwater having $\delta^{34}\text{S}$ near -0.0‰ during Pliocene and Pleistocene erosion and deposition of the overlying till. Surface waters from PE drainageways, which are predominantly from till and shale porewater, have a relatively tight $\delta^{34}\text{S}$ range from about -10 to -15‰, and with a mean of -12.7‰. PE contributions to aquifer sulfate by recharge should be between this range and approximately 0.0, depending on the amount of runoff from precipitation. Sulfate contributions to the EVA from oxidation of local pyrite through direct oxidation or autotrophic denitrification should both contribute sulfate having $\delta^{34}\text{S}$ similar to the pyrite being weathered. Pyrite $\delta^{34}\text{S}$ in the basal silt and till under the EVA is in the BSR range identified for shale bedrock sources. Heavier $\delta^{34}\text{S}$ in their porewater could have been caused by several possible processes:

- i) pyrite oxidation followed by subsequent BSR and removal of sulfide as FeS;
- ii) by dissolution of other diagenetic minerals containing substituted sulfate;
or
- iii) by long-term diffusion of sulfate following oxidation.

5. RESULTS

Sulfate and nitrate-N concentrations on Transect A-A' are shown on Fig. 17. All bottom sulfate concentrations are elevated with respect to the middle of the aquifer, and all but one (Site 6) have highest concentrations near the bottom. Sulfate concentrations near the surface are highly variable.

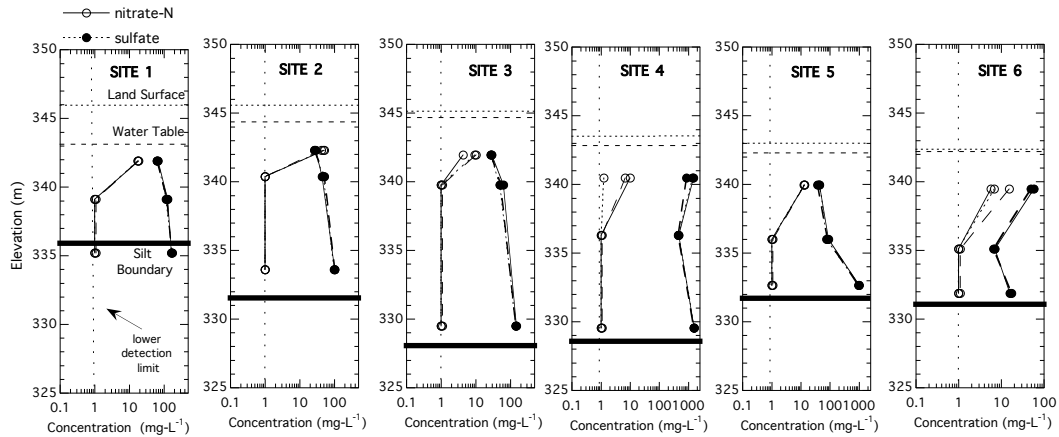


Figure 17. Sulfate and Nitrate-N concentrations for Transect A-A'.

5.1 Transect Hydrology

The stratigraphy and water levels for Transect A-A' are shown on Fig. 18. Site 3 was the primary recharge site in July of 1997 with water flowing northwestward at Sites 2 and 1 respectively toward the Turtle River, and southeastward (Sites 4, 5, and 6) toward Hazen Brook (which flows into the Turtle River) and other seeps flowing into the Goose River. By November Site 2 was the primary recharge site, and Site 3 was within the southeastward flow path. The difference was caused by flooding of the area east of County Drain #14 by waters draining from the PE in the Spring of 1997, which was the year of record flooding in the upper Red River Valley.

5.2 General Chemistry on Transect A-A'

General chemistry for shallow, middle and deep wells on Transect A-A' is shown on Fig. 19. Comparative parameters, including gravimetric sulfate-to-chloride, and sodium to chloride ratios for Transect A-A', and other sources, including seawater and local bedrock are on Table 9.

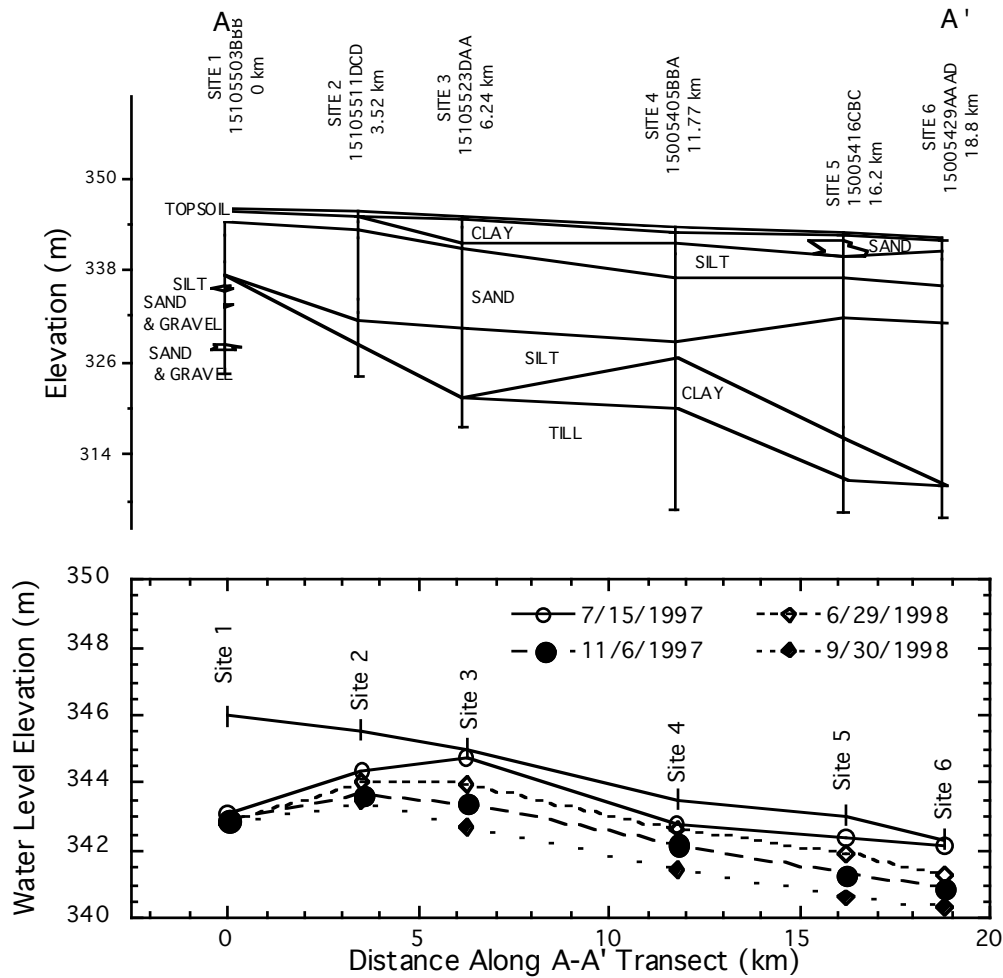


Figure 18. EVA stratigraphy and piezometric profiles for Sites 1-6, Transect A-A'.

The sulfate distribution profiles on Figs. 17 and 19 indicate that sulfate concentrations are highly variable, stratified, and predominantly governed by bottom sources. Elevated concentrations in the shallow oxidized zone that are separated from highest concentrations in the deep unoxidized zone by lower sulfate water in the mid aquifer indicate that weathering and precipitation processes in the vadose zone and the upper aquifer are affecting the shallow portion of the aquifer. However, there is no evidence that deep or shallow sulfate are increasing or decreasing with distance along the flow path. Sites 4 and 5 have elevated sulfate in both the shallow and deep EVA. On Site 4 locally depressed pH in both layers and enhanced reduced iron concentrations support the premise of local pyrite oxidation at both depths. In addition, x-ray diffraction and scanning electron microscopy (SEM) conducted on a bottom silt sample on Site 6 (Appendix 3) have indicated the likely presence of FeCO_3 which may have been

mobilized by temporary acidification in the bottom layers on Site 4. Iron concentrations are insufficient to account for large sulfate concentrations through pyrite oxidation and are transitory, decreasing over time, possibly due to oxidation with transitory DO discussed below. Elevated calcium (deep) and magnesium (shallow and deep) are consistent with acid weathering of carbonate minerals following pyrite oxidation, and elevated sodium (deep and shallow) are consistent with cation exchange resulting from the weathering of carbonate minerals.

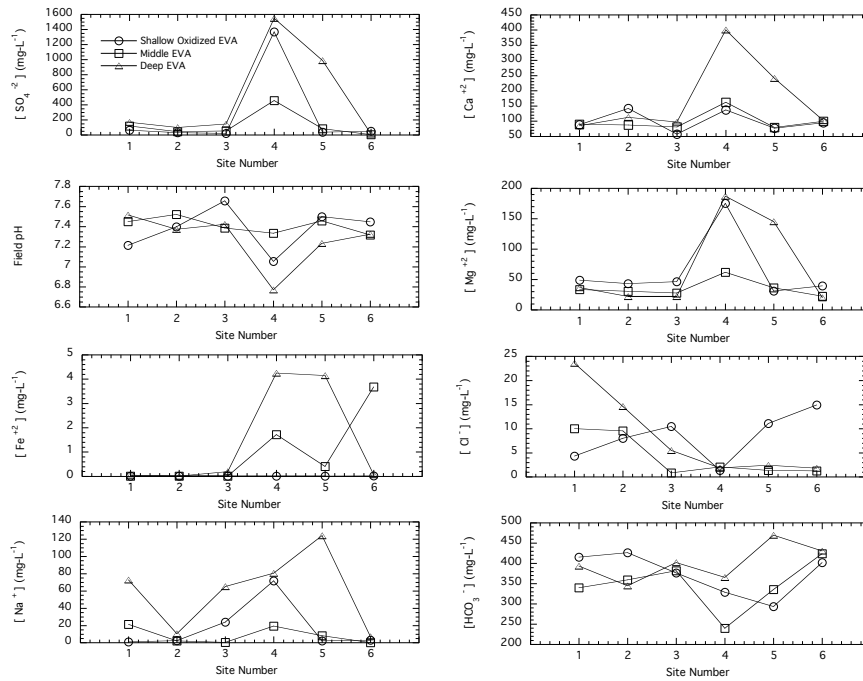


Figure 19. Water chemistry composition for wells on Transect A-A'.

The only consistent trend on Fig. 19 is decreasing chloride in the deep EVA moving from west to east along the transect. The primary source of chloride is in the underlying Carlile and Niobrara shale bedrock which has been identified as having a chemical composition similar to seawater with an approximate 80% freshwater dilution, and slightly elevated sulfate, calcium and sodium from in situ oxidation (Fig. 13). Using diffusion models for local till aquitard thicknesses and published approximate times of deposition, we have found that chloride concentration profiles from the deep EVA through the silt and till aquitard layers to the underlying shale can be accounted for almost entirely by long-term upward diffusion from the shale. The decreasing northwest-southeast chloride trend on Transect A-A' is thus a result of the thickening silt and till

aquitard layer with distance from the PE and its effect on long-term diffusion from the shale source. Chloride in the lower EVA should thus be a good indicator of bedrock influence. Another chloride source is PE water which is a surrogate for the underlying Pierre shale. Drainageways on the PE are incised into the shale and are separated from them only by thin till or sediment within the drainageways. Their base flows receive waters from the shale, thus the increased chloride content.

Sulfate vs. EC for the middle and deep EVA and the underlying silt and shallow till is slightly more enriched with sulfate than PE waters (Fig. 20). The relative difference in EC is in higher Cl^- (200 to 500 $mg-L^{-1}$) in the PE (Table 9) compared with $< 20 mg-L^{-1}$ in the EVA, silt, and shallow till aquitard). A summary of sulfate- and sodium-to-chloride ratios (Table 9) is useful for establishing some general comparative trends.

Sulfate-to-chloride ratios (SO_4^{2-}/Cl^-) for the EVA are higher than underlying shales because the shale bedrock is a primary source of chloride, and contains little sulfate. Strong increases in ratios of the deep and mid aquifer proceeding from west to east (Table 9), are caused by both decreasing chloride and elevated sulfate, which indicates that the PE is not the main modern source of deep sulfate.

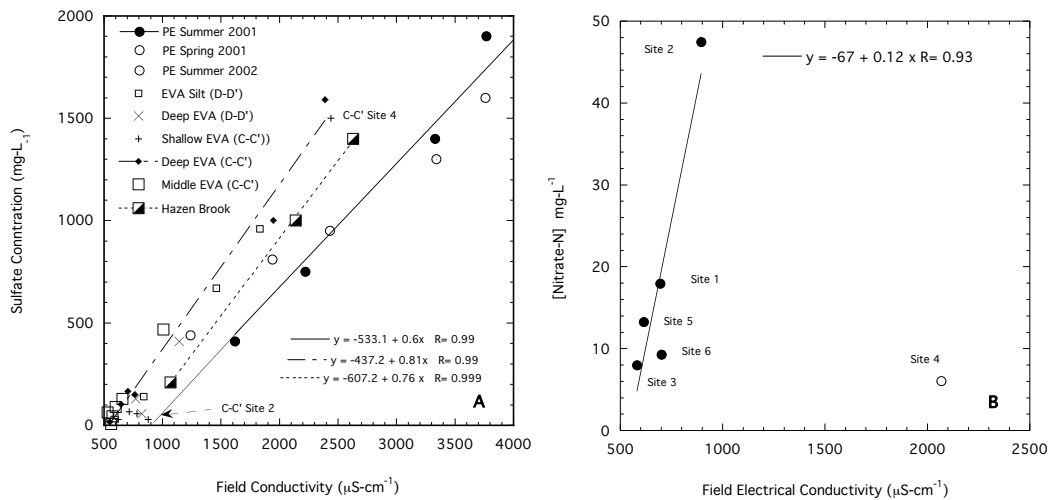


Figure 20. EVA sulfate vs. EC (A), and shallow EVA nitrate vs. EC (B).

SO_4^{2-}/Cl^- on the PE itself are much smaller (*approx.* 5) because of the proximate chloride source in the Pierre shale under the thin till mantle. Sites 1 and 2, those closest to the PE, have SO_4^{2-}/Cl^- similar to, or only slightly elevated from those of the PE.

These may indicate the influence of PE recharge waters themselves, or they may indicate a common source or process, since deep aquifer wells at these western sites are separated from the underlying shale by a thinner aquitard, a condition more similar to the tills overlying the PE. Slightly elevated chloride and very low local ratios (less than those of the PE) at some shallow sites is likely due to increased chloride from muriate of potash (KCl, 40% Cl^- by weight) which has been applied in large quantities (approx. 50 to 200 $kg\text{-ha}^{-1}\text{-y}^{-1}$) as an agricultural fertilizer since the 1950s.

Sodium is a companion ion to chloride in diffusion from the shale source, but it is also released through cation exchange caused by acid weathering of carbonates resulting from sulfide oxidation (Eq. 2). Systematically increasing sodium concentrations southeastward on the transect occur only in the deep aquifer (Fig. 19). Because chloride is decreasing with increasing sodium, as indicated by increasing Na^+/Cl^- , cation exchange is the probable source. Increasing Na^+ and Na^+/Cl^- only in the deep aquifer and not in the middle indicate that the zone of active weathering and exchange (and therefore active sulfate production) lies in the deep aquifer, and that the likely source of mid aquifer sulfate is diffusion from the deeper unit. Na^+/Cl^- in the PE are only slightly higher than the deep unoxidized shales. Ratios in the mid EVA are small and possibly related to PE concentrations only at Sites 1 through 3.

Shallow EVA SO_4^{2-}/Cl^- are mostly low (with the exception of Site 4). They are below SO_4^{2-}/Cl^- for precipitation and the PE (both approx. 10), and are likely affected by muriate of potash additions. Shallow oxidized EVA waters are generally lower in EC ($< 800 \mu\text{S}\text{-cm}^{-1}$), and have lower sulfate than would be predicted by either PE or aquifer (and silt) transfer functions. The shallow EVA, unlike deeper units, exhibits no correlation between sulfate and EC (Fig. 20-A). Rather, there is a strong correlation between NO_3^- and EC (Fig. 20-B). The shallow oxidized portion of the aquifer appears to be freshened with low-sulfate recharge water which is laden with nitrate fertilizer. In addition, SO_4^{2-}/Cl^- in the shallow oxidized zone are determined mainly by Cl^- .

A plot of all SWC data for 267 wells indicates a general relationship for the EVA in which SO_4^{2-}/Cl^- for all $SO_4^{2-} > 400 \text{ mg}\text{-L}^{-1}$ are correlated primarily with sulfate (Fig. 21-A) while ratios for all lower sulfate ($< 400 \text{ mg}\text{-L}^{-1}$) samples are correlated with a power function of chloride (Fig. 21-B). The data for the shallow aquifer on all sites except Site 4 belong to the low sulfate and chloride-correlated data group (Fig. 21-B). Both EC and SO_4^{2-}/Cl^- in the shallow oxidized zone support the presence and chemical influence of fertilizer as nitrate and muriate of potash and less from sulfate.

Table 9. Chemical indicators of recharge-water sources in the shallow oxidized strata of the Elk Valley aquifer (Sites 1-6), and related source materials. The dilution factor is the ratio of sulfate concentration in County Drain #14 abutting the aquifer and the Escarpment (PE) drainage waters - to shallow EVA sulfate concentrations. 'S' is shallow, 'M' is middle and 'D' is deep.

Site Number	Distance on Transect	[SO ₄ ²⁻]	[Cl ⁻]	[Na ⁺]	[SO ₄ ²⁻] / [Cl ⁻]	[Na ⁺] / [Cl ⁻]	Dilution Factor *
A-A' B-B' (#)	km on A-A'	mg-L ⁻¹	mg-L ⁻¹	mg-L ⁻¹	g/g	g/g	
Seawater		2560	18980	10560	0.13	0.56	
Meteoric		0.82	0.08		10.3		
Carlile #7		66	2370	1600	0.16	0.72	
Niobrara #8		66	1220	920	0.054	0.75	
Carlile #9		210	1340	970	0.028	0.68	
PE		1300	250	330	5.2	1.3	
PE		1600	350	380	4.6	1.1	
PE		1800	380	480	4.7	1.3	
1-S	0	64	4	1.40	14	0.35	15
2-S	3	32	8	3.15	4	0.40	30
3-S	6	22	10	22.3	2	2.2	43
4-S	11	1367	1	113	1012	113	0.73
5-S	16	37	11	1.15	3	0.1	26
6-S	18	50	14	3.05	3	0.22	19
1-M	0	120	10	20.5	12	2.1	8
2-M	3	45	9	1.75	4	0.19	22
3-M	6	54	0	0.300	64	*	18
4-M	11	458	2	17.0	221	8.5	2
5-M	16	83	1	7.55	61	7.1	12
6-M	18	6	1	0.100	4	0.1	155
1-D	0	170	23	73.8	7	3.2	5
2-D	3	100	14	10.9	6	0.78	9
3-D	6	146	5	66.7	26	13.3	6
4-D	11	1550	1	93.2	828	93.2	0
5-D	16	987	2	117	408	58.5	1
6-D	18	16	1	5.45	8	5.45	61
Goose R.		5,700	91	460	62.6	5.1	
Hazen B.		210	18	13	11.7	0.72	
Hazen B		1,400	41	54	34.1	1.3	
Hazen B		1,000	17	45	58.8	2.7	

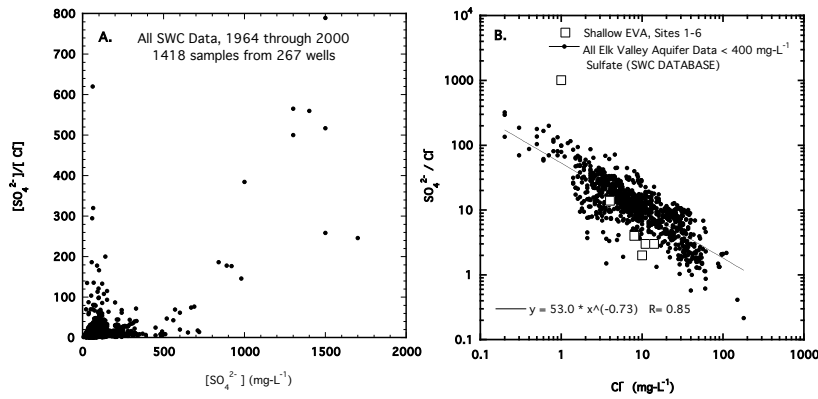


Figure 21. SO_4^{2-}/Cl^- vs. SO_4^{2-} for all SWC wells in the EVA (A), and SO_4^{2-}/Cl^- vs. Cl^- for all wells having $SO_4^{2-} < 400 \text{ mg-L}^{-1}$ (B).

5.3. Dissolved Oxygen (DO) of the EVA

The oxidation status of the EVA and interacting hydrologic units is a key property for examining the plausibility of sources and processes affecting sulfate generation and retention.

DO measurements in the shallow (oxidized) zone on Transect A-A' ranged from 1 to 6 mg-L^{-1} , but were usually between 2 and 4 mg-L^{-1} in areas identified on Fig. 18 as recharge areas (Sites 1, 2, and 3). Schlag (1995) measured DO ranging from 2.1 to 2.8 mg-L^{-1} in the transitional zone just below the oxidized zone at an experimental site within a few meters of Site 2.

DO measurements in September 1997, were $\sim 1 \text{ mg-L}^{-1}$ in the middle (unoxidized) EVA of all sites on Transect A-A' (Table 10). They increased slightly on Sites 1, 2, and 3 during the winter of 1997, and then declined. Measurements on Sites 4, 5, and 6 declined throughout the measurement period. Temporary slightly elevated DO (1 to 2 mg-L^{-1}) in the middle aquifer, followed by much lower values, were likely influenced by the spring events of 1997. DO declined to less than one on all sites by the end of 1998.

DO measured in the deep EVA (on Transect A-A'), with some slight variance following the recharge events of spring 1997, were almost all near or below 1 mg-L^{-1} and were generally lower than mid aquifer values. The deepest EVA wells, those located just above the silt boundary (Transect B-B'), and wells in the silt, till aquitard, and shale on Transect B-B' were all below 1 mg-L^{-1} (Table 11).

Table 10. Dissolved oxygen (DO) in mg-L⁻¹ for the shallow oxidized (S), mid unoxidized (M), and deep unoxidized (D) strata of the Elk Valley Aquifer on Transect A-A', Sites 1-6.

Date	Site 1			Site 2			Site 3			Site 4			Site 5			Site 6		
	S	M	D	S	M	D	S	M	D	S	M	D	S	M	D	S	M	D
9/17/1997	2.70	0.99	1.01	3.89	0.96	1.20	2.48	0.84	1.24	0.97	1.49	3.03	1.59	1.30	1.73	0.84	1.23	1.17
12/12/1997	3.66	1.29	2.16	5.04	1.63	2.40	3.13	1.35	1.13	1.09	1.15	1.58	3.13	0.71	1.19	2.34	0.67	1.09
4/3/1998	3.78	-	0.41	6.36	1.17	0.47	3.13	1.93	0.40	0.43	0.95	0.48	0.70	0.37	0.38	-	-	-
10/20/1998	1.06	0.08	0.07	3.10	0.05	0.03	4.52	0.01	0.01	5.24	0.02	0.01	0.15	0.02	0.03	-	0.03	0.00

Table 11. Dissolved oxygen (DO) in mg-L⁻¹ measurements (February 2002) for the B-B' Transect.

Location	Strata	DO mg-L ⁻¹
Site 7 15105523BBB	EVA	0.6
	Silt	0.4
	Shallow Till	0.6
	Carlile Shale	0.8
Site 8 15105419CCC	EVA	0.4
	Silt	0.6
	Shallow Till	0.6
	Deep Till	0.6
	Niobrara Shale	0.7
Site 9 (15005405ABB)	EVA	0.8
	Silt	0.6
	Shallow Till	0.8
	Deep Till	0.6
	Carlile Shale	0.8

These data indicate variable oxidation states in the upper aquifer, with a predominance of more highly oxidized waters in areas of high recharge near the PE. The predominant oxidation state of the middle and deep aquifer is low, with some small variance in the mid aquifer in areas close to the PE following exceptionally large recharge events. The deep EVA, just above the silt layer, and the underlying silt, till, and shale are characterized by $\text{DO} < 1 \text{ mg-L}^{-1}$.

5.4 Summary of General Relationships

The main source of chloride in the deep and middle EVA is bedrock shale. General chloride trends in the deep and mid aquifer decrease along Transect A-A' due to increasing thickness of the till aquitard between the bedrock source and the EVA. The predominant sulfate source seems to be in the deep aquifer which provides a current dispersive source of sulfate for the mid aquifer. Sulfate, chloride, and sodium on Sites 1 and 2 may be influenced by PE waters, or by processes similar to those forming PE waters augmented somewhat by in situ sulfide oxidation. The anionic composition of EC in the deep and middle EVA is governed by nitrate. EC in the shallow oxidized portion of the aquifer is not correlated with sulfate, and its anionic composition is dominated by chloride and sulfate. Chloride in the shallow aquifer appears to have been affected by a source other than the underlying shale, likely fertilizer potash. Sulfate in the shallow EVA is highly variable and does not appear to be strongly influenced by bottom processes. Elevated calcium, magnesium and sodium in high sulfate areas of the deep and shallow EVA suggests in situ acid weathering of pyrite. Their absence in the middle EVA, with indications of covariance with bottom chloride, suggest that the sulfate source in the middle portion of the aquifer is dispersive transport from the bottom. Dissolved oxygen in the shallow oxidized zone varies from ~ 1 to 6 mg-L^{-1} . DO in the middle and deep aquifer approached ~ 2 to 3 mg-L^{-1} following a very large recharge event, but reduced to $< 1 \text{ mg-L}^{-1}$ within one year. DO in the deep EVA, and the underlying silt, till aquitard and shale was found to be $< 1 \text{ mg-L}^{-1}$.

6. ANALYSIS

Hypotheses offered for high sulfate in the EVA include: (1) evaporative concentration in discharge areas, (2) gypsum mobilization, (3) vadose pyrite oxidation and leaching, (4) pyrite oxidation through autotrophic denitrification, (5) addition through sulfatic fertilizer, and (6) runoff from the PE.

In this section we will: (1) briefly examine the major hypotheses; (2) analyze sulfate sources and processes contributing to each of the three measured strata of the aquifer (shallow oxidized, middle unoxidized, and deep oxidized); and (3) examine sulfur and oxygen isotopes, and their relationship to sources of modern sulfate concentrations.

6.1 Major Hypotheses

The previous section concluded that some sulfate concentrations in the shallow and middle depths of EVA on Sites 1 and 2 may be affected by runoff water from the PE. The PE does not, however, appear to be a major determinant of concentrations in the EVA. We have previously examined potential precipitation, organic matter and fertilizer sources (Sections 3.2, 3.6, 3.7) and have determined that they are not the major sources of elevated sulfate in the south EVA. They do, however, contribute to the overall sulfate pool and influence sulfate concentrations in the near surface environment. Their contribution will be further examined in the Sections on the Shallow EVA (Section 6.2.3) and on Isotopic Evidence of Sulfate Sources (Section 6.4).

6.1.1 Hypothesis: Gypsum Mobilization

Gerla's (1992) hypothesis that ongoing dissolution of gypsum is the source of sulfate (measured predominantly in deep aquifer wells) cannot be supported as a currently viable process. Saturation indices (SI) were calculated using WateqF (Plummer et al. 1978) for all Transect A-A' and B-B' sites and depths, and at three additional SWC deep EVA well sites having relatively high sulfate concentrations. Results (Table 12) indicate that water at all sites and depths is undersaturated with respect to gypsum. Field pH was used on sites A-A', while lab pH values were used on sites B-B' and the SWC well sites. Indices were computed using DO according to the Sato relation (described by Truesdell and Jones, 1974). Arndt and Richardson (1989) used gypsum saturation indices for soil saturation extracts from samples taken in a flow-through wetland to demonstrate that gypsum was stable only at EC values $> 3,800 \mu\text{S-cm}^{-1}$. None of the EC measurements taken in the EVA or in the silt layer approach this EC. Saturation indices computed for the deep EVA, upper till, and silt layers on transect B-B'

corresponded well with the SI versus EC relationship established by Arndt and Richardson (1989). These determinations indicate that modern sulfate sources within and underlying the EVA are not from gypsum. They do not exclude the possibility, however, of gypsum dissolution in the vadose zone and leaching to the upper portion of the aquifer during recharge events.

Table 12. Summary of saturation indices (Wateqf, Plummer et al. 1976) for water chemistry samples taken in the Elk Valley aquifer, silt, and shallow till wells on Sites 1-9.

Site	Strata	LOG [IAP/KT]	Site	Strata	LOG [IAP/KT]	Site	Strata	LOG [IAP/KT]
1#	Shallow EVA	-1.714	4#	Shallow EVA	-0.699	7#	Deep EVA	-0.699
	Mid EVA	-1.428		Mid EVA	-0.764		Silt	-0.764
	Deep EVA	-1.347		Deep EVA	-0.145		Shallow Till	-0.145
2#	Shallow EVA	-1.915	5#	Shallow EVA	-2.64	8#	Deep EVA	-2.64
	Mid EVA	-1.803		Mid EVA	-1.620		Silt	-1.620
	Deep EVA	-1.427		Deep EVA	-1.329		Shallow Till	-1.329
3#	Shallow EVA	-2.225	6#	Shallow EVA	-1.783	9#	Deep EVA	-1.783
	Mid EVA	-1.791		Mid EVA	-2.606		Silt	-2.606
	Deep EVA	-1.339		Deep EVA	-2.183		Shallow Till	-2.183

6.1.2 Hypothesis: Bedrock Porewater Source

A sulfate source for the EVA from underlying bedrock could occur either from upward diffusion from sulfate in the bedrock shale, or upward extrusion of porewater from bedrock under the weight of glacial ice during the Pleistocene as proposed by (Cherry, 1972). Water samples collected from the Carlile and Niobrara shales underlying the EVA on Transect B-B' have indicated that sulfate concentrations in the shale are too low to provide a substantial source. Water samples taken from wells of the deeper Cretaceous Dakota Mbr. of the Lakota F. in the proximity of the EVA have sulfate concentrations similar to elevated concentrations in the lower EVA ($\sim 1,500 \text{ mg-L}^{-1}$). However, they have a much elevated EC ($\sim 7,000 \mu\text{S-cm}^{-1}$) compared with EVA samples (Section 3.3, Fig. 11). Moreover, data for porewater (Section 4, Table 7) indicate that Dakota Mbr. porewater has a relatively heavy $\delta^{34}\text{S}$ isotope composition similar to lower Cretaceous seawater ($\sim +15$ to $+17\%$) compared with modern EVA porewater ($\sim -10\%$),

a difference having a BSD probability of < 0.04 (Section 4, Table 8). Sulfate from deeper evaporite sources in bedrock would likely have an even heavier $\delta^{34}\text{S}$ isotope composition (Section 4). Diffusion or extrusion from bedrock is not a plausible source.

6.1.3 Hypothesis: Evaporative Concentration

Sulfate profiles on Transect A-A' indicate that the largest sulfate concentrations are on the bottom of the aquifer, and that the middle and sometimes the surface of the aquifer have relatively lower concentrations. Predominant evaporative discharge, which concentrates salts at the locus of evaporation, is inconsistent with this profile. Individual instances of high sulfate concentrations near the surface (Ex. Site 4) may involve dissolution and leaching of evaporite minerals in the vadose zone. Predominant discharge soils in associations (Fig. 7) overlying the south EVA are Calciaquolls. These frequently have gypsum deep in the soil profile. However, they are relatively mildly expressed net discharge soils [an average of $< -3 \text{ cm}\cdot\text{y}^{-1}$ (Knuteson et al. 1989)]. Strongly expressed evaporative soils are predominantly along drainageways of the PE, and are not characteristic of the EVA. Terminal discharge is not a plausible primary cause of high sulfate in the south EVA.

6.1.4 Hypothesis: In Situ Pyrite Oxidation

Swanson (1992) proposed aerated oxidation (Eq. 1), and Korom et al. (2005) proposed autotrophic denitrification of pyrite (Eq. 2) in the vadose zone and shallow EVA as a sulfate source. Mineral assays have indicated substantial pyrite in the EVA grain matrix (Section 3.5, Fig. 14). Pyrite is generally depleted in the topsoil through the upper (oxidized EVA), although it is variably present. Pyrite is most common in the deltaic silt underlying the EVA sands, it is somewhat depleted in the lower EVA, and better preserved in the middle (unoxidized) EVA. Sulfur ($\delta^{34}\text{S}$) isotope data summaries (Table 3) indicate that the range (-29 to -14‰) of $\delta^{34}\text{S}$ in EVA and silt layer are similar to the range (-46 to -16‰) of potential source bedrock data from the Carlile, Niobrara, and Pierre (Pembina and DeGrey Mbr.) Formations sampled in eastern North Dakota, although slightly on the heavy end of the range. In this respect they are similar to the local bedrock Carlile and Niobrara F. sample range (-25 to -16.1‰, Table 4). These similarities suggest that pyrite in the EVA, silt and underlying till is derived from erosion and weathering of the local bedrock. The abundant supply of pyrite suggests that non-microbial and microbial oxidative weathering of pyrite may be a major sulfate source.

6.2 Analysis of EVA Sulfate Sources by Depth

Preliminary analyses of water chemistry indicated that highest sulfate concentrations are usually in the lower aquifer, highest variability is near the surface of the aquifer, and lowest local concentrations and most evidence of sulfate formation are in the middle of the aquifer. In this section we will examine sulfate sources by depth.

6.2.1 Deep Unoxidized EVA

Highest sulfate in the deep EVA suggests a source in underlying boundary materials. Extrusion of underlying sulfatic bedrock porewater, dissolution of gypsum along the EVA flow path, evaporative concentration, runoff from the PE, and fertilizer and precipitation have been eliminated as predominant sources for the deep EVA. Deep EVA, silt, till aquitard and bedrock wells on Transect B-B' indicate that the modern proximate source of sulfate is in the silt layer.

Figure 12 shows depth profiles of chloride and sulfate at Sites 7, 8 and 9. Chloride gradients decline nearly monotonically from maxima in the bedrock shale through the till and silt to minima in the EVA. We hypothesize that this is due to a chloride source from residual connate water in the shales that supplies chloride to the basal units of the aquifer sequence by diffusion driven by this gradient. Proportions of ions relative to chloride in the shale and deep till ground waters are similar to seawater (Fig.13, a, e and f), supporting the connate water hypothesis. The sulfate profiles in Fig. 12-B are different, exhibiting maxima in the silt layer – or in the till immediately below the silt at Site 7 - where the sulfate maximum is much depressed relative to Sites 8 and 9. Thus the shale and deep till cannot represent a source of sulfate to the aquifer as true of chloride; rather the silt (or till immediately below) is the modern proximate source of sulfate and sulfate diffuses from the silt into the aquifer above and till below. We have determined that modern evaporative concentration, gypsum mobilization, and bedrock porewater are not plausible sources for sulfate in the lower EVA. The remaining hypothesis is that of authigenic pyrite oxidation.

The EVA and silt contain substantial pyrite (Fig. 14, Tables 5 and 6). The pyrite source is the shale portion of the EVA and silt matrix. Pyrite-S profiles are similar for all sites. They are depleted in the surficial soil and vadose zones and upper aquifer, more abundant in the mid-aquifer, somewhat depleted in the deep aquifer just above the silt layer, and most abundant in the silt layer. Oxidation of pyrite can generate sulfate and thus pyrite oxidation is a potential source of the elevated sulfate concentrations in the silt. Figure 13 b, c and d show different distributions of sulfate and cations relative to the deep till and shale (Fig. 13 e and f). Sulfate is enriched relative to chloride, as are Ca^{2+} , Mg^{2+}

and Na^+ . This is consistent with elevation of sulfate concentrations by pyrite oxidation (Equation 1) accompanied by weathering of carbonate minerals by the acid produced. Ion exchange reactions, driven by increases in Ca^{2+} concentration from carbonate weathering, cause Na^+/Cl^- (and possibly Mg^{2+}/Cl^-) to rise.

The deep EVA, silt and shallow till all have elevated SO_4^{2-}/Cl^- compared to the deeper units (Fig 13a), though this is in part due to the increasing chloride concentration with depth (Fig. 12-A). To corroborate the findings from this single transect we used the larger SWC database that contains water chemistry records, well-construction data and lithology for 265 wells. Partitioning by SO_4^{2-}/Cl^- for all SWC wells indicated that where waters evolved to high SO_4^{2-}/Cl^- , sulfate concentrations are elevated above $400\text{ mg}\cdot\text{L}^{-1}$. Almost all wells having sulfate $>400\text{ mg}\cdot\text{L}^{-1}$ have well screen intervals within, partly within or immediately above the silt layer (Fig. 22, Table 15). The silt layer thus represents the modern source of high sulfate across the entire deep EVA.

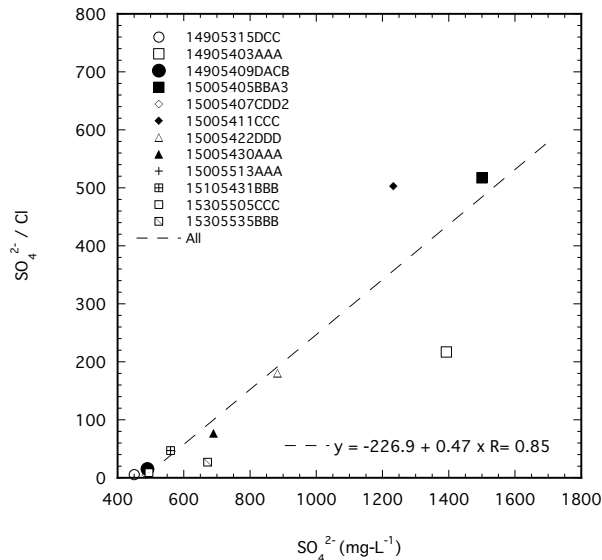


Figure 22. SO_4/Cl for EVA wells having SO_4 concentration $> 400\text{ mg}\cdot\text{L}^{-1}$

6.2.1.1 Sulfur Isotope Composition

Sulfur isotopic compositions of solid samples and silt and underlying till ground water are presented in Tables 5 and 6. One third of the EVA aquifer and silt samples have pyrite $\delta^{34}S$ between -14 and -18 ‰ , whilst the remainder have a range of more negative $\delta^{34}S$ (to -29.8 ‰). This range reflects variability in the original shale source rocks. Ground-water sulfate at Sites 8 and 9 has very closely similar sulfur

isotopic compositions in both silt and deep till, between -14.7 and -16.7 ‰. At Site 7, ground-water sulfate has less negative $\delta^{34}\text{S}$, -11.7 ‰ in the till and -6.2 ‰ in the silt. Since oxidation of pyrite to sulfate involves negligible isotopic fractionation (Nakai and Jensen 1964; Toran and Harris 1989) the deep EVA, silt and till aquitard ground-water sulfate compositions are consistent with a predominantly pyrite source (see Section 4.3 for full discussion).

There is thus geochemical evidence to support the hypothesis of pyrite oxidation as the source of sulfate in the deep units of the EVA and underlying silt. We next consider the possible scenarios under which sulfide oxidation might have taken place in the deep aquifer.

Table 13. Summary of well-screen placements for SWC having $\text{SO}_4^{2-} > 400 \text{ mg-L}^{-1}$, and their proximity to the silt layer.

Location	Material Depth Interval	Grain Matrix m	Well SI m
14905403AAA	3.6-32.3	Silt	5.5-7
15005411CCC	4-6.4	Silt	8-9.4
	6.4-9.8	Sand	
	9.8-27.7	Silt	
15005422DDD	3.7-15	Sand	12.8-14.3
	15-	Silt	
15105431BBB	3.7-10.4	Sand	9.5-10.1
	10.4-28	Silt	
15005531AAA	11-15.2	Sand 95% shale	14.6-15.6
	15.2-19.2	Silt	
15305505CCC	2.7-11.9	Sand	10.4-11.3
	11.9-15.9	Till, mostly shale	
15305535BBB	10.7-12.2	Sand	10.7-11.6
	12.2-19.2	Silt	

6.2.1.2 Oxidizing Processes

Lacking other plausible external sources it is clear that at some time an oxidizing event (OE) occurred during which in-situ pyrite-S was oxidized to sulfate and entered the silt layer. The modern sulfate profile (Fig. 12B) establishes that since that time the silt layer has, through hydraulic resistance, served as a "conserving" layer, slowly feeding sulfate into the less sulfatic EVA and till aquitard, primarily through diffusion. We wish to determine where [in what layer(s)] this may have occurred, whether the oxidizing process is modern or historical, an approximate time frame for its occurrence, and a plausible mechanism(s) for its redistribution to match the modern profile.

To examine the range of plausible scenarios we employ a semi-generic advection-dispersion process model, using locally measured hydraulic properties, or, in some cases, properties for similar and similarly derived materials from the literature. The model structure, properties and parameters are described in Appendix 1. The modeling approach is to establish plausible initial boundary conditions and sulfate concentrations, and examine the temporal progress of advective and dispersive processes to match the modern sulfate distribution on Sites 7, 8, or 9. The main target layers for matching are the till aquitard and silt layers. These are selected because they are the most hydrologically conservative, having slow conductive properties. They are thus less affected than the EVA by hydrodynamic dispersion, the spatial and temporal variability of hydraulic properties, variations in the natural flow system, and potential vertical advective flow components caused by local recharge and discharge regimes. Recharge and discharge conditions are treated in two separate models. The first, called CDM for "closed depression model", uses a radial model to simulate a closed depression intra-annual recharge and discharge regime similar to the Calciaquoll-Haplaquoll association described for the south EVA. The second, labeled FTM for "flow-through model," simulates a linear flow path similar to the east part of south EVA. The structures, properties and parameters of both models are discussed in Appendix 1.

6.2.1.3 Hypothesis: Contemporary Oxidizing Event (OE)

We first examine the possibility that deep sulfate may be forming through ongoing oxidation in the deep EVA. Greater depletion of pyrite-S in the deep EVA (Fig. 14) suggests that this may have been the source. However two factors indicate that contemporary pyrite oxidation is unlikely to be the sulfate source. Firstly, oxygen diffusion from the atmospheric interface cannot support sufficiently large sulfate concentrations in the silt layer at 16.5 m below the water table. As observed by Marshall (1977, p. 13) " the presence of a saturated zone effectively blocks the movement of these gases [CO_2 and O_2] over appreciable distances." Secondly, there are both lower sulfate concentrations and higher matrix pyrite-S concentrations in the overlying parts of the aquifer. The matrix pyrite-S indicates a large chemical oxidation demand (COD) between the EVA surface and the target layer.

Dissolved oxygen (DO) was measured on Transect A-A' from 9/1997 through 12/1998 (Table 10), and on transect B-B' in 2/2002 (Table 11). Results for 1997-8 (Table 10) show a single period of relatively high DO in the deep EVA on one high sulfate site (Site 4) in 9/1997. However, DO immediately began to decrease at all sites and depths until it was nearly below detection by 12/1998. The single large DO occurred when the

EVA was subjected to an uncharacteristic recharge event in a year of record spring floods. The large initial reading was thus likely caused by local advection of oxygenated water from uncommonly large surficial recharge. It was not, however, repeated in subsequent measurements. DO for the deep EVA, silt, till and shale is usually $< 1 \text{ mg-L}^{-1}$.

To simulate a "conservative" case we applied the 1990 climate CDM to Site 9 for the conditions: constant DO concentration of 10 mg-L^{-1} in all surface nodes; initial DO of 0.9 mg-L^{-1} at all depths; all $\text{DO} > 0.9 \text{ mg-L}^{-1}$ removed in the target layer (silt at 16.5 m), as represented by a constant concentration node of 0.9 mg-L^{-1} at 17.5 m; and no chemical interference or reduction in strata overlying the target depth. This should simulate a maximum possible oxygen-diffusion rate (ODR) to the target layer. The aquifer diffusion coefficient D^* for O_2 was calculated using $D = 1.8 \times 10^{-5} \text{ cm}^2\text{-s}^{-1}$ and multiplying by η^2 (η is porosity) for each layer (Hendry, Cherry and Wallick 1986). Results indicated about 200 years to first DO response at 16.5 m followed by a long-term ODR of about $0.04 \text{ mg-L}^{-1}\text{-y}^{-1}$ into the target layer. Integrating the ODR over 8 ky indicated that a total DO of 81 and 74 mg-L^{-1} would have reached the target layer under the net recharge and discharge areas, respectively. If that DO were consumed by pyrite oxidation (Eq. 2, p. 5), an estimated maximum sulfate concentration of 456 and 417 mg-L^{-1} would have formed under net recharge and discharge zones after 8 ky (from the Eq. 2, gravimetric sulfate = $\text{DO} \times 5.63$). For diffusion without advection, simulated first response in the target layer was about 1 ky, and the maximum equivalent concentration of oxygen was 16 mg-L^{-1} or 90 mg-L^{-1} sulfate in the target layer. All cases are less than half of the modern sulfate concentration of 970 mg-L^{-1} . All simulated concentrations in the target layer are too low to increase sulfate concentrations the shallow-till aquitard at 31.5 m from an initial concentration of 140 mg-L^{-1} to the modern (640 mg-L^{-1}) concentration.

For a second model approach we used the maximum measured DO (3 mg-L^{-1}) in the deep EVA on Table 10 and assumed that a single large DO entry of that magnitude reaches the deep EVA aquifer each year, followed by immediate oxidation of pyrite to sulfate and a final $\text{DO} < 1 \text{ mg-L}^{-1}$. We applied the same CDM model conditions as above, but with the following differences: constant DO of 0.9 mg-L^{-1} in all surface nodes; initial $\text{DO} = 0.9 \text{ mg-L}^{-1}$ in the EVA and silt, and 140 mg-L^{-1} in the till aquitard; and the bottom five meters of the EVA (to 12.5 m) treated as internal nodes with constant sulfate flux of $12.8 \text{ mg-L}^{-1}\text{-y}^{-1}$ (derived from a stoichiometric conversion (Eq. 2, p. 5) of 2.25 mg-L^{-1} reducible DO to sulfate). Results indicated that within the ambient recharge-discharge system sulfate concentrations reached 970 mg-L^{-1} only near the outer boundary

of the net discharge zone between 3.2 and 5.2 ky, and there was little effect on the till aquitard after 8 ky.

In addition to simulated results, large COD from ample pyrite-S at mid aquifer and in the silt layer (above the target depths), and published reaction rates for pyrite-S (McKibben and Barnes 1986, Anderson et al. 2001) render even the maximum simulated rates of sulfate accretion in the silt and till aquitard target depths implausible. A modern source of high sulfate in the deep EVA thus is not feasible.

6.2.1.4 Hypothesis: Historical Oxidation in the Silt Layer

Because the largest pyrite-S concentration is in the silt layer (Fig. 14) we propose that one possible scenario is that higher particle densities of pyrite may have caused preferential accumulation of pyrite in the silt layer during deltaic deposition. An OE then occurred in which pyrite-S oxidized within the silt layer. For reasons determined in the previous section (6.2.1.3) the required oxidizing conditions could only have occurred during glaciofluvial deposition (approx. 12 to 10 cal. ky B.P.), or during a climatic episode with a much lower water table.

We employ both the "flow-through model" FTM and the "closed-depression model" CDM described in the Appendix, with an initial high uniform sulfate concentrations (C_o) in the silt layer and EVA. The models are used to measure the redistribution time (t_f) required to match modern concentrations in the till and silt. During redistribution sulfate increases in the till aquitard (through diffusion from the silt layer) and decreases in the silt through diffusion to the till and lower EVA. Larger C_o take longer to deplete from the silt layer, but diffuse more quickly to the underlying till aquitard due to the larger diffusion gradient. Because silt depletion and till enhancement functions are inverse we can establish a unique t_f and C_o at which modern concentrations in both the silt and till match (Fig. 23).

Using the FTM model, the matching C_o for Site 9 is 1.6 g-L^{-1} and t_f is 3.9 ky following the OE. The matching C_o for Site 8 is 1.4 g-L^{-1} and t_f is 6.2 ky following the OE. Sulfate profile matches and initial concentrations are shown on Fig. 24, and on Table 23 (FTM#6.2.1.4-1 and FTM#6.2.1.4-2).

The CDM model was employed for Sites 8 and 9 using both 1990 and 1993 climate scenarios. An example of the t_f vs. C_o matching procedure applied to net recharge and discharge zones using the CDM model is shown on Fig. 25. Simulated C_o for both Sites were between 1.4 and 2 g/L under the net recharge areas, and were slightly lower under the net discharge areas (Table 14, CDM#6.2.1.4-3 through CDM#6.2.1.4-6). Matching t_f were between 1.9 and 2.6 ky under the net recharge area and between 2.6 and

3.3 ky under the net discharge area. For Site 8 matching t_f were between 3.1 and 4.4 ky under the net recharge area and between 4.1 and 6 ky under the net discharge area. Profile fits for the CDM (not shown) are similar to those for the FTM (Fig. 24).

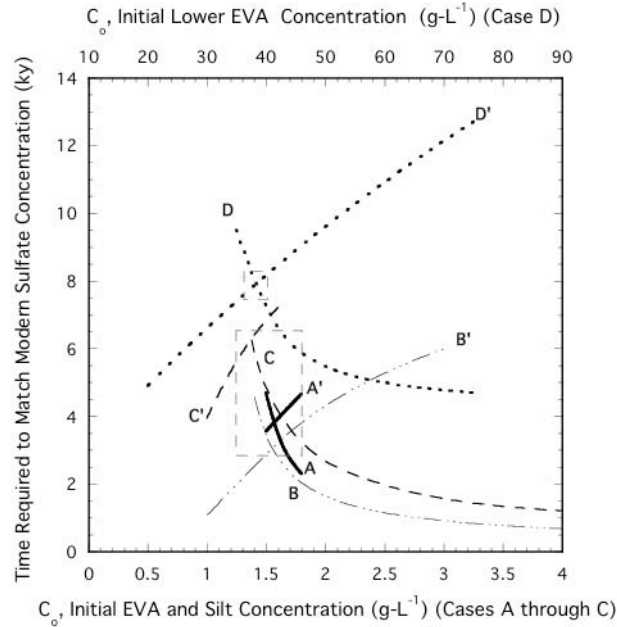


Figure 23. Simulated time from the oxidizing event and initial uniform sulfate concentrations in the silt layer required to match the modern sulfate profile in the silt (A through D) and underlying till aquitard (A' through D') using the FTM Model. Simulated values are determined by the matched intersecting lines. Paired simulations D and D' are for the FTM applied to a maximum sulfate concentration in the bottom of the EVA (top axis scale) following an oxidizing event in the lower EVA.

Site 7 represents a variant case in which the maximum sulfate is in the shallow till rather than the silt. We propose that this occurred because of the thinness of the silt layer (4 m) near the western boundary of the EVA compared with thicker (15 m) silt on Sites 8 and 9. The thinner silt layer (and smaller total sulfate pool) resulted in earlier depletion of sulfate. At some time after the OE, sulfate in the silt decreased to a concentration equal to that in the underlying till. We call this the "crossover time." Thereafter the till became the conserving layer, back-feeding sulfate to the silt layer as it continued to deplete into the overlying EVA. In this case, since both the silt and till are decreasing, we cannot identify a unique converging C_o and t_f as in Sites 8 and 9. We can, however,

Table 14. Simulated sulfate concentration, C_o , in the EVA and silt layer, duration of oxidizing conditions, t_s , and redistribution time, t_r , following the oxidizing event, OE, for the silt-layer source model scenarios, discussed in Section 6.2.1.4.

Model			Site	Year	Net Recharge Area				Net Discharge Area			
Type	#	Description			Center (CDM)*		Periphery		Inner Boundary		Outer Boundary	
					C_o g/L	t_r ky	C_o g/L	t_r ky	C_o g/L	t_r ky	C_o g/L	t_r ky
FTM	6.2.1.4-1	Net Recharge = 0.007 m/y, Gradient = 0.00024	9	-	1.6	3.6	-	-	-	-	-	-
FTM	6.2.1.4-2	Net Recharge = 0.007 m/y, Gradient = 0.00007	8	-	1.4	6.2	-	-	-	-	-	-
FTM	6.2.1.4-1a	Net Recharge = 0.007 m/y, $\nabla_x = 0.00015$	9		1.57	3.75	-	-	-	-	-	-
FTM	6.2.1.4-1a	Net Recharge = 0.007 m/y, $\nabla_x = 0.00023$	9		1.59	3.55	-	-	-	-	-	-
FTM	6.2.1.4-1a	Net Recharge = 0.007 m/y, $\nabla_x = 0.0004$	9		1.62	3.22	-	-	-	-	-	-
FTM	6.2.1.4-1a	Net Recharge = 0.007 m/y, $\nabla_x = 0.0008$	9		1.66	2.99	-	-	-	-	-	-
FTM	6.2.1.4-1b	Net Recharge = 0.01 m/y, $\nabla_x = 0.00024$	9		1.64	3.16	-	-	-	-	-	-
FTM	6.2.1.4-1b	Net Recharge = 0.03 m/y, $\nabla_x = 0.00024$	9		1.9	2	-	-	-	-	-	-
FTM	6.2.1.4-1b	Net Recharge = 0.08 m/y, $\nabla_x = 0.00024$	9		2.15	1.5	-	-	-	-	-	-
FTM	6.2.1.4-1b	Net Recharge = 0.16 m/y, $\nabla_x = 0.00024$	9		3.2	0.8	-	-	-	-	-	-
FTM	6.2.1.4-1c	Net Recharge = 0.007 m/y, $\nabla_x = 0.0008$ $d(x) = 0.003\text{m}\cdot\text{y}^{-1}$	9		1.53	3	-	-	-	-	-	-
CDM	6.2.1.4-3	0.9 g/m ³ influx nodes	9	1990	2	1.9	1.83	2.49	1.79	2.58	1.73	2.85
CDM	6.2.1.4-4	0.9 g/m ³ influx nodes	9	1993	1.93	2	1.75	2.6	1.73	2.79	1.66	3.32
CDM	6.2.1.4-5	0.9 g/m ³ influx nodes	8	1990	1.68	3.1	1.51	4	1.48	4.15	1.4	5
CDM	6.2.1.4-6	0.9 g/m ³ influx nodes	8	1993	1.6	3.24	1.43	4.42	1.43	5.1	1.36	6
CDM	6.2.1.4-7	43 g/m ³ influx nodes	9	1990	1.98	1.92	1.82	2.53	1.78	2.62	1.72	2.99
CDM	6.2.1.4-7	120 g/m ³ influx nodes	9	1990	1.96	2	1.79	2.68	1.76	2.72	1.7	3.2
CDM	6.2.1.4-8	1/2 x K	9	1990	1.96	1.84	1.82	2.46	1.78	2.54	1.72	2.84
CDM	6.2.1.4-8	2 x K	9	1990	1.98	2	1.82	2.47	1.82	2.68	1.72	2.86
CDM	6.2.1.4-9	1/2 x D	9	1990	2.2	2.76	1.97	3.94	1.93	4	1.88	4.3
CDM	6.2.1.4-9	2 x D	9	1990	1.82	1.2	1.7	1.5	1.67	1.58	1.61	1.8
CDM	6.2.1.4-10	Long ($r_r=60\text{m}$)	9	1990	2	1.42	1.86	1.79	1.82	1.96	1.64	2.58
CDM	6.2.1.4-11	Annual Mean Net Discharge and Recharge	9	1990	1.54	4.2	1.49	5.2	1.45	6.28	1.4	8.5

* FTM results are from the simulated location (x on L_x) corresponding to the hydraulic gradient for the designated Site (7,8, or 9).

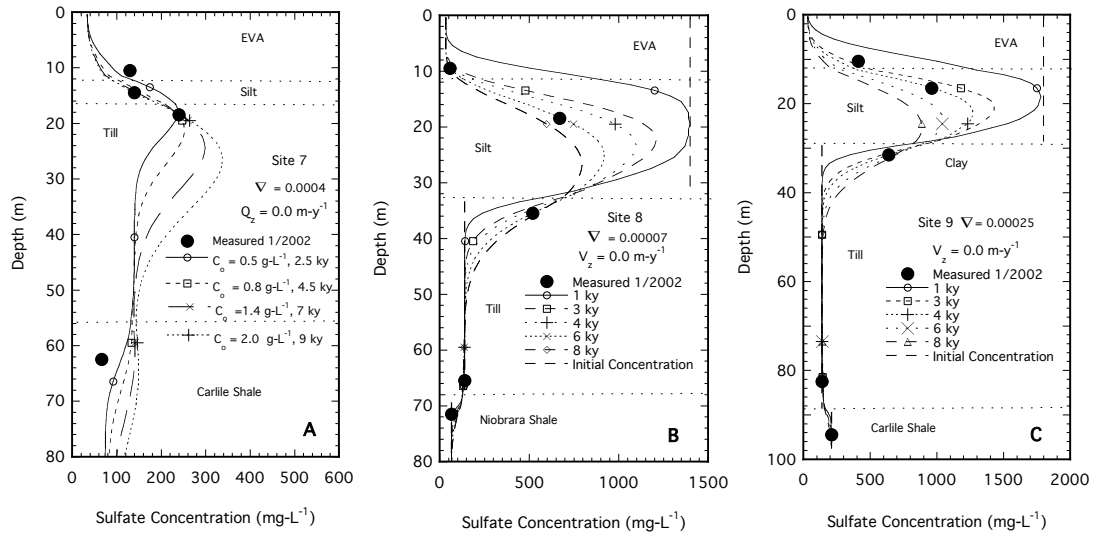


Figure 24. Temporal changes in simulated sulfate redistribution profiles and comparison with the modern distribution for Sites 7 (A), 8 (B) and 9 (C) on Transect B-B'.

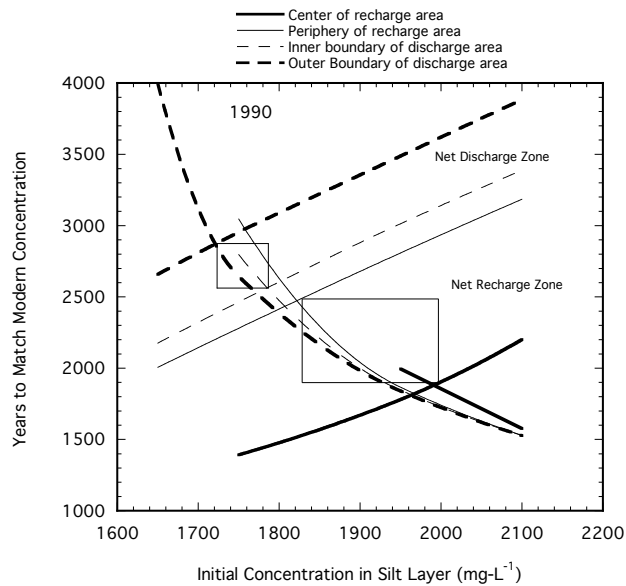


Figure 25. Simulated redistribution times (t_f) following the OE and required initial sulfate concentrations (C_0) in the EVA and silt layer, following the OE, to match the modern sulfate distribution on Site 9 using the CDM model.

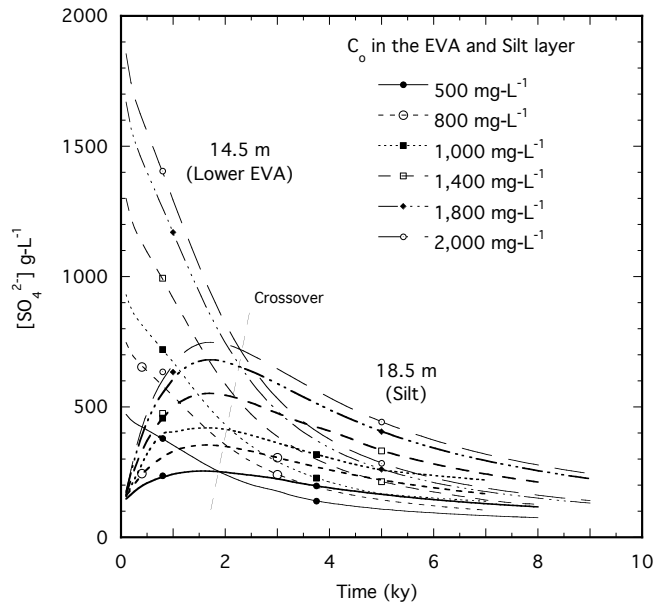


Figure 26. Simulated sulfate concentrations in the silt and shallow till layers vs. simulated redistribution time for varying initial sulfate concentrations in the silt layer. The "crossover" is the time and concentration at which the sulfate concentration in the silt source depletes to that of the till sink, and the till becomes the new source.

identify the "crossover time." Using the FTM model, crossover times for C_0 in the approximate range of those identified for Sites 8 and 9 are shown on Fig. 26. All are near 2 ky. This provides a lower limit for times required to match the modern sulfate profile. Profile matches for Site 7 using several C_0 are shown on Fig. 24A. Best fits were for $t_f > 4.5$ ky.

6.2.1.5 Model Sensitivity

Several model parameters and boundary conditions were tested for sensitivity using the silt-layer source hypothesis with both FTM and CDM models.

First, the effect of using the 0.9 mg-L^{-1} constant concentration in the surface nodes during recharge periods was examined. The 0.9 mg-L^{-1} value is based on 10 years of mean sulfate concentrations measured in rainfall at Icelandic State Park during the 1990s. It is arguable that modern and historical oxidation of sulfide certainly occurred and continues to occur in the upper aquifer and in the overlying vadose zone. This is

indicated by modern surface concentrations which are usually between 43 and 120 $\text{mg}\cdot\text{L}^{-1}$ in the upper aquifer. Results for simulations using the CDM and upper boundary concentrations of 43 and 120 $\text{mg}\cdot\text{L}^{-1}$ (Table 14, CDM#6.2.1.4-7) indicate low sensitivity of long-term results in the silt and deep till aquitard.

Second, sensitivity to K and D were examined by varying parameter values in all layers by 0.5x and 2x. Results for K (Table 16, CDM#6.2.1.4-8) indicated little effect on outcomes. Results for D (Table 16, CDM#6.2.1.4-9) indicated that simulated t_f was 700 to 800 years less under 2xD, and 1.05 to 1.45 ky more under 0.5xD. Similar results were determined using the FTM.

The effect of variability of path length in the CDM model was examined by simulating a closed depression having 3x the radial path length in both net recharge and net discharge zones. A 24 to 28% decrease in t_f was found. The decrease was larger under the net recharge area than under the net discharge area.

The FTM is not sensitive to simulation path length (L_x) as long as model q_x and ∇_x for the point of comparison are constant. Simulated t_f decreases with increasing ∇_x for a given q_x (∇_x increases with increasing x on L_x). However, the difference is < 1 ky over an order of magnitude change in ∇_x (Table 16, FTM#6.2.1.4-1a). Time is highly sensitive to, and decreases as a power function of q_x for a given ∇_x (Table 16, FTM#6.2.1.4-1b). This is an important relationship and will be discussed more fully later.

Finally, we examined the effect of using a single composite net annual recharge ($\sim 5 \text{ cm}\cdot\text{y}^{-1}$) and discharge ($\sim 3 \text{ cm}\cdot\text{y}^{-1}$) for the CDM model, in place of the intra-annual recharge-discharge regime based on the rainfall distribution and root extraction. Results (Table 16, CDM#6.2.1.4-11) indicated somewhat longer t_f . Between 4.2 and 5.2 ky were required under the net recharge area, and 6.2 to 8.5 ky were required under the net discharge area.

6.2.1.6 Hypothesis: Historical oxidation in the lower EVA

One possibility, supported by the apparent relative depletion of pyrite-S in the lower 5 m of the EVA (Fig. 14), is that the OE occurred in the lower EVA. In this case, we propose that the water table receded during a period of prolonged drought, allowing for oxidizing conditions in the bottom of the aquifer. Because of the distance across the silt layer, large concentrations of sulfate would be required in the lower EVA to create a concentration gradient sufficient to match the modern concentration in the upper till aquitard. If it is assumed that pyrite in the silt layer has undergone little oxidation, and that the original % pyrite-S was similar in the silt and deep EVA, the maximum

equivalent concentration of sulfate that could have resulted from oxidation of sulfide over a short period of time is shown on Fig. 27. The mean concentration for the bottom 5 m of the EVA (allowing for porosity) could have been about 33 g-L⁻¹, with a maximum concentration of 75 g-L⁻¹ about 1.5 m above the upper boundary of the silt layer.

Sulfate concentrations of this or larger magnitude have, in fact, been both predicted and observed in situations where there is low flow through pyrite-rich media (Wisotsky, 1998). Such large sulfate concentrations assume sufficient quantities to overwhelm calcium so that sulfate is not precipitated as gypsum. The chemical environment, common in mine spoils, would be extremely acidic and would have dissolved calcite early in the acidification process. Lack of calcite in modern bottom sediments (Appendix 3) is consistent with a historical system of this nature.

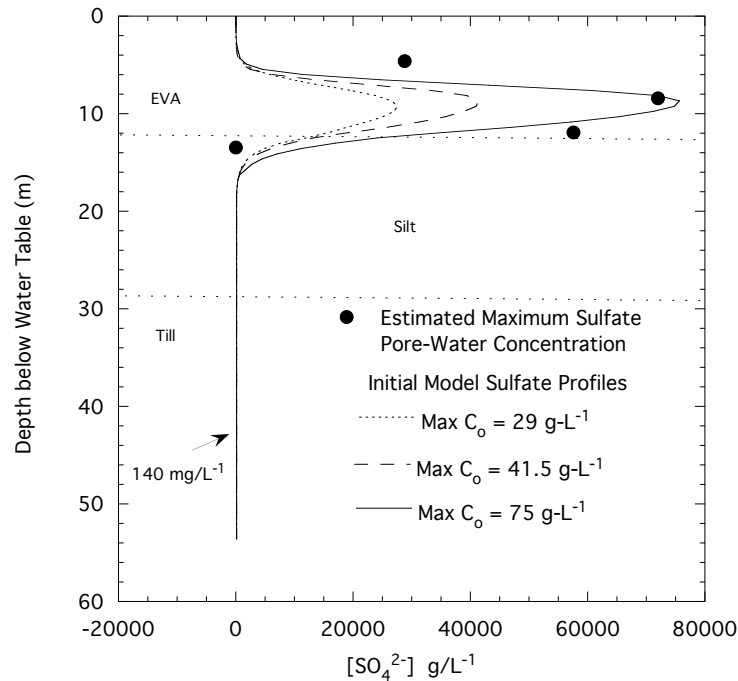


Figure 27. Estimated maximum possible sulfate concentration in the lower EVA from short-term oxidation of pyrite-S, calculated from sulfide depletion in relation to the underlying silt layer.

We first apply the FTM with the C_o profile matching or proportional to the sulfate profile shown in Fig. 16. In discussion C_o regimes are identified by their maximum value in the aquifer profile. Optimal C_o and t_f are determined as discussed for the silt-layer source model above. If we assume that the sulfide oxidation was effectively

instantaneous (within a few years), an initial maximum concentration of 39 g-L^{-1} and a redistribution time 7.9 ky would have been required (Fig. 23, Table 15, FTM #6.2.1.6-1).

Alternately, we propose a scenario in which the water table declined, and remained low and essentially static for a period of time, labeled t_s , during a period of prolonged drought. We assume that, during t_s , low water tables, uncoupled ET, negligible recharge and negligible local flow occur. During this static period DO enters the lower EVA and reacts with pyrite-S at a rate limited by the ODR, or by the pyrite reaction surface (McKibben and Barnes 1986, Anderson et al. 2001). To simulate gradual sulfate oxidation within the deep EVA we apply individually several trial $\frac{dC}{dt}$ for sulfate as constant solute flux stresses within designated interior nodes for the bottom 5 m over t_s . C_o are 0.9 mg-L^{-1} in the EVA and Silt layers and 140 mg-L^{-1} in the till aquitard. The maximum allowable t_s is 4.5 ky, based on an approximate duration of the Hypsithermal Interval (Bluemle 1991). This is discussed further in Section 4.1. This simulation is followed by a subsequent dynamic time period, t_d , over which the aquifer quickly refills to modern levels and the modern flow system is simulated. For the simulated t_d period, C_o are the final C values from the t_s simulation. Constant solute flux in interior nodes are not employed during t_d . Sulfate concentrations are determined entirely by surface influx and advective and dispersive redistribution within the ambient FTM net recharge and flow regime. Total sulfate oxidation and redistribution time t_f is the sum of t_s and t_d . For several trial $\frac{dC}{dt}$ scenarios (Table 15, FTM #6.2.1.6-2) t_f vs. t_s are optimized for matches with known modern concentrations. All simulated t_s are between 0.4 and 2.4 ky, and all t_f are between 8 and 9.5 ky.

For the CDM model, we examined several C_o profiles assuming near instantaneous oxidation similar to FTM #6.2.1.6-1 (Table 15) but employing the static time for the high initial value as in FTM #6.2.1.6-2. Results (Table 15, Model CDM #6.2.1.6-3) indicated that t_s is between 1.04 to 3.6 ky under the net recharge regime and between 0.85 and 2.8 ky under the net discharge regime for all $C_o > 35.3 \text{ g-L}^{-1}$. For C_o of 25.2 g-L^{-1} all t_s were above the maximum allowable 4.5 ky. All optimal t_f were between about 5 and 6.5 ky under the net recharge area, and between 5.3 and 7.2 ky under the net discharge area.

We also employed a CDM model that assumed a gradual oxidation of pyrite-S to sulfate within the bottom 5 m of the EVA, using constant solute flux into interior nodes similar to Model FTM #6.2.1.6-2 (Table 15). Results (Table 15, Model CDM 6.2.1.6-4) indicated that t_s varied from 0.84 to 2.4 ky under both the net recharge and net discharge

areas. Final t_f were between 4.4 and 6.3 ky under the net recharge area and 5.2 and 7 ky under then net discharge area. In this case, however, the largest $\frac{dC}{dt}$ applied (62.1 mg-L⁻¹-y⁻¹) resulted in a maximum C value of 88 g/L in the lower EVA, which is larger than the maximum possible (75 g-L) concentration for semi-instantaneous oxidation of pyrite-S, based on pyrite-S mineral measurements. The lower rate (15.3 mg-L⁻¹-y⁻¹) results in a profile maximum within the allowed range.

Table 15. Simulated initial sulfate concentration, C_o ; or (as indicated) the rate of sulfate formation, $\frac{dC}{dt}$, through local in-situ oxidation in the deep EVA; duration of oxidizing conditions (t_s); and total final redistribution time (t_f) following the deep EVA oxidizing-event (OE) sulfate source-layer scenario (Section 6.2.1.6).

Model			Site	Net Recharge Area				Net Discharge Area			
Type	#	C_o / $\frac{dC}{dt}$		Center (CDM) †		Periphery		Inner Boundary		Outer Boundary	
				t_s ky	t_f ky	t_s ky	t_f ky	t_s ky	t_f ky	t_s ky	t_f ky
FTM	6.2.1.6-1	39 g-L ⁻¹	9	0	7.9	-	-	-	-	-	-
FTM	6.2.1.6-2	12.5 mg-L ⁻¹ -y ⁻¹	9	2.4	9.5	-	-	-	-	-	-
FTM	6.2.1.6-2	25	9	1.36	8.5	-	-	-	-	-	-
FTM	6.2.1.6-2	50	9	0.71	8.38	-	-	-	-	-	-
FTM	6.2.1.6-2	100	9	0.4	8	-	-	-	-	-	-
						-	-	-	-	-	-
CDM	6.2.1.6-3	68.5 g-L ⁻¹	9	1.4	4.95	1.04	5.05	0.94	5.3	0.85	5.8
CDM	6.2.1.6-3	54.2	9	2	5.2	1.53	5.68	1.48	5.68	1.35	6.2
CDM	6.2.1.6-3	41.5	9	2.86	5.8	2.4	6	2.16	6.09	2.04	6.65
CDM	6.2.1.6-3	35.3	9	3.56	6.29	3.02	6.5	2.84	6.6	2.6	7.2
CDM	6.2.1.6-3	25.2	9	>4.5	-	>4.5	-	4.55	7.7	-	8
CDM	6.2.1.6-4	15.3 mg-L ⁻¹ -y ⁻¹	9	2.4	6	2.2	6.3	2.19	6.4	2.15	7
CDM	6.2.1.6-4	62.1 ¶	9	0.94	4.4	0.84	4.8	0.85	5.21	0.85	6

† FTM, results are from the simulated location (x on L_s) corresponding to the hydraulic gradient for the designated Site (7,8, or 9).

§ Maximum simulated sulfate concentration reached = 43 g-L⁻¹

¶ Maximum simulated sulfate concentration reached = 88 g-L⁻¹

6.2.1.7 Discussion of Deep EVA Sources

The data indicate that the proximate modern source of high sulfate concentrations in the deep EVA is in the underlying silt layer. From the silt layer the sulfate is transported, primarily through diffusion, to the underlying till aquitard and to the overlying EVA where it is eventually removed through seepage or evaporative discharge.

Eventually, and more quickly if the conserving silt layer is thin, or if the overlying recharge regime is larger, the sulfate in the silt layer is depleted to a concentration less than the underlying till aquitard. The latter then becomes the conserving layer, slowly back-feeding sulfate into the silt layer. The modern proximate source in the deep EVA is not gypsum. There is ample pyrite throughout the aquifer and in the underlying silt. The most plausible source of sulfate, therefore, is in-situ oxidation of pyrite-S.

Advection-dispersion models for a closed-depression hydrologic system similar to that of the prevailing soils, and for a flow-through hydrologic system indicate that the OE cannot be recent. Moreover, it cannot have occurred primarily in the shallow aquifer, or through long-term influx of DO to the deep EVA under modern flow-system and water-table conditions. A much reduced water-surface elevation would have been required to enable the OE in the deep EVA or silt layer. Using hydrologic models we have explored the possibilities of a historical oxidizing event in either the silt layer, or in the deep EVA. Both historical sources were found to be feasible. For both FTM and CDM models, all simulated redistribution times following the oxidizing event required several thousand (2.5 to 8 ky) years to match the modern sulfate profile. Varying major model parameters within a reasonable range ($\times 2$ or 0.5) did not alter this conclusion.

6.2.1.8 Climatic Cause of the OE

We cannot identify with certainty the specific event that caused the OE. However, the general time frame established suggests that a plausible time would be the Hypsithermal Interval, a period of prolonged drought that occurred locally from about 8 to 4.5 cal. ka (Bluemle, 1991). Forman et al. (2001) have summarized studies indicating aridity in the northern and eastern border of the Great Plains between 9 and 5 cal. ka, with peak aridity between 7.5 and 5 cal. ka. In central Minnesota increased aridity from 4.8 to 4.3 cal. ka were also noted. Hendry et al. (1986) determined that a 15-m lower water table required to form the modern sulfate profile in a glacial till (in southern Alberta) from the oxidation of organic matter could only have occurred during the Hypsithermal Interval. To determine potential aquifer drawdown over a prolonged (3-4 ky) drought we employed a variation of the FTM using the same properties and parameters as those previously described, but with a seepage face through both the sand and silt layers, to simulate the incised Turtle River, and distance of 15 km from the flow barrier (PE) to the river. To simulate the effect of a prolonged drought we assumed negligible net annual recharge. This same recharge assumption was made by Hendry et al. (1986) in their hydrologic model. The feasibility of this assumption is supported by chloride profile studies in the arid Sudan (Edmunds et al., 1990) which have indicated a

long-term average recharge of only $0.72 \text{ mm}\cdot\text{y}^{-1}$. Results (Fig. 28) indicate that over a 1 to 3 ky nil-recharge period the EVA water level could approach the upper boundary of the silt boundary, but that the hydraulic resistance of the silt layer would be sufficient to retain water. An exception would be near (within 1 to 3 km) the seepage face.

6.2.1.9 Stratigraphic Location of the OE

We have proposed the deep EVA and the silt layer as potential locations for the OE. The retention of water in the silt layer indicated by the seepage model means that sulfide oxidation in the silt layer would depend on the ODR and the COD of that layer. Hendry et al. (1986) employed an oxygen diffusion model combined with COD estimates for oxidation of organic sulfur in a till and determined that, over the Hypsithermal Interval, the oxidized layer would likely be $< 2 \text{ m}$ beneath the water table. The thickness of the modern EVA shallow-oxidized zone, which is $< 2\text{m}$, indicates similar limits for the EVA. Large modern COD represented by pyrite-S in the silt layer and evidence of persistent saturation in the silt layer indicate that historical oxidation in the silt layer is unlikely except, perhaps, near the surface of the silt layer. The limits of dewatering combined with depleted sulfate-S in the deep EVA indicate that the deep EVA is a more plausible principle source for sulfate oxidation during the OE.

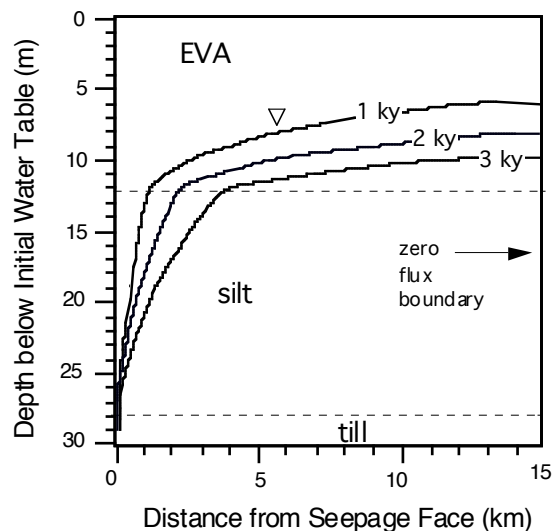


Figure 28. Simulated water-table depth for a seepage face at the Turtle River with zero net annual recharge.

The deep EVA scenario would have created an acid environment. However, the ambient flow system has been predominant for more than 4 ky, and sulfide oxidation in the lower EVA and upper silt has been minimal for that time. With a mean cycling time of about 117 years, EVA water has been replaced many times. Sulfate-to-chloride ratios for the deep EVA and shallow till aquitard (Fig. 13b,c, and d) are consistent with acidification, dissolution of carbonate minerals, release of calcium, and subsequent sodium mobilization through cation exchange. SEM and x-ray diffraction analysis (Appendix 3) of one silt sample (Site 6, just below the EVA boundary) has indicated that four of five points analyzed are low in mineral calcium (<3.25% wt.), and one point having large calcium (46.9% wt.) most likely indicates dolomite (20.23% Mg by wt.). The likely presence of iron as iron carbonate and iron sulfate is also indicated. The modern pH for the deep and shallow till are between 7.8 and 8, while those of the deep EVA are silt and are below 7.6 and range as low as 6.8, indicating that they are not buffered by calcite. These are consistent with a relic acidified environment in the deep EVA and silt layers.

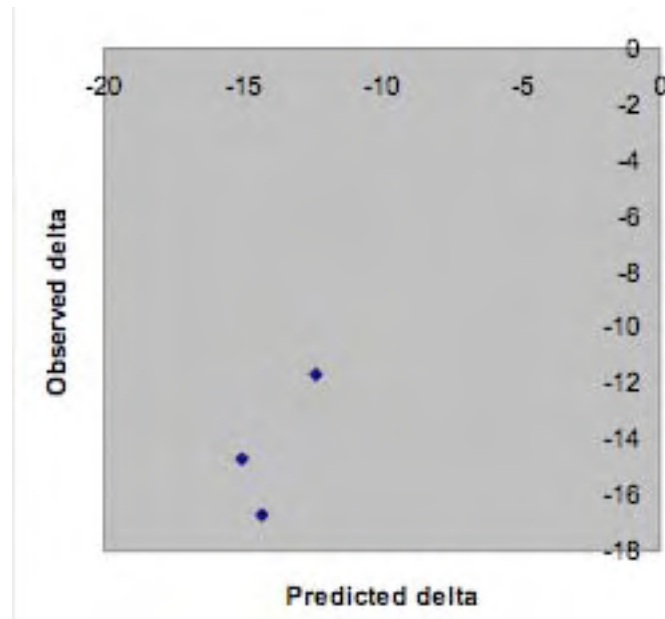


Figure 29. Comparison of observed sulfate $\delta^{34}S$ in basal silt/till with that predicted from Rayleigh fractionation applied to the diffusional loss model.

6.2.1.10 Impact of Long-Term Diffusion on Sulfate $\delta^{34}S$ in the Retentive Layer

Diffusion of sulfate out of the silt layer will be accompanied by a small isotopic effect, since the diffusion coefficient for lighter $^{32}\text{SO}_4^{2-}$ molecules is slightly greater than that for heavier $^{34}\text{SO}_4^{2-}$ molecules. Over time, diffusive loss of sulfate would cause $\delta^{34}S$ of residual sulfate to increase (become less negative); this process can be described by a Rayleigh fractionation trend. We assume that the sulfate initially present in the lower EVA and silt layers had a $\delta^{34}S$ equal to the mean of the measured pyrite compositions (since there is no isotopic fractionation on pyrite oxidation: Nakai and Jensen 1964; Toran and Harris 1989) and that initial sulfate concentration in the lower EVA and silt layers was 45 g L^{-1} (as indicated by models discussed in Section 6.1.2.6). In this case a fractionation factor of around -4‰ (i.e. $D[^{34}\text{SO}_4^{2-}] = 0.996(D[^{32}\text{SO}_4^{2-}])$, where D is the diffusion coefficient for each isotopomer) can reasonably successfully predict the present distribution of sulfate $\delta^{34}S$ in the silt (or at Site 7 the underlying till) by diffusive loss of sulfate to the present observed concentration (Fig. 29). The isotopic fractionation factor for diffusion of sulfate based purely on the masses of the isotopomers (Graham's Law) is -4.5‰, so the present distribution of sulfate isotopic compositions is entirely consistent with isotopic redistribution during diffusive loss of sulfate from the retentive layer. Therefore the coincidence of predicted and observed sulfate $\delta^{34}S$ both: (i) explains why the present sulfate $\delta^{34}S$ does not correspond identically with the average $\delta^{34}S$ of the pyrite source; and (ii) provides additional confirmation of the chemical evolution of the retentive basal layer by diffusional loss of sulfate from an initial high concentration reservoir with an isotopic composition derived by pyrite oxidation.

6.2.1.11 Soil Great Group Taxa as Indicators of Hydrologic Conditions in the Deep EVA

The soil hydrology of the EVA was explained in Section 1.4. Calciaquoll and associated Haplaquoll soils predominate over areas of the EVA hydrologically characterized as closed depressions or flow-through areas having very small net recharge or small gradients (Fig. 4, Fig. 7). This is most evident in the south EVA. The CDM model was designed to simulate closed-depression hydrology conforming to published Calciaquoll and Haplaquoll intra-annual net recharge and discharge characteristics. Our simulated times for the net discharge area (Calciaquoll) for the OE in the silt layer were about 2.5 to 6 ky. Comparative simulated times for the OE in the deep EVA were 5.3 to 8 ky. These compare well with the simulated time (approx. 5 to 6 ky with net discharge $< 3 \text{ cm-y}^{-1}$) for Calciaquoll soil formation (Knuteson et al. 1989). Both simulated time frames correspond well with the end of the Hypsithermal interval.

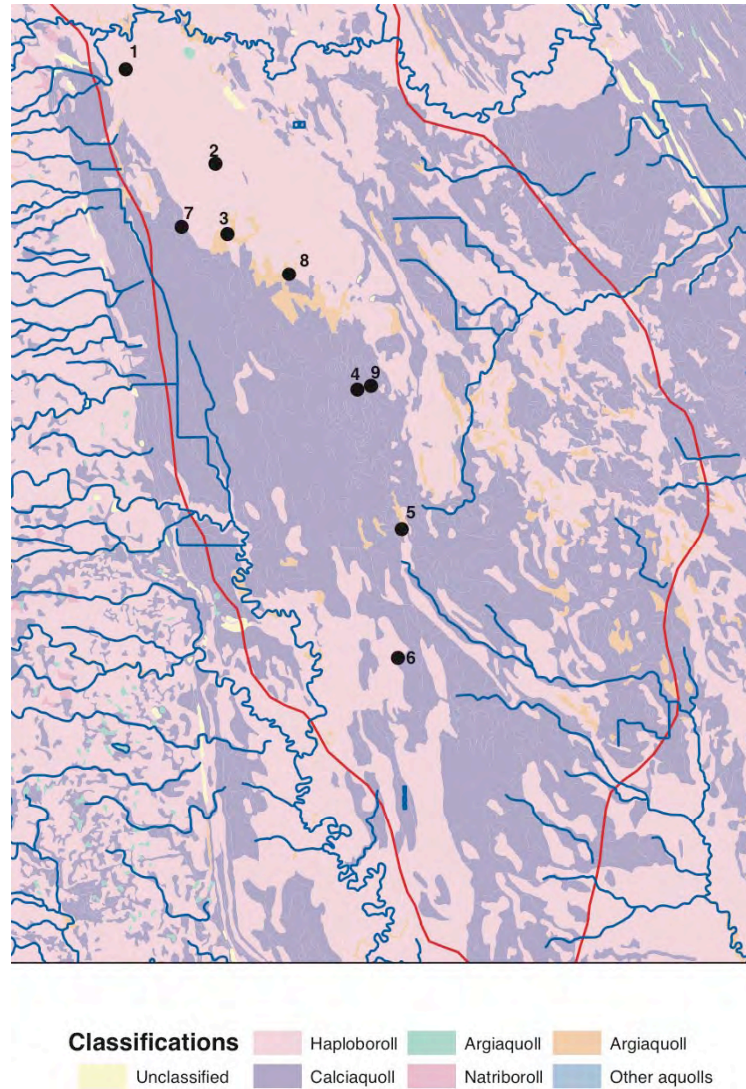


Figure 30. Relationship of sulfate measurement sites on Transect A-A' and B-B' to soil Great Group taxa in the south EVA.

Conversely, the Haploboroll soils predominate over areas of the aquifer having better integrated drainage to the Turtle River and its tributaries and areas of lower water table (Fig. 4, Fig. 7). In these areas, steeper piezometric gradients result from larger cumulative recharge with distance along the flow path, drawdown near discharge zones, and larger local net recharge because of decreased ET with greater water table depth. Haploboroll soils have been measured to have net recharges of about 15 to 18 $\text{cm}\cdot\text{y}^{-1}$ (Oakes citation in Section 1.5 above, and Schuh et al. 1993). These conditions are simulated using the FTM (Table 14, FTM #6.2.1.4-1a and FTM #6.2.1.4-1b). Times as short as 0.8 ky are simulated for the net recharge values in the designated range.

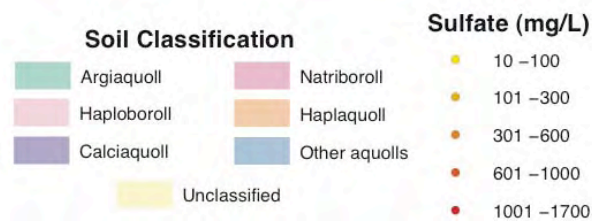
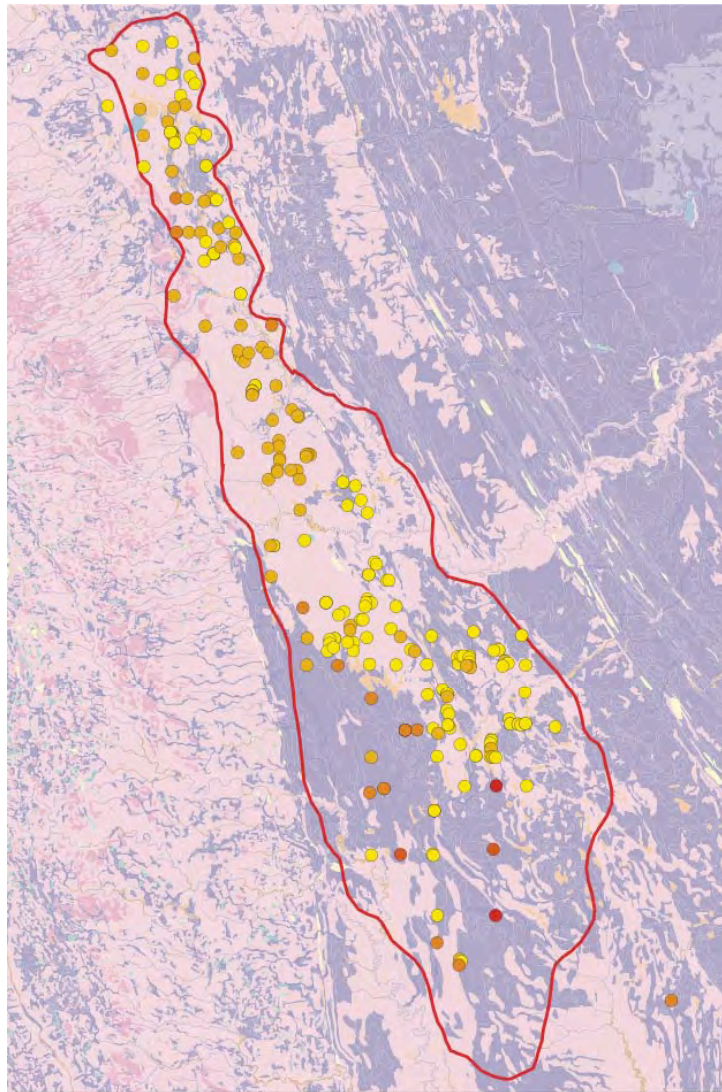


Figure 31. Map of soil Great Group taxa and sulfate concentrations measured for all EVA wells from the SWC database.

This means that the redistribution of sulfate and its depletion from the conserving silt layer occur most slowly under the Calciaquolls, slightly more quickly under the hydrologic regimes represented by the Haploborolls. Based on our simulations, we

would expect that the sulfate concentrations in the deep EVA and silt would be largest under the Calciaquoll soils and least under the Haplaborolls. On Fig. 30 we observe that all cases of elevated ($> 400 \text{ mg-L}^{-1}$) sulfate on the A-A' and B-B' Transects (Sites 4, 5, 7, 8, and 9) are located within or immediately down-gradient from areas mapped as Calciaquoll soils. All experiment sites (Sites 1, 2, 3, and 6) having low sulfate ($< 400 \text{ mg-L}^{-1}$) are located in or immediately down-gradient from areas mapped to Haplaboroll soils. To further test the robustness of this observation we examine the distribution of sulfate concentrations in deep EVA and silt wells in the larger (264 well) SWC database. Results (Fig. 31) indicate that the Calciaquoll-Haplaquoll soil association does, indeed, serve as general indicators of higher sulfate concentrations in the deep aquifer, and that generally lower sulfate concentrations in the deep EVA and silt occur underlying the Haplaboroll soils. This occurs despite the occurrence of fresher water between the deep EVA and aquifer surface, which is hydrologically most directly related to soil formation.

6.2.2 Middle EVA

Our advection-dispersion models for lower-boundary silt sulfate sources predict a monotonically decreasing sulfate profile from the silt layer (or where the silt layer is thin from the underlying till aquitard) to the EVA surface (Fig. 24). Similar models for bedrock-source chloride (not discussed in this report) predict monotonically decreasing chloride from bedrock to the EVA surface. All measured sulfate profiles for the EVA on Transect A-A' conform qualitatively to this expectation at mid aquifer for both sulfate (Fig. 17) and chloride (Table 14). Pyrite-source profiles (Fig. 14) indicate that the middle EVA has the highest pyrite retention. This suggests minimal historical oxidative weathering. Porewater chemistry (Fig. 19) for 1997 and 1998 demonstrate that the middle EVA has the least indicators of acid oxidative weathering ($< \text{pH}$, $> \text{Ca}^{2+}$, $> \text{Mg}^{2+}$, $> \text{Na}^+$), even on sites (Sites 4 and 5) showing signs of recent oxidative activity in the deep and/or surface layers. All of these observations indicate that the middle EVA is least active as a sulfate source and most distance from proximate sulfate sources. It appears to be primarily a receiving layer, with sulfate mainly in the underlying EVA and underlying boundary materials, and some local contributions from the shallow EVA and overlying boundary materials.

6.2.3 Shallow EVA

As discussed in Section 6.2.2 (Middle EVA), the predominance of bottom boundary sources for both chloride and sulfate predict monotonically decreasing sulfate

and chloride to the surface - unless active sulfate sources are operative in the EVA surface layer and in boundary materials.

Chloride concentrations increase in EVA surface porewater compared with mid and deep EVA (Table 14). Despite oxidizing conditions, sulfate-to-chloride ratios for Sites 2, 3, 5, and 6 are smaller in shallow EVA porewater than in locally measured precipitation (Table 14). These indicate that chloride in shallow EVA porewaters are enriched from other surface sources. The most likely source is muriate of potash (KCl) from agricultural fertilizer (Section 3.6).

Waters from locations strongly affected by active sulfate sources exhibit strong and fairly robust relationships for sulfate vs. EC (Fig. 11). While there is a significant correlation for deep and middle EVA sulfate vs. EC (Fig. 20), however, there is no significant relationship between shallow sulfate concentration on Transect A-A'. For all low-sulfate ($<400 \text{ mg-L}^{-1}$) water samples in the SWC data set for the EVA, sulfate-to-chloride ratios correlate mainly with chloride (Fig. 21-B). All shallow EVA sample sites, with the exception of Site 4, correspond with this relationship (Figure 21-B).

In addition there is a strong positive correlation between shallow EVA porewater nitrate-N concentrations and EC, again with the exception of Site 4. These indicate that chemistry of shallow EVA waters are affected by constituents of vadose waters, and particularly the introduction of agricultural fertilizer as chloride and nitrate.

The exception of Site 4 for the relationship between EC and sulfate-to-chloride ratio with chloride and nitrate is explained by the predominance of sulfate and evidence of $< \text{pH}$ and bicarbonate, and locally enhanced sodium and magnesium in shallow porewater (Fig. 19). Site 4 is unique in that unoxidized pyrite remains in the topsoil (Fig. 14) and is depleted in the lower vadose zone and upper EVA. This differs with all other sites on Transect A-A', which are depleted of pyrite in the topsoil. On Site 4 it thus appears that the predominant sulfate source is oxidation of pyrite according to Eq. 1 in the topsoil and subsequent leaching to the shallow EVA. This mechanism, which was proposed by Swanson (1992), is only observed on Site 4.

6.3 Autotrophic Denitrification

The possibility of autotrophic denitrification as a sulfate source in the EVA was first presented by Mayer (1992). Mayer observed the presence of stratified nitrate in the EVA which decreased with depth, and observed that nitrate and sulfate were inversely stratified. He also identified the presence of denitrifying bacteria, but did not differentiate between autotrophic and heterotrophic denitrifiers. Patch and Padmanabhan (1994) measured and reaffirmed the stratification observed by Mayer, and used stratified

$\delta^{15}\text{N}$ isotope profiles to confirm denitrifying activity in the upper EVA. They also used an advection-dispersion model to determine that nitrate stratification with depth could not be accounted for by dilution through advection and dispersion alone.

Stratification of nitrate-N concentrations, and temporal fluctuation of concentrations in the upper EVA (Fig. 32) confirm the observations of Mayer (1992), and indicate that denitrification may be occurring on Transect A-A' sites. On Sites 2, 3 and 5, the lowest concentrations are in spring, followed by increased nitrate concentrations in summer. Site 1 concentrations are also lowest in spring, but the differences from other times are very small and likely insignificant. Sites 4 and 6 have smallest concentrations in December. Both have increased nitrate again in spring and summer, and Site 6 exhibits a large flush of nitrate in the spring of 1998.

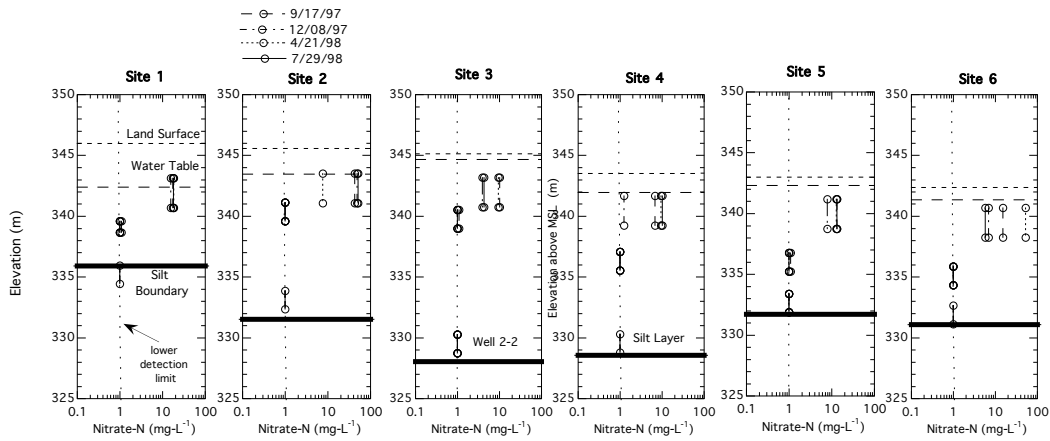


Figure 32. Nitrate-N concentration profiles for water samples collected on 9/17/97, 4/21/98, 12/8/97 and 7/29/98 on Transect A-A'.

6.3.1 Denitrification Rates

Dr. Scott Korom and his students have installed instrumentation on Site 2 to directly measure and quantify denitrification and to identify the relative contributions of carbon, sulfide and iron electron donors. The Larimore EVA site (Site 2) is one of nine sites located in Minnesota (MN) and North Dakota (ND) at which denitrification has been studied using situ mesocosms (ISMs). ISMs are stainless steel chambers that isolate aquifer sediments below the water table. The design, construction, and installation of the ISMs, and how denitrification tracer tests are employed and interpreted are reported in Korom et al. (2005). The resulting aquifer mesocosms allow nitrate to be studied in situ and permit insights into denitrification rates and the associated kinetic orders, apparent

isotopic enrichment factors, and the donors that contribute electrons to the reactions. The Larimore set was installed at Site 2 in 1997, shortly after the construction of Transect A-A'. ISMs were placed at 4.6-6.1 m below land surface, about a meter below first visual evidence (gley) of reducing conditions. Six denitrification tracer tests were conducted at this site, and their results are presented on Table 16. The average denitrification rate for all six Larimore tracer tests is $0.16 \pm 0.06 \text{ mg-L}^{-1}\text{-d}^{-1}$.

Table 16. Summary of denitrification rates, $\delta^{15}\text{N}$ isotopic enrichment, and % of denitrification attributed to pyrite oxidation.

Tracer Test	Start Dates	End Dates	Zero-Order Rate (mg/L/day)	R ²	First-Order Rate (/day)	R ²	$\delta^{15}\text{N}$ Isotopic Enrichment ϵ (‰) ¹	R ²	Denitrification By Pyrite (%) ²
1	12/1/1997	8/30/1998	0.23	0.93	0.013	0.65	-20.4	1.00	62
2	10/27/1998	11/30/1999	0.11	0.95	0.0063	0.72	-27.7	0.92	49
3	9/4/2000	8/29/2001	0.19	0.96	0.0071	0.81	-40.8	1.00	75
4	10/8/2001	10/21/2002	0.20	0.98	0.0065	0.89	-45.1	1.00	80
5	11/13/2002	3/24/2004	0.12	0.90	0.0074	0.66	-38.9	0.99	79
6	6/14/2004	ongoing	0.097	0.94	0.0025	0.93	-32.4	1.00	73

¹ Based only on results reported by the University of Waterloo Environmental Isotope Laboratory.

² With denitrification by pyrite (FeS_2), 14/15 is by sulfide and 1/15 is by Fe(II). These results are based on the final samples taken for each tracer test; the amount of denitrification attributed to pyrite varies from sample to sample.

6.3.2 Denitrification Kinetic Models

The data from all six tests are better fit by zero-order kinetic models than first-order models (Fig. 33). For comparison, examples of fits for two additional kinetic models (labeled Karlsruhe-S) from another aquifer, the Karlsruhe aquifer in north-central North Dakota are also shown. The first-order EVA kinetic model shown on Figure 32 does a good job of representing the data except for the last point, which represents a nitrate-N concentration $< 20 \text{ mg/L}$. This is a typical result for the EVA data. Denitrification rates at most of the other ND and MN sites were better fit by first-order models, but, unfortunately, most of these tests did not have sufficient denitrification rates to reduce the amended nitrate to low levels ($< 20 \text{ mg-L}^{-1}$) during the testing periods (Korom, 2005). However, the two tracer tests at the Karlsruhe-S site (Fig. 33) had sufficient rates to reduce nitrate-N concentrations to this level and first-order models still better fit the data. The initial concentrations (104 mg-L^{-1} for the EVA vs. 99 mg-L^{-1} for Karlsruhe-S) and final concentrations (15.2 mg-L^{-1} for Larimore vs. 12.8 mg-L^{-1} for Karlsruhe-S) for the first and last data points on Figures 1-4, respectively, are similar.

The observation of a zero-order model better fitting the data may be explained by the Michaelis-Menten model for reaction rates:

$$V = \frac{V_{\max} [S]}{K_m + [S]} \quad (5)$$

where V is the rate of reaction, V_{\max} is the maximum rate of reaction, K_m is Michaelis rate constant, and $[S]$ is the substrate concentration. When $[S] \gg K_m$, $V = V_{\max}$, and the reaction is zero-order. When $K_m \gg [S]$, $V = V_{\max} [S]/K_m$, or $V = K' [S]$, which is a first-order reaction. This is the basis of our hypothesis that the rate of the reaction can be used to infer the availability of electron donors relative to the nitrate loading. The rates of denitrification at the Larimore site were about two to 20 times those of the Karlsruhe ISMs. Based on Eq. (5) these observations indicate that the Larimore site has more available electron donors, which is true based on electron donor analysis (Tesfay 2006). Larimore has more pyrite, which seems to be a preferred electron donor at our sites (compared to organic carbon and ferrous iron), and more organic carbon. The Karlsruhe sites have comparable levels of ferrous iron. Furthermore, the Larimore site has the fastest denitrification rates in our network of ISMs.

During denitrification, ^{15}N is enriched in the remaining nitrate (e.g., Wellman et al., 1968; Delwiche and Steyn, 1970; Blackmer and Bremner, 1977). Denitrification takes several steps (Firestone, 1982); however, Mariotti et al. (1982) showed that it can be successfully modeled in soil as a single-step, unidirectional model such that the isotopic composition of nitrate during denitrification increases proportionally with the natural logarithm of the residual nitrate fraction (Mariotti et al., 1988):

$$\delta_s = \delta_{s_0} + \epsilon \ln(C/C_0) \quad (6)$$

where δ_s is the isotopic composition of the nitrate at time, t , and δ_{s_0} that of the initial nitrate. C is the concentration of nitrate at t and C_0 that of the initial nitrate. ϵ is the isotopic enrichment factor; greater enrichment results in a more negative value. Bryan et al. (1983) using cultures of *Pseudomonas stutzeri* found a negative correlation between ϵ and denitrification rate (greater rates resulted in smaller negative values for ϵ) when the rate was increased by adding more electron donor (succinate). Mariotti et al. (1982) also found in laboratory experiments with soils that higher denitrification rates were accompanied by less enrichment (smaller negative numbers). Citing this work, several

investigators have made qualitative estimates on aquifer denitrification rates based on values of “apparent” isotopic enrichment values (e.g., Mariotti et al., 1988; McMahon et al., 1999; Böhlke et al., 2002). McMahon et al. (1999) and Böhlke et al. (2002) correctly use the term “apparent” isotopic enrichment values. Unlike the work of Bryan et al. (1983) it is unlikely that a single bacterium is involved in aquifer denitrification.

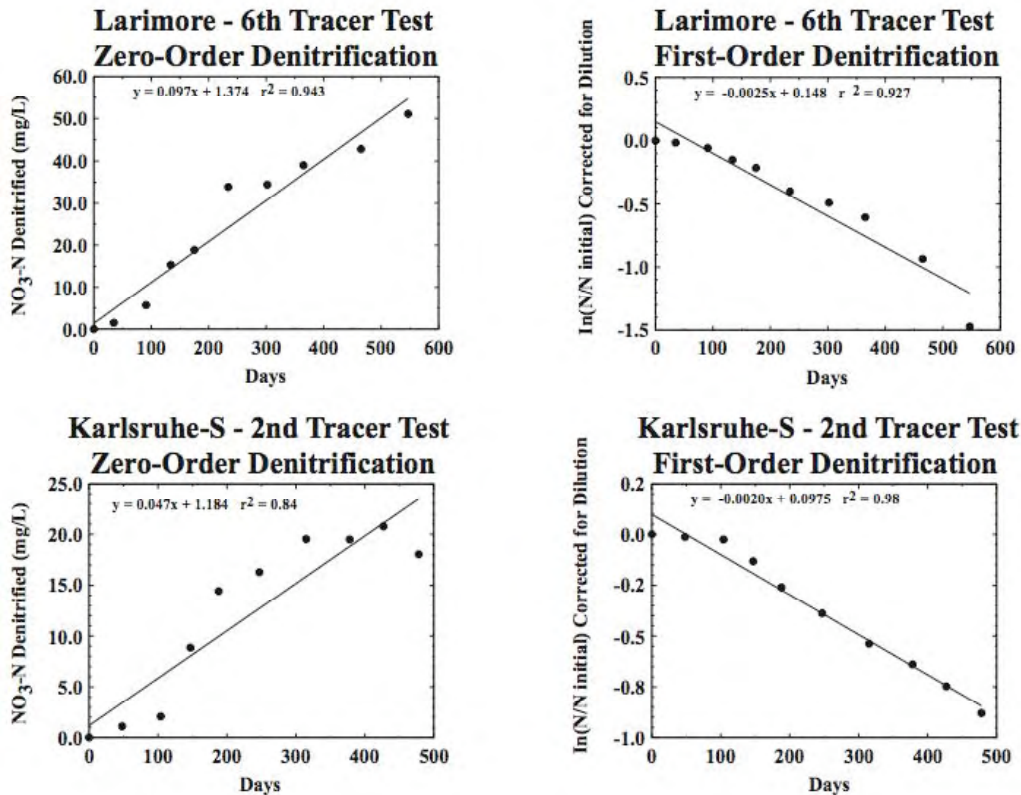


Figure 33. Comparison of zero- and first-order kinetic models for denitrification for in-situ measurements of the EVA (Larimore) and Karlsruhe aquifer ISM sites.

Rather, aquifer denitrification research tends to integrate processes over a large area and with a suite of electron donors (Korom, 1992). For example, McMahon et al. (1999) found evidence of denitrification by organic carbon and ferrous iron, Böhlke et al. (2002) found evidence of denitrification by sulfide and ferrous iron, and Korom et al. (2005) found evidence of denitrification by sulfide, ferrous iron, and organic carbon in the Larimore site nitrate ISM. Having various electron donors implies that various types of microorganisms are responsible for the denitrification. If a relationship between apparent ϵ and denitrification rates can be established, it would be a valuable tool; apparent isotopic enrichment factors are relatively easy to measure, while estimating in situ

denitrification rates are more expensive and difficult. Unfortunately, there is no such correlation between apparent isotopic enrichment factors vs. rate for the Larimore data (the slope of the line and R^2 are < 0.001).

6.3.3 Estimating Long-Term Aquifer Denitrification Potential

Because nitrate-N in water supplies is considered detrimental to public health, and because it is considered to be one of the most serious contaminants in ground water on a world-wide scale, pyrite oxidation through denitrification is a highly beneficial process and serves as a cleansing mechanism for pyrite-containing aquifers. Pyrite-S sources are finite and autotrophic denitrification will cease once pyrite sulfur and iron are fully oxidized. Remaining denitrification will then be limited by organic carbon supplies and processes controlling heterotrophic denitrification, and the supply of non-pyrite ferrous iron. An estimate of the sustainability of aquifer pyrite at current rates of nitrate loading is therefore of interest. Total pyrite-S was estimated numerically for each site by integrating the weight of pyrite-S over depth using the "sum of the trapezoids":

$$S_{pyrite} = \int_0^{z_{max}} \rho_b S_z dz / 100 \quad (7)$$

where S_z is the percent by weight pyrite-S measured at depth z , and ρ_b is the estimated bulk density (assumed approx. $1,700 \text{ kg-m}^{-3}$). To estimate the sustainability of the supply of pyrite-S electron donors for denitrification we first calculate total nitrate-N mass for each site as:

$$N_t(g) = \bar{N}_c \left(\frac{g}{m^3_{water}} \right) \cdot z(m) \cdot \theta \left(\frac{m^3_{water}}{m^3} \right) \cdot A(m^3) \quad (8)$$

where \bar{N}_c is the mean nitrate-N concentration in porewater, z is the depth or thickness of the aquifer column having nitrate in porewater, and θ is water-filled porosity. On all sites substantial nitrate was measured only in the top well having a screen-length of 1.5 m, which we use for z . For a unit water column area (A) = 1. For consistency with the estimated bulk density we use 0.36 as an estimate for θ . To estimate the nitrate-N loading rate, we assume that the measured nitrate-N (N_t) measured for each site represents an annual load which is fully denitrified for each year. The conservative assumption of approximate full annual denitrification is justified by denitrification rates

described in Table 16 (p. 82). For computation we use $N_t^* = N_t/1,000$ in units of $\text{kg}\cdot\text{y}^{-1}$ for comparative conversion to kg units.

Table 17. Nitrate-N concentrations and estimated total pyrite-retention time (t) at current rates of nitrate loading in the EVA from Eq. 7, 8, and 9.

Site	Depth (m)	$\int_0^{z_{\max}} S_z dz$	Total Pyrite-S kg	Nitrate-N mg/L or g/m^3 water	N_t^* kg	t years
1	11.58	0.914	179.93	18	0.0097	11,356
2	21.95	5.65	2108.3	52	0.028	46,062
3	19.2	4.71	1537.3	10	0.0054	174,653
4	16.5	4.85	1360.4	10	0.0054	154,555
5	12.8	3.97	863.87	13	0.0070	75,495
6	12.8	3.86	839.94	15	0.0081	63,617

The stoichiometry of Eq. 3 requires 1.63 g of S for each gram of nitrate-N denitrified. From this, the maximum potential time for pyrite sulfur depletion by denitrification alone, based on aquifer matrix S, is estimated as:

$$t_p(y) = \frac{S(\text{kg})}{1.63 \left(\frac{\text{kg-S}}{\text{kg-N}} \right) \cdot N_t^* \left(\frac{\text{kg-N}}{\text{y}} \right)} \quad (9)$$

It is important to note that the 1.63 effective ratio includes electrons donated by pyrite iron (Eq. 3). Nitrate-N denitrified and maximum potential time thus include autotrophic denitrification from both pyrite ferrous iron and sulfide. Results on Table 17 indicate that remaining pyrite supplies are sufficient to sustain denitrification at modern loading rates for 11,000 to 175,000 years, depending on location and loading rate. Realization of estimated long-term denitrification potential is dependent on the flow system. These computations assume slow, well-mixed and effectively vertical local nitrate penetration to a receding unoxidized zone and the absence of substantial preferential flow. They also assume maintenance of unoxidized conditions through sustained water levels. Depleted water levels would cause oxidized conditions and would cause the accelerated depletion of pyrite electron donors.

The molar ratio of $\frac{\text{NO}_3^-}{\text{SO}_4^{2-}}$ is 1.4 and the mass ratio is 1.1. Annual denitrification of nitrate-N concentrations on Table 17 would result in the production of $246 \text{ mg}\cdot\text{L}^{-1}$ sulfate in the maximum case and $47 \text{ mg}\cdot\text{L}^{-1}$ in the minimum case.

6.3.4 Summary of Denitrification Effect on the EVA

Data presented for the ISMs at the Larimore EVA site support the following conclusions: (1) Denitrification rates have been zero-order with an average rate of $0.16 \pm 0.06 \text{ mg-L-d}^{-1}$; (2) Denitrification rates are the highest in our network of ISMs.; (3) The major electron donor for denitrification at the Larimore site is sulfide as pyrite; and (4) There is no correlation between isotopic enrichment factors for the denitrification observed at the Larimore site and denitrification rates. Pyrite-S measurements for Transect A-A' indicate that there is sufficient pyrite to oxidize nitrate for many thousands of years at current loading rates. Sulfate production from pyrite at *approx.* 50 to 250 $\text{mg-L}^{-1}\text{-y}^{-1}$ can occur in the denitrifying zone through autotrophic denitrification.

6.4 Isotopic Evidence of Sulfate Sources

Isotopic analyses of groundwater sulfate, sulfate extracted from the solid-phase aquifer matrix, and sulfate from applied fertilizers as shown in Fig. 34 (sulfur) and Fig. 35 (oxygen). Isotopic compositions of pyrite sulfur from the aquifer matrix are also plotted on Fig. 34. Sample depths are plotted on an arbitrary scale relative to the water table to remove the effects of variable depth to water table, etc. In this section we consider the isotopic evidence independently. In the next section (6.5) we will compare the isotopic evidence to hydrologic and water chemistry evidence discussed in previous sections.

6.4.1 Sulfur Isotopes

Sulfate data show broadly similar trends at Sites 1 to 5 (Transect A-A'). There is a general trend in sulfate $\delta^{34}\text{S}$ from more ^{34}S -enriched values in shallower samples to more ^{34}S -depleted values in deeper ones. At Sites 1 and 2, sulfate in surficial solid-phase samples has $\delta^{34}\text{S}$ similar to ^{34}S -enriched fertilizer compositions; $\delta^{18}\text{O}$ of these samples is also similar to fertilizers (see Fig. 35) and indicates a large fertilizer sulfate component here. Surficial samples from Site 3 are more ^{34}S -depleted, presumably the result of a greater component of sulfate from pyrite oxidation at shallow depths. The general trend to more ^{34}S -depleted sulfate compositions in ground water with depth indicates pyrite oxidation as the source of increased sulfate concentrations at depth. Some of the solid-phase sulfate samples have $\delta^{34}\text{S}$ markedly different from ground water in the same wells. In three cases (samples 5-5, 5-7 and 5-11, Table 4) pyrite $\delta^{34}\text{S}$ was measured in the same aquifer matrix sample and is always close to the solid-phase sulfate value (Fig. 34). In all these samples the solid-phase sulfate concentration is higher than could be attributed to sulfate in sample porewater (Table 5, see Section 4). In these samples, secondary sulfate

minerals must have been generated by pyrite oxidation, and, since there is no isotopic fractionation during this process (Nakai and Jensen 1964; Toran and Harris 1989), sulfate is isotopically identical to the pyrite source. At Sites 1 to 5, ground-water sulfate isotopic compositions represent a mixture of spatially-averaged pyrite-derived sulfur and more ^{34}S -enriched surficial (fertilizer) sources, with pyrite-derived sulfur becoming more dominant with depth.

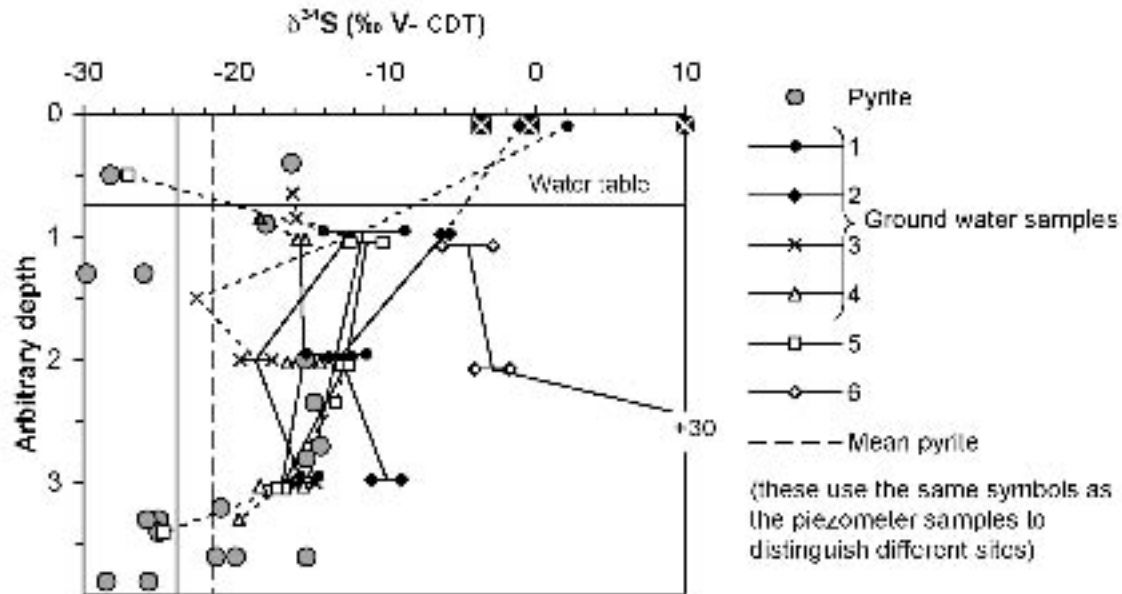


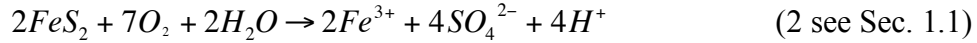
Figure 34. Stratigraphic distribution of $\delta^{34}\text{S}$ in grain pyrite and porewater sulfate for Transect A-A'. "Arbitrary Depth" is scaled for relative reference to (0) topsoil, (1) the shallow-EVA oxidized zone well, (2) the mid-EVA (unoxidized) wells, and (3) the deep EVA wells. (See Fig. 35 for fertilizer key)

At Site 6 (the furthest downstream on transect A-A') the shallowest ground-water sulfate $\delta^{34}\text{S}$ is similar to that at the other sites, but the trend with depth is to more ^{34}S -enriched compositions, up to $\sim +30\text{‰}$ in the deepest sample. Since at this site sulfate concentrations decrease with depth (Fig. 15), the isotopic data demonstrate that this is the result of bacterial sulfate reduction, which enriches ^{34}S in residual sulfate (Nakai and Jensen 1964; Strebel et al. 1990).

6.4.2 Oxygen Isotopes

Sites 1 to 5 (Fig. 35) exhibit broadly similar trends at depth while Site 6 shows strong ^{18}O enrichment in the deepest sample, consistent with bacterial sulfate reduction

identified on the basis of sulfur isotopic compositions (Strebel et al. 1990). Surficial sulfate at Sites 1 and 2 has $\delta^{18}O$ in the relatively ^{18}O -enriched range of fertilizer values, confirming the conclusion from S isotopes that they are dominated by fertilizer-derived sulfate. On the basis of S-isotopic composition, the surficial samples at Site 3 contained sulfate from a pyrite source, the ^{18}O -enriched composition in this case is the result of pyrite oxidation in the shallow oxic zone where O_2 is available as an electron acceptor:



This reaction allows a large proportion of ^{18}O -enriched (+23 ‰) atmospheric oxygen to be incorporated into the sulfate molecules (Lloyd 1967).

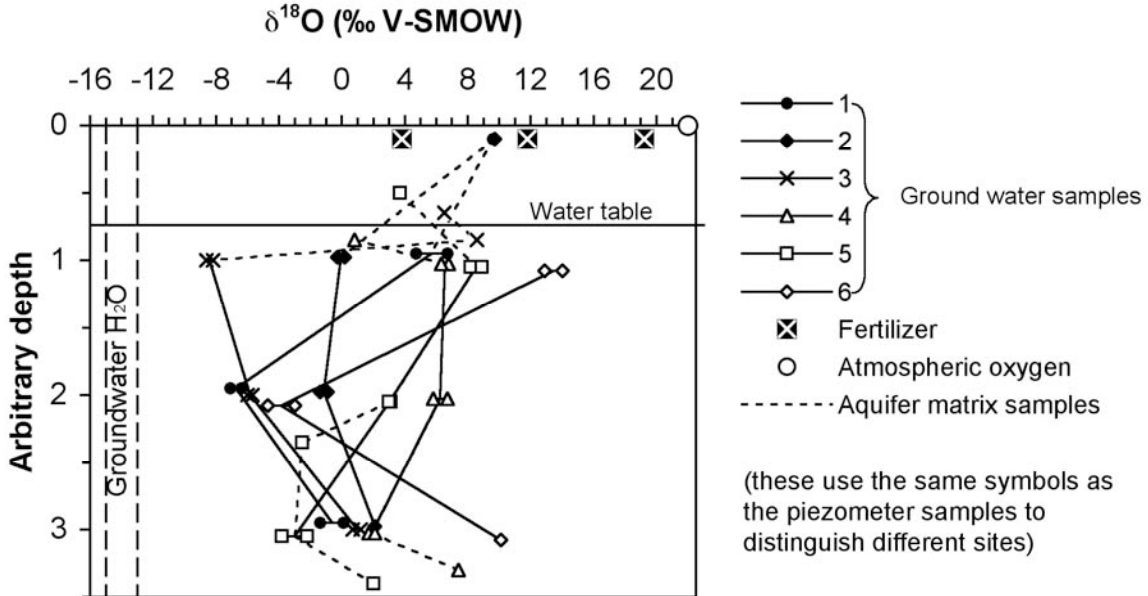
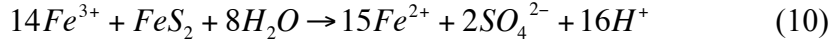


Figure 35. Stratigraphic distribution of $\delta^{18}O$ in grain pyrite and porewater sulfate for Transect A-A'. "Arbitrary Depth" is scaled for relative reference to (0) topsoil, (1) the shallow-EVA oxidized zone well, (2) the mid-EVA (unoxidized) wells, and (3) the deep EVA wells.

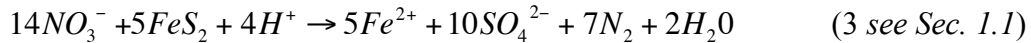
The shallowest ground-water sulfates have a wide range of $\delta^{18}O$, reflecting mixtures of fertilizer sulfate, pyrite oxidized in the oxic zone (both ^{18}O -enriched compositions, above) and pyrite weathered anoxically. Compositions as ^{18}O -depleted as Site 3 can be produced by a reaction such as:



which incorporates oxygen molecules into sulfate from ground water without isotopic fractionation (Lloyd 1967; Toran and Harris 1989; McCarthy et al. 1997), producing sulfate with $\delta^{18}O \sim -13 \text{ ‰}$ reflecting the isotopic composition of local ground water (*see Fig. 35*).

Toward the base of the EVA, ground-water sulfates at Sites 1-5 converge on a relatively narrow range of $\delta^{18}O$ between -3 and +3 ‰. This is consistent with a common sulfate source in the deep aquifer, and is thus consistent with sulfate supply by diffusion from a deeper reservoir as proposed in Section 6.2.1. Since these samples are dominated by pyrite-derived sulfur (see above) this should approximate to the $\delta^{18}O$ of sulfate produced by the pyrite oxidation mechanism during the postulated Oxidizing Event. The range of values found, close to 0‰ is indicative of oxidation in an environment with restricted aerobic influence, as would be the case in a deeply drained EVA.

Sulfate in the middle part of the aquifer has a moderately wide range of $\delta^{18}O$. Except at Site 4, this is lower than the $\delta^{18}O$ of the shallow water at the same site and is the minimum $\delta^{18}O$ in the profile at three sites. Pyrite oxidation below the oxic zone requires an alternative electron acceptor to the O_2 utilized in reaction (2), possibilities being reaction (3) above and:



As described above, reaction (10) generates sulfate with $\delta^{18}O$ of $\sim -13 \text{ ‰}$. Reaction (3) incorporates oxygen molecules into sulfate from nitrate; this nitrate would have formed originally in the oxic zone by oxidation of NH_4^+ (no nitrate-N fertilizers are used in this area, anhydrous ammonia, urea and ammonium sulfate being the most common nitrogen fertilizers) and would have incorporated O from both ground water (-13 ‰) and atmospheric O_2 (+23 ‰). The detailed isotopic systematics of NH_4^+ oxidation are not yet well understood, but generation of sulfate with $\delta^{18}O$ in the range observed is consistent with what we understand of reaction (3), thus providing support for the hypothesis that nitrate reduction is occurring via pyrite oxidation on an aquifer-wide scale.

6.5 Synthesis of Isotopic Composition, Hydrology and Water Chemistry

The heavier $\delta^{34}S$ characteristic of fertilizer sulfate and $\delta^{18}O$ characteristic of fertilizer sulfate and nitrate indicated for the vadose zone and shallow EVA on Sites 1, 2

are consistent with local soil hydrology in which they are characterized as predominant recharge sites (Fig. 30). Lighter sulfate $\delta^{34}\text{S}$ with depth on Site 2 indicates progressive mixing of sulfate from fertilizer and precipitation sources with the local pyrite source. Indications of large denitrification on Site 2 (Table 16) are of particular comparative interest. The ISMs measure effects of a semi-isolated system with sediments identical in composition to the neighboring grain-matrix and wells, but isolated from other ambient sulfate sources and deliberately and directly loaded with nitrate-N $> 100 \text{ mg-L}^{-1}$ for each tracer test. Despite the strong influence of fertilizer and atmospheric sulfate in the shallow EVA on this site, pyrite contribution of sulfate from denitrification clearly occurs at this site, resulting in intermediate (mixed) pyrite and surficial sources, as reflected in somewhat lighter $\delta^{34}\text{S}$ concentrations in the middle of the aquifer.

Soil hydrology indicates that Site 6 is also a predominant recharge site (Fig. 30). Site 6 also has relatively heavy $\delta^{34}\text{S}$ and $\delta^{18}\text{O}$ in the upper EVA indicating a likely fertilizer source (Section 6.4). These are consistent with nitrate and chloride data which indicate that leached fertilizer nitrate and chloride from muriate of potash are significant components of the chemistry of the upper EVA porewater on Sites 1, 2, 3, 5, and 6 (Fig. 20). On Site 4 their effect is minimal compared to other processes (discussed below).

The lighter (pyrite-source) $\delta^{34}\text{S}$ in the shallow EVA on Sites 3 and 4 are consistent with the water chemistry of the upper EVA. Site 4 has strong hydrogeochemical indicators of pyrite oxidation, including the highest sulfate concentration of all sites, depressed pH, and increased magnesium and sodium (Section 5.2, Fig. 19). Site 4 also has the highest pyrite retention in its topsoil (Fig. 14), which is available for oxidative weathering and leaching to the shallow water table of the shallow EVA. Relatively heavier $\delta^{18}\text{O}$ is consistent with an atmospheric oxygen source. There is also evidence of denitrification occurring in the shallow EVA on Site 4 (Fig. 32). But the major sulfate source on Site 4 appears to be aerated oxidation (Eq. 2), and both $\delta^{34}\text{S}$ and $\delta^{18}\text{O}$ isotopes indicate a strong component of sulfate formed from aerated oxidation in the shallow unoxidized EVA beneath the oxidized zone.

At Site 3 light $\delta^{34}\text{S}$ and relatively heavy $\delta^{18}\text{O}$ both indicate aerated weathering of pyrite in the oxidized shallow EVA (Sec. 6.4). There are no significant complimentary indicators of aerated oxidation in water chemistry data as on Site 4, but the concentrations of sulfate formed are small (varying temporally from 12 to 29 mg-L^{-1}) compared with the concentrations (varying temporally from 871 to 1,731 mg-L^{-1}) on Site 4. As on Site 4, fluctuations of nitrate concentrations in the shallow oxidized EVA on Site 3 (Fig. 32) provide evidence of denitrification. But in addition, the lightest $\delta^{34}\text{S}$ and

lightest $\delta^{18}O$ of all sites in the shallow unoxidized EVA beneath the oxidized zone indicate that autotrophic denitrification is the dominant source of sulfate in the shallow EVA on Site 3.

The shallow oxidized EVA on Site 5 has sulfate concentrations (32 to 44 mg-L⁻¹) intermediate between the predominant fertilizer source and pyrite source groups discussed above. Isotope indicators are also intermediate, indicating varying sources. Relatively heavy $\delta^{18}O$ indicates sulfate sources from fertilizer or aerated weathering, while intermediate $\delta^{34}S$ indicate a likely mixture of fertilizer and pyrite sources.

At mid aquifer $\delta^{34}S$ for all sites with the exception of Site 6 approach the pyrite range (Section 6.4), which is consistent with the known ubiquity of autotrophic denitrification in the shallow unoxidized zone (Section 6.3). Mid-aquifer $\delta^{34}S$ on Site 6 appears to be influenced (likely by diffusion) by sulfate sources affected by BSR in the lower EVA. All sites, except Site 4, have relatively light $\delta^{34}S$ at mid aquifer, and all of these sites, except Site 3 (which has strongest indicators of autotrophic denitrification at slightly shallower depths) have lightest local $\delta^{34}S$ at mid aquifer. Mixture with aerated sources is consistent with the sulfate-formation history of the lower EVA which provides a source of sulfate in the lower aquifer through upward diffusion to the middle EVA, and with the known contribution of autotrophic denitrification in the shallow to middle unoxidized EVA.

Measurements of deep porewater chemistry in the EVA and underlying boundary materials have indicated that the primary source of sulfate in the lower EVA is in the underlying silt (Section 3.4, Fig. 12). Sulfate was most likely oxidized from local pyrite under oxidizing conditions caused by lower water tables during an ancient period of prolonged drought, likely the Hypsithermal Interval approx. 4 to 8 thousand years ago (Section 6.2.1). Oxidation likely occurred in the lower EVA, the underlying silt, or possibly in a combination of the lower EVA and upper silt layers. Sulfate has been gradually depleting through diffusion since the oxidizing event. Isotopic evidence for all sites, with the exception of Site 6, is consistent with this scenario. $\delta^{34}S$ for Sites 1, 3, 4, and 5 are all within the pyrite range. Deeper samples from Sites 4 and 5, both having high deep EVA sulfate concentrations, exhibit the lightest $\delta^{34}S$, which conform to the lighter tendencies of deeper pyrite samples (Fig. 34), and confirm them as a likely source.

Sulfate $\delta^{18}O$ in deep EVA ground water has a general tendency to heavier values than in the mid aquifer, indicating a likely residual effect from the original atmospheric source during the oxidizing event. The tendency toward heavier $\delta^{18}O$ in the deep EVA is particularly marked in the deepest samples from Sites 4 and 5. These two sites also have

the highest deep EVA sulfate concentrations. Both $\delta^{34}\text{S}$ and $\delta^{18}\text{O}$ are consistent with conclusions drawn from long-term advection and dispersion models discussed in Section 6.2.1. In addition, sulfate $\delta^{34}\text{S}$ in the underlying silt porewater is narrowly represented near the heavier boundary of the pyrite range, which has been shown to be consistent with long-term diffusion of sulfate following the oxidizing event (Section 6.2.1.10).

Site 6 is unique and different from all other sites in that isotopic data indicate the likely modern occurrence of BSR. Heavy $\delta^{18}\text{O}$ in the deep aquifer is accompanied by heavy $\delta^{34}\text{S}$. Both are consistent with BSR and combined they indicate its likely occurrence. This is consistent with local deep EVA sulfate concentrations, which are the lowest of all sites from all transects measured ($< 20 \text{ mg-L}^{-1}$). It is also consistent with consistent low local DO values in the deep EVA (Tables 10 and 11).

6.6 Trace Element Products of Pyrite Oxidation

One of the ancillary water-quality concerns related to sulfate generation from pyrite is the release of trace elements which may be toxic or otherwise harmful for certain beneficial uses of water. Oxidation of high-organic shale pyrite has been associated with elevated arsenic and selenium, and possibly molybdenum in porewater (Schultz et al. 1980, p. B69). van Beek and Hettinga (1989), at the Vierlingsbeek well field in the Netherlands, and Larsen and Postma (1997), at the Beder well field in Denmark, considered changes in trace element concentrations associated with pyrite oxidation. Larsen and Postma (1997) provided more insights into the mobilization of Ni associated with pyrite oxidation. They noted that Ni concentrations were particularly high in the unsaturated zone and in recently resubmerged portions of the saturated zone. They postulated that Ni accumulates on Mn oxides during pyrite oxidation. With a rising water table, oxygen supplies become limited and ferrous iron reduces the Mn oxides, thereby releasing Ni to the ground water.

Trace elements were measured as a part of the shallow EVA denitrification study. These data provide some information on trace-element release under an oxidizing regime controlled by denitrification. Six tracer tests were conducted in ISMs. (Korom et al. 2005) installed just below the oxidized zone in the EVA. Control ISMs (C) were treated with a bromide tracer (as KBr in the first two tests, and as NaBr in the last four tests). Treatment ISMs (N) were amended with nitrate at initial concentrations ranging from 98 to 135 mg-L^{-1} (as nitrate) in addition to the bromide tracer. Changes in general water chemistry, Fe, and SiO_2 within the ISM's are shown on Table 18. Changes in trace elements are shown on Table 19. Trends were identified by the nonparametric Mann-

Kendall two-tailed test (Mann 1945; Kendall 1975) for $p \leq 0.05$. This test uses only relative magnitudes of the data, not their measured values (Gilbert, 1987); therefore trends may be significant with only small consistent changes in analyte values. For analyte concentrations below detection, a value of 90% of the detection level was used for the trend test. Trends are indicated on the tables as increasing (+), decreasing (-), or no effect (0).

Table 18. Trends of increasing (+), decreasing (-) or non detectable changes in solute species for principle cations and anions, and Fe, Mn and SiO₂ in ISM porewater during tracer tests. C indicates a control ISM, amended only with bromide tracer. N indicates a treatment ISM amended with nitrate and bromide. Trends are identified using the Mann-Kendall two-tailed test (Mann 1945; Kendall 1975) for $p \leq 0.05$.

Tracer Test	Na	Mg	K	Ca	Mn	Fe	NH ₃ -N	SiO ₂	F	Cl	SO ₄	NO ₃ -N	Inorganic Carbon	Organic Carbon	Field pH
1C	0	0	-	0	+	0	0	0	0	0	-	0	+	0	0
1N	0	-	-	-	-	0	0	0	+	-	+	-	-	0	0
2C	0	0	-	0	+	0	0	-	0	0	-	0	0	0	0
2N	+	-	-	-	-	0	0	-	+	0	+	-	-	0	0
3C	-	0	0	0	+	0	0	0	0	0	0	0	0	0	0
3N	-	-	0	0	0	0	0	0	+	0	+	-	-	0	0
4C	-	0	0	0	+	0	0	0	0	0	0	0	0	0	+
4N	-	0	0	0	0	0	0	-	0	0	+	-	0	0	+
5C	-	0	+	0	+	0	0	-	0	0	0	0	-	0	0
5N	-	0	+	0	0	0	0	-	+	0	+	-	0	0	0
6C	-	0	0	0	+	0	0	0	0	0	0	0	0	0	0
6N	-	0	+	0	+	0	0	0	0	0	+	-	0	0	0

As discussed previously, NO₃ (only added to the nitrate ISM) consistently decreased in the nitrate ISM through denitrification (Korom, 2005). Concomitant with denitrification, SO₄ increased in the nitrate chamber in every tracer test by the oxidation of pyrite (Korom et al., 2005), and inorganic carbon (mainly as HCO₃⁻ at the pH values in the ISMs) decreased significantly in the nitrate chamber in three of the six tracer tests, presumably by the oxidation of sediment OC and the subsequent precipitation as Ca- and Mg-carbonates (Korom et al., 2005).

F increased in four of the six tracer tests in the nitrate chamber. Elsewhere Tesfay (2006) showed that ferrous-iron-silicate minerals are likely involved in denitrification

reactions in our region. Biotite ($\text{KMg}_{2.5}\text{Fe}^{2+}_{0.5}\text{AlSi}_3\text{O}_{10}(\text{OH})_{1.75}\text{F}_{0.25}$) is such a mineral that also happens to have small amounts of F. The increase of F in the N-ISM is consistent with the use of ferrous iron in biotite as an electron donor for denitrification, with the concomitant release of F. Cl showed no clear trends. Oxidation of pyrite iron during autotrophic denitrification would produce relatively insoluble ferric iron.

Table 19. Trends of increasing (+), decreasing (-) or non detectable changes in trace elements during four (tests 3 through 6) tracer tests. C indicates a control ISM, amended only with bromide tracer. N indicates a treatment ISM amended with nitrate and bromide. Trends are identified using the Mann-Kendall two-tailed test (Mann 1945; Kendall 1975) for $p \leq 0.05$.

Tracer Test	Ag	Al	As	B	Ba	Be	Cd	Cr	Cu	Ni	Pb	Sb	Se	Tl	Zn
3C	0	0	0	0	0	0	0	0	0	+	0	0	0	0	0
3N	0	0	0	0	-	0	0	0	0	0	0	+	+	0	-
4C	0	0	0	0	0	0	0	0	0	+	0	0	0	0	0
4N	0	0	0	0	-	0	0	0	0	0	0	0	+	0	0
5C	0	0	0	0	0	0	0	0	0	0	-	0	0	0	0
5N	0	0	0	0	-	0	0	0	0	0	0	0	+	0	0
6C	0	0	0	0	0	0	0	0	0	0	0		0	0	0
6N	0	0	0	0	0	0	0	0	0	0	0		0	0	0

Trace elements were measured only in the last four (tests 3 through 6) tracer tests (Table 19). Barium (Ba) is the most abundant trace element measured in ground-water samples from the chambers (order of magnitude = $10^2 \mu\text{g-L}^{-1}$). It decreased in the nitrate chamber in three of the four tracer tests. With the increase of SO_4 in the nitrate chamber, barite precipitation (BaSO_4), an insoluble sulfate mineral, possibly explains the decrease in Ba. Ni increased in the control chamber in two of the four tracer tests. The only analyzed trace element to increase in the nitrate chambers was Se and it increased in three of the four tracer tests. While increasing arsenic was not indicated during denitrification in these tests, the possibility of arsenic release during weathering of pyrite under a more aggressive oxidizing regime with higher DO concentrations remains.

6.7 Contemporary Significance of the OE Findings

These results indicate that sulfate in the deep EVA is decreasing rather than increasing, through long-term advective and dispersive depletion. However, they also indicate that aquifers, like the EVA, with pyrite-bearing matrix materials are vulnerable to the effects of oxidation during aquifer derogation that could result from overabstraction or climate change or both. Local water supplies may also be affected by oxidation caused by local depressions and surging from pumping. Effects could include increasing sulfate, acidification (dependent on local buffering minerals), possible elevation of arsenic (Schreiber et al. 2000, Gotkowitz et al. 2004), selenium and molybdenum (Schultz et al. 1980 p. B69), where these elements are present with pyrite. Pyrite oxidation is occurring at a relatively fast rate in the shallow unoxidized zone of the aquifer. The main effect of denitrification is the removal of nitrate, and is therefore mainly beneficial. Denitrification strongly protects against additions of nitrate through leaching losses from natural and agricultural sources. Sulfate bi-products of denitrification are substantial, but within the time of this study (5 years) do not appear to be collecting and temporally increasing sulfate in the upper EVA. This is likely because of the hydrologic activity of the upper EVA, with active evaporative discharge (resulting in gypsum deposition in lower profiles local Calciaquoll soils) and discharge to local streams through rejected waters during periods of high water table.

7. CONCLUSIONS

Sulfate sources in the EVA are many and vary with depth, location and local hydrology. By far the largest source of sulfate is oxidation of local pyrite in aquifer and underlying sediments. The entire stratigraphic column of fluvial sediments was formed from the elutriated glacio-fluvial deposition of weathered shale. Local dark shale bedrock parent materials, including Carlile, Niobrara and various members of the Pierre Formation all contain pyrite. EVA sediments vary in modern pyrite concentration with depth and location, depending on historical weathering and hydrologic processes affecting the oxidation of pyrite.

The largest aquifer sulfate reservoir is in the deep EVA. Least is in the middle, and surficial sulfate is highly variable. Large sulfate in the deep EVA has a proximate source in the underlying silt layer which generally has the largest sulfate stored in the stratigraphic column from the surface, through the underlying silt and till materials, and including the basal Cretaceous shale bedrock. Sulfate in the silt layer was derived from local pyrite in the mineral fraction of the sediments. Sulfate in the silt layer and the lower EVA was most likely formed by oxidation of pyrite during an oxidizing event which likely occurred several (4 to 8) thousand years ago, plausibly during the Hypsithermal Interval, during which the water table was lower and more oxidizing conditions prevailed in the lower aquifer and upper silt layer. Following sulfate formation, and since its formation, sulfate has been transported through diffusion to the underlying till and to the overlying aquifer where it has been transported through advection and dispersion in the prevailing flow system to discharge sites. In some cases, thinness of the silt layer and more aggressive local advective and dispersive conditions have led to depletion of the sulfate in the silt layer, and the till underlying the silt is now the proximate source, feeding sulfate back into the silt and the lower aquifer. Evidence supporting these processes included multiple measurements of deep water chemistry data in the aquifer and underlying materials, advection-dispersion models, mineral analysis, and sulfur and oxygen isotope analyses of sulfate. The bottom sulfate reservoir represents the largest sulfate source, and the most substantial sulfate-depleting processes in the EVA are those of long-term and ongoing depletion from the bottom layers through transport to surface streams.

The rates of depletion of sulfate from silt and the lower EVA are affected by the local flow system. Because the EVA constitutes a shallow water-table hydrologic system, and because local hydrology dominates soil formation, soil Great-Group taxa serve as integrators of the historical hydrologic regime and can be used as indicators

sulfate-removing processes. Depletion occurred most quickly under predominant recharge areas identified by soils of the Hapliboroll (USDA) or Hapludoll soil Great-Group taxa. They occurred most slowly under the fluctuating, but slightly evaporative discharge-weighted soils of the Calciaquoll Great Group. They occurred slightly more rapidly under associated fluctuating, but slightly recharge-weighted soils of the Haplaquoll Great Group. Soil Great-Group taxa maps serve as general indicators of the modern deep sulfate disposition. The largest modern sulfate concentrations in the lower EVA occur under recharge areas and smallest modern concentrations occur under net discharge areas. Modern sulfate concentrations in the lower EVA are also affected by the thickness of the silt layer, and in rare cases by biological sulfate reduction. On one site low sulfate concentrations in the lower EVA were shown (by $\delta^{34}\text{S}$ and $\delta^{18}\text{O}$) to be caused by modern secondary biological sulfate reduction. This site had the lowest sulfate concentration in the deep EVA of all sites measured.

Sulfate concentrations in the upper EVA are highly variable ($< 20 \text{ mg-L}^{-1}$ to $> 1,500 \text{ mg-L}^{-1}$) and are affected by many sources and processes. In almost all cases, lowest local sulfate concentrations are in the upper oxidized EVA and vary from as low as 23 mg-L^{-1} to as high as 64 mg-L^{-1} . Pyrite supplies in the vadose zone and oxidized upper aquifer are generally depleted, and the chemical composition of this low-sulfate water is affected by fertilizer nitrate, chloride and sulfate sources and somewhat by rainfall. These surficial sulfur sources are small compared with pyrite sulfur retained in the unoxidized zone, and are small in comparison with existing sulfate sources in the lower aquifer and underlying silt. In some locations, as indicated by one experiment site, sufficient pyrite has been retained in the vadose zone to cause a large ($> 1,500 \text{ mg-L}^{-1}$) increase in sulfate in the upper aquifer through oxidation and leaching from the vadose zone. These processes are identified by complimentary water chemistry data and by sulfate $\delta^{34}\text{S}$ and $\delta^{18}\text{O}$ data.

In the transition from the upper oxidized zone to the underlying unoxidized portions of the EVA there is a large supply of pyrite. In this transition zone autotrophic denitrification using pyrite as an electron donor is a major contributor to sulfate concentrations. The range of mean nitrate-N concentrations (*approx.* 10 to 50 mg-L^{-1}) detected in 1.5 m well-screens on six sites, if fully denitrified, were sufficient to form 50 to 250 mg-L^{-1} sulfate concentrations in a stratigraphic column of similar length, or a total addition of about 150 to 375 g of sulfate in a square meter area.

Denitrification rates measured by Korom et al. (2005) and additional data reported here have indicated that the range of nitrate concentrations measured can be fully denitrified within a year. In six measured replications, denitrification rates on Site 2

ranged from 0.1 to 0.23 mg-L⁻¹-d⁻¹, of which pyrite electron donors accounted for 49% to 80%, depending on the replicate. $\delta^{34}\text{S}$ and $\delta^{18}\text{O}$ data confirmed the contribution of denitrification in transitional zone. Based on local pyrite-S and measured N loading rates, it is estimated that there are sufficient electron donors on each site to denitrify for 11,000 to 175,000 years, depending on the individual site and loading rate. There is sufficient pyrite to maintain denitrification at least 4,300 years at the maximum measured rate of nitrate influx on the minimum pyrite-containing site, and an average of 50,000 on the mean pyrite-containing site. These estimates are general and would be locally affected by the local flow system.

Influx of surface water from the Pembina Escarpment may influence the sulfate composition of the shallow water near the western boundary of the EVA, but appears to have little effect the overall sulfate composition of the aquifer. Sulfate contributions from precipitation occur, and are consistent with increased $\delta^{34}\text{S}$ near the aquifer surface (along with fertilizer contributions), but are small and contribute little to the overall sulfate budget of the aquifer.

Under current conditions, the pool of reduced sulfur in the pyrite fraction of EVA sediments appears to be oxidizing very slowly at rates controlled by limited periodic influx of dissolved oxygen, and ongoing denitrification which is limited by the rate of nitrate influx. However, large changes could occur under climatic or water use scenarios that would cause local or general aquifer depletion. Under current conditions it is expected that placement of high capacity wells will cause aeration within the mixing zones affected by those wells. It is thus expected that the placement and operation of high-capacity well fields will cause sulfur oxidation and sulfate formation within their own zones of influence. Thus, after initiation of well operation increasing sulfate in waters pumped is expected.

Shale sources from which EVA pyrite is derived frequently contain trace elements, including arsenic and selenium. Pyrite oxidizing conditions may, in some cases, cause their release. Elevated selenium has been identified as a bi-product of pyrite weathering during autotrophic denitrification in the shallow unoxidized EVA. Because pyrite oxidation is an acidifying process, and because some portions of the aquifer appear to be depleted of calcium carbonate, there is also concern that problems from liberation of some heavy metals may, in some cases, be exacerbated by acidifying conditions. Future work should investigate the trace-element constitution of EVA minerals. Users of high-capacity wells may also wish to monitor changes in arsenic concentrations after well placement. Finally, in pyrite-containing aquifers, like the EVA, we must beware of

management or climatic scenarios which would allow large water-table depression and aeration within the portion having large residual pyrite.

Sulfur and oxygen isotopes were useful, and in some cases essential for discerning sources and processes affecting the sulfate distribution. Combined isotope analysis enabled the separation of fertilizer and pyrite sources, and the identification of some key electron receivers in sulfate oxidation. Sulfur isotope analysis also enabled the broad identification of parent materials for the aquifer grain matrix, and provided supplementary data supporting hypotheses of historical oxidation in the silt layer.

8. CITATIONS

Anderson, Martin Sogaard, Flemming Larsen, and Dieke Postma. 2001. Pyrite oxidation in unsaturated aquifer sediments. Reaction stoichiometry and rate of oxidation. *Environ. Sci. Technol.* 2001. 35:4074-4079.

Arndt, J.L. and J.L. Richardson. 1989. Geochemistry of hydric soil salinity in a recharge-throughflow-discharge prairie-pothole wetland system. *Soil Sci. Soc. Am. J.* 53:848-855.

Benz, L.C., E.J. Doering, G.A. Reichman. 1981. Watertable management saves water and energy. *Trans. ASAE.* 24:4:995-1001.

Berner, R.A. 1974. Kinetic models for early diagenesis of nitrogen, sulfur, phosphorus, and silicon in anoxic marine sediments. In (Ed.) E.D. Goldberg: *The Sea: Vol. 5, Marine Chemistry.* John Wiley and Sons. NY. p. 393-425.

Blackmer, A.M. and J.M. Bremner. 1977. Nitrogen isotope discrimination in denitrification of nitrate in soils. *Soil Biology and Biochem.* 9:2:73-77.

Bloom, P.R., W.M. Schuh, G.L. Malzer, W.W. Nelson, and S.E. Evans. Effect of N fertilizer and corn residue management on organic matter in Minnesota mollisols. *Agron. J.* 74:161-163.

Bluemle, J.P. 1991. *The face of North Dakota.* Educational Series 21. North Dakota Geological Survey. Bismarck, ND. 177 p.

Böhlke, J.K., R. Wanty, M. Tuttle, G. Delin and M. Landon. 2002. Denitrification in the recharge area and discharge area of a transient agricultural nitrate plume in a glacial outwash sand aquifer, Minnesota. *Water Resour. Res.* 38:7:101-1026.

Bottrell, Simon H., Neil Webber, John Gunn, and Stephen R.H. Worthington. 1996. The geochemistry of sulphur in a mixed allogenic autogenic karst catchment, Castleton, Derbyshire, UK. *Earth Surface Processes and Landforms.* 25:155-165.

Bottrell, S.H. and Raiswell, R. 2000. Sulphur isotopes and microbial sulphur cycling in sediments. In (Ed.) R.E. Riding and S.M. Awramik: *Microbial Sediments* Heidelberg, Springer-Verlag. p. 96-104

Bottrell, S.H., Moncaster, S.J., Tellam, J.H., Lloyd, J.W., Fisher, Q.J. and Newton, R.J. 2000a. Controls on bacterial sulphate reduction in a dual porosity aquifer system: the Lincolnshire Limestone aquifer, England. *Chemical Geology* 169:461-470.

Bottrell, S.H., Parkes, R.J., Cragg, B.A. and Raiswell, R. 2000b Isotopic evidence for deep anoxic pyrite oxidation and stimulation of bacterial sulphate reduction. *Journal of the Geological Society* 157: 711-714.

Bouwer, H., and R.C. Rice. 1976. A slug test for determining hydraulic conductivity of unconfined aquifer with complete or partially penetrating wells. *Water Resour. Res.* 1:3:423-428.

Brown, C.J. and Schoonen, M.A.A. 2004. The origin of high sulfate concentrations in a coastal plain aquifer, Long Island, New York. *Applied Geochemistry* 19:343-358.

Bryan, B.A., G. Shearer, J. L. Skeeters, and D. H. Kohl. 1983. Variable expression of the nitrogen isotope effect associated with denitrification of nitrate. *J. Biological Chem.* 258:8613–8617.

Buckman, H.O. and N.C. Brady. 1969. *The Nature and Properties of Soils*. Seventh Ed. MacMillan Co., N.Y. 653 p.

Burdett, J.W., Arthur, M.A., Richardson, M., 1989. A neogene seawater sulfur isotope age curve from calcareous pelagic microfossils. *Earth and Planetary Science Letters* 94: 189-198.

Chambers, L.A and Trudinger, P.A. 1978. Microbiological fractionation of stable sulphur isotopes: A review and critique. *Geomicrobiology Journal* 1: 249-293.

Cherry, J.A. 1972. Geochemical processes in shallow groundwater flow systems in five areas in southern Manitoba, Canada, *Proc. Int. Geol. Congr.* 24th: p. 208-221.

Claypool, G.E., W.T. Holser, I. R. Kaplan, H. Sakai, and I. Zak. 1980. The age of curves of sulfur and oxygen isotopes in marine sulfate and their mutual interpretation. *Chemical Geology*. 28: 199-260.

Clayton, Lee, and S.R. Moran. 1981. Chronology of Late Wisconsinan glaciation in middle North America. *Quaternary Science Reviews*. 1: 55-82.

Delwiche, C.C., and P.L. Steyn. 1970. Nitrogen isotope fractionation in soils and microbial reactions. *Environ. Sci. Technol.* 4:929-935.

Doorenbos, J. and Pruitt, W.O. 1975. Crop water requirements. *Irrigation and Drainage Paper 24*. Food and Agriculture Organization of the United Nations. Rome. 179 p.

Duursma, E.K. 1966. Molecular diffusion of radioisotopes in interstitial water of sediments. IAEA, Vienna SM 72/20.

Edmunds, W.M., W.G. Darling, and D.G. Kinniburgh. 1990. Solute profile techniques for recharge estimation in semi-arid and arid terrain. In (Ed.) D.N. Lerner, A.S. Issar and Ian Simmer: *Groundwater Recharge*. IAH Vol. 8. p. 257-270.

Edwards, W.M. 1982. Predicting tillage effects on infiltration. In (Ed.) Kral, D.M. and Hawkins, S. *Predicting Tillage Effects on Soil Physical Properties and Processes*. Am. Soc. Agron. Spec. Publ. No. 434. P. 105-115.

Firestone, M. K. 1982. Biological denitrification. In (Ed.) F. J. Stevenson et al. *Nitrogen in Agricultural Soils*. Agronomy Monograph 22. American Society of Agronomy, Madison, Wisconsin. p. 289-326.

Forman, Steven L., Robert Oglesby, and Robert S. Webb. 2001. Temporal and spatial patterns of Holocene dune activity on the Great Plains of North America: megadroughts and climate links. *Global and Planetary Change*. 29:1-29.

Garlick, G.D. and Eugster, H.P. 1969. Oxygen. Chapter 8 in: (Ed.) K.H. Wedepohl: *Handbook of Geochemistry*. Springer. Berlin.

Garrels, R.M., and E.A. Perry. 1974. Cycling of carbon, sulfur, and oxygen through geologic time. (In)Ed. E.D. Goldberg, *The Sea: Vol. 5, Marine Chemistry*. John Wiley and Sons. NY. p. 303-336.

Gelhar, L.W., Claire Welty, and K.R. Rehfeldt. 1992. A critical review of data on field-scale dispersion in aquifers. *Water Resour Res.* 28: 1955-1974.

Gerla, Phillip J. 1992. Pathline and geochemical evolution of ground water in a regional discharge area, Red River Valley, North Dakota. *Ground Water.* 30:5. 743-754.

Gilbert, R.O. 1987. *Statistical Methods for Environmental Pollution Monitoring*. Van Nostrand Reinhold. New York.

Gilkeson, Robert H., Eugene C. Perry, and Keros Cartwright. 1981. Isotopic and geologic studies to identify the sources of sulfate in groundwater containing high barium concentrations. Final Report Project No. A-100-I211. Contract/Grant Report: 1981-4. Illinois Dept. of Energy and Natural Resources State Geological Survey Division, Champaign, Ill.

Gill, Games, R. and William Cobban. 1965. Stratigraphy of the Pierre Shale, Valley City and Pembina Mountain areas North Dakota. Geological Survey Professional paper 392-A. United States Government Printing Office, Washington.

Goldhaber, M.B. and I.R. Kaplan. 1974. The sulfur cycle. In (Ed.) E.D. Goldberg, *The Sea: Vol. 5, Marine Chemistry*. John Wiley and Sons. New York. p. 569-658.

Gotkowitz, Madeleine B., Madeline E. Schreiber, and J.A. Simo. 2004. Effects of water use on arsenic release to well water in a confined aquifer. *Ground Water.* 42:4:568-575.

Hansen, Dan E. and Jack Kume. 1970. Geology and Ground Water Resources of Grand Forks County: Part 1, Geology. Bulletin 53. North Dakota Geological survey. 76 p.

Harker, Brook D., Karen Bolton, Lawrence Townley-Smity and Bill Bristol. 1997. A Prairie-wide perspective of nonpoint agricultural effects on water quality. Prairie Farm Rehabilitation Administration, Regina SK, CD. 86 p.

Harkness, R.E., N.D. Haffield, and G.L. Ryan.. 1986. Water resources data: North Dakota water year 1986. U.S. Geological Survey Water-Data Report ND-86-1. U.S. Government Printing Office.

Harkness, R.E., N.D. Haffield, and W.R. Berkas. 1990. Water resources data: North Dakota water Year 1990. U.S. Geological Survey Water-Data Report ND-90-1. U.S. Government Printing Office.

Harkness, R.E., N.D. Haffield, W.R. Berkas, S.W. Norbeck, and M. Strobel. 1995. Water resources data: North Dakota water Year 1995. U.S. Geological Survey Water-Data Report ND-95-1. U.S. Government Printing Office.

Harkness, R.E., W.R. Berkas, S.W. Norbeck, and S.M. Robinson. 1999. Water resources data: North Dakota Water Year 1999. U.S. Geological Survey Water-Data Report ND-99-1. U.S. Government Printing Office.

Healy, R.W. 1990. Simulation of solute transport in variably saturated porous media with supplemental information on modifications to the U.S. Geological Survey's computer program VS2D. Water-Resources Investigation Report 90-4025. U.S. Geological Survey, Denver, CO. 122 p.

Hem, John D. 1959. Study and interpretation of the chemical characteristics of natural water. Geological Survey Water-Supply Paper 1473. U.S. Government Printing Office, Washington.

Hendry, M.J., J.A. Cherry, and E.I. Wallick. 1986. Origin and distribution of sulfate in a fractured till in southern Alberta, Canada. *Wat. Resour. Res.* 22:1. 46-61.

Holser, W.T. and I.R. Kaplan. 1966. Isotope geochemistry of sedimentary sulfates. *Chem. Geol.* 1: 93-135.

Kelly, T.E. and Q.F. Paulson. 1970. Geology and ground water resources of Grand Forks County: Part III, ground water resources. Bulletin 53. North Dakota Geological survey. 58 p.

Kendall, M.G. 1975. Rank Correlation Methods. Oxford University Press. New York.

Klute, A. 1986. Laboratory measurement of hydraulic conductivity of saturated soil. In (Ed.) A. Klute: *Methods of soil analysis* (2nd ed.). Agronomy 9. p. 210-220.

Knuteson, J.A., J.L. Richardson, D.D. Patterson, and Lyle Prunty. 1989. Pedogenic carbonates in a Calciaquoll associated with a recharge wetland. *Soil Sci. Soc. Am. J.* 53:495-499.

Kolle, W., O. Strelbel, and J. Boettcher. 1985. Formation of sulfate by microbial denitrification in a reducing aquifer. *Water Supply.* 1:35-40.

Korom, S.F. 1992. Natural denitrification in the saturated zone: a review. *Water Resour. Res.* 28:1657-1668.

Korom, S.F. 2005. Section 319 Project Report for North Dakota Department of Health.

Korom, Scott F., Allen J. Schlag, William M. Schuh, and Alison K. Schlag. 2005. In situ mesocosms: denitrification in the Elk Valley aquifer. *Ground Water Monitoring and Remediation.* 25:1:787-89.

Krouse, H. R. and B. Mayer 2000. Sulfur and oxygen isotopes in sulphate. In (Ed.) (Ed. P.G. Cook and A. L. Herczeg: *Environmental Tracers in Subsurface Hydrology.* p.195 – 231. Kluwer Academic Press. Boston, MA.

Larsen, F., and D. Postma. 1997. Nickel mobilization in a groundwater well field: Release by pyrite oxidation and desorption from manganese oxides. *Environmental Science and Technology.* 31: 2589-2595.

Lloyd, R. Michael. Oxygen-18 composition of oceanic sulfate. *Science.* 156: 1228-1231.

MacNamara, J. and H.G. Thode. 1950. Comparison of the isotopic composition of terrestrial and meteoritic sulfur. *The Physical Review.* 78:307-308.

McCarthy, M.D.B., R.J. Newton, and S.H. Bottrell. 1998. Oxygen isotopic compositions of sulfate from coals: implications for primary sulfate sources and secondary weathering processes. *Fuel,* 77: 677-682.

Manheim. 1970. The diffusion of ions in unconsolidated sediments. *Earth and Planetary Science Letters*. 9:307-309.

Mann, H.B. 1945. Nonparametric tests against trend, *Econometrica*. 13:3:245-259.

Mariotti, A., J.C. Germon, and A. Leclerc. 1982. Nitrogen isotope fractionation associated with the $\text{NO}_2 \rightarrow \text{N}_2\text{O}$ step of denitrification in soils. *Canad. J. Soil Sci.* 62:227-241.

Mariotti, A., A. Landreau, and B. Simon. 1988. ^{15}N isotope biogeochemistry and natural denitrification process in groundwater: Application to the chalk aquifer of northern France. *Geochimica et Cosmochimica Acta*. 52:1869-1978.

Marshall, C.E. 1977. *The Physical Chemistry and Mineralogy of Soils: II. Soils in Place*. Wiley-Interscience. NY. p13.

Mayer G.G. 1992. Denitrification in the Elk Valley aquifer, northeastern North Dakota: Ph.D. Dissertation. Department of Geology and Geological Engineering. University of North Dakota, Grand Forks, ND. 234 p.

McKibbin, M.A. and H.L. Barnes. 1986. Oxidation of pyrite in low temperature acidic solutions: Rate laws and surface textures. *Geochimica et Cosmochimica Acta* 50:1509-1520.

McMahon, P.B., J.K. Bohlke, and B.W. Bruce. 1999. Denitrification in marine shales in northeastern Colorado. *Water Resour. Res.* 35:5:1629-1642.

Merrill, S.D. and D.L. Tanaka. 1998. Root growth of crops alternative to wheat in dryland rotations. Poster paper, Soil Science Society of America Annual Meeting, October 18-22, Baltimore MD. 9 p. Submitted by: USDA-ARS Northern Great Plains Research Laboratory, Mandan, ND.

Mermut, A.R. and M.A. Arshad. 1985. Significance of sulfide oxidation in soil salinization in southeastern Saskatchewan, Canada. *Soil Sci. Soc. Am. J.* 51:247-251.

Moncaster, S.J., S.H. Bottrell, J.H. Tellam, J.W. Lloyd, and K.O. Konhauser. 2000. Migration and attenuation of agrochemical pollutants: insights from isotopic analysis of groundwater sulphate. *J. Cont. Hydrol.* 43:147-163.

Moran, Stephen R., Lee Clayton, Mary W. Scott, and John A. Brophy. 1973. Catalog of North Dakota Radiocarbon Dates. North Dakota Geological Survey Miscellaneous Series 53. 49 p.

Mualem, Y.I. 1976. A new model for predicting the hydraulic conductivity of unsaturated porous media: *Wat. Resour. Res.* 12:3:513-522.

Nakai, N. and M.L. Jensen. 1964. The kinetic isotope effect in the bacterial reduction and oxidation of sulfur. *Geochimica et Cosmochimica Acta.* 28:1893-1912.

Newton, R.J., S.H. Bottrell, S.P. Dean, D. Hatfield, and R. Raiswell. 1995. An evaluation of the use of the chromous chloride reduction method for isotopic analyses of pyrite in rocks and sediment. *Chemical Geology.* 125: 317-320.

Niles, C.A., S.E. Morgan, and W.S. Edwards. 2002. Case report-sulfur-induced polioencephalomalacia in beef steers consuming high sulfate water. *NDSU Animal and Range Science.* 36:2:101-104.

Ohmoto, Hiroshi, Takeshi Kakegawa, and Donald R. Lowe. 1993. 3.4-billion-year-old biogenic pyrites from Barberton, South Africa: sulfur isotope evidence. *Science.* 262:555-556.

Patterson, D.D., and C.J., Heidt. 1987. A taxonomic guide to the soils of North Dakota. Department of Soil Science Research Report No. 20. Agricultural Experiment Station. North Dakota State University, Fargo, ND.

Patch Jon C. and G. Padmanabhan. 1994. Investigation of vertical nitrate gradients in a shallow unconfined aquifer in North Dakota. Water Resource Investigation No. 31. North Dakota State Water Commission. Bismarck, ND. 99 p.

Paytan, Adina, Miriam Kastner, Douglass Campbell, and Mark H. Thiemens. 2004. Seawater sulfur isotope fluctuations in the Cretaceous. *Science.* 304:1663-1665.

Plummer, N.L., B.F. Jones, and Alfred H. Truesdell. 1978. WATEQF-a FORTRAN IV version of WATEQ, a computer program for calculating chemical equilibrium of natural waters. U.S. Geological Survey Water-Resources Investigations 76-13.

Porter and O'Brien Consulting Engineers. 1962. Subsurface site investigations WS-133A operational facilities Minot and Grand Forks air force bases, North Dakota. vols 1-13 (Minot), vols 1-12 (Grand Forks). Los Angeles, California: Porter and O'Brien.

Poulton, S.W., S.H. Bottrell, and C.J. Underwood. 1998. Porewater sulphur geochemistry and fossil preservation during phosphate diagenesis in a Lower Cretaceous shelf mudstone. *Sedimentology* 45:875-888.

Rightmire, C.T., F.J. Pearson, Jr., W. Back. 1974. Distribution of sulphur isotopes of sulphates in ground waters from the Principal Artesian Aquifer of Florida and the Edwards Aquifer of Texas, United States of America. *Isotopes Techniques in Groundwater Hydrology, 1974: Proceedings of a Symposium*. International Atomic Energy Agency Publication IAEA-SM-182. p. 191-207.

Schlag. A.J. 1999. In-situ measurement of denitrification in the Elk Valley aquifer. M.S. thesis. Department of Geology and Geological Engineering. University of North Dakota. Grand Forks, ND. 104 p.

Schlehuber, A.M. and Billy B. Tucker. 1967. Culture of Wheat. In (Ed.) K.S. Quisenberry and L.P. Reitz: *Wheat and Wheat Improvement*. ASA No. 13. American Society of Agronomy. Madison, WI. p. 117-116.

Schreiber, M.E., J.A. Simo, and P.G. Freiberg. 2000. Stratigraphic and geochemical controls on naturally occurring arsenic in groundwater, eastern Wisconsin, USA. *Hydrogeology Journal*. 8:161-176.

Schuh, W.M., R.L. Cline, and M.D. Sweeney. 1988. Comparison of a laboratory procedure and a textural model for predicting in situ soil water retention. *Soil Sci. Soc. Am. J.* 52:1218-1227.

Schuh, W.M., R.L. Cline, and M.D. Sweeney. 1991. Unsaturated soil hydraulic properties and parameters for the Oakes area, Dickey County, North Dakota. Water Resources investigation No. 18. North Dakota State Water Commission. 343 p.

Schuh, W.M., R. Meyer, M.D. Sweeney, and J.C. Gardner. 1993. Use of an integrated transient flow and water budget procedure to predict and partition components of local recharge. *J. Hydrol.* 148:1-4:27-60.

Schuh, W.M. and D.L. Klinkebiel. 2003. Effects of microtopographically concentrated recharge on nitrate variability in a confined aquifer: model simulations. *Nat. Resour. Res.* 12:4:257-272.

Schultz, Leonard G., Harry A. Tourtelot, James R. Gill, and Josephine G. Boerngen. 1980. Composition and properties of the Pierre Shale and equivalent rocks, Northern Great Plains Region. (Geochemistry of the Pierre Shale and equivalent rocks of the late Cretaceous age.) Geological Survey Professional Paper 1064-B.

Seelig, B.D. and J.L. Richardson. 1994. Sodic soil toposequence related to focused water flow. *Soil Sci. Soc. Am. J.* 58:156-163.

Shaver, R.B. 1998. The determination of glacial till specific storage in North Dakota. *Groundwater.* 36:44:552-557.

Seelig, B.D. and J.L. Richardson. 1994. Sodic soil toposequence related to focused water flow. *Soil Sci. Soc. Am. J.* 58:156-163.

Strauss, Harald. 2001. 4 GA of seawater evolution-evidence from sulfur isotopes. Session No. 37-0. GSA Annual Meeting.

Strebel, O., J. Bottcher, and P. Fritz. 1990. Use of isotope fractionation of sulfate-sulfur and sulfate-oxygen to assess bacterial desulfurication in a sandy aquifer. *J. Hydrol.* 121:155-172.

Swanson, Kevin D. 1992. Discussion of "Pathline and Geochemical Evolution of Ground Water in a regional discharge area, Red River Valley, North Dakota," by Philip J. Gerla. *Ground Water* 495-499.

Tesfay, T. 2006. Modeling groundwater denitrification by ferrous iron using PHREEQC. Phd Dissertation. Department of Geology and Geological Engineering. University of North Dakota. Grand Forks, ND.

Tisdale, S.L. and W.L. Nelson. 1966. Soil Fertility and Fertilizers. 2nd Ed. The MacMillan Co., N.Y. 694 p.

Toran, L. and R.F. Harris. 1989. Interpretation of sulfur and oxygen isotopes in biological and abiological sulfide oxidation. *Geochimica et Cosmochimica Acta*. 53: 2341-2348.

Tourtalot, Harry A. 1962. Preliminary investigation of the Geologic setting and chemical composition of the Pierre shale Great plains Region. Geological Survey Professional Paper 390. United States Government Printing Office, Washington.

Truesdale, A.H. and B.F. Jones. 1974. WATEQ, a computer program for calculating chemical equilibria of natural waters. *U.S. Geol. Survey Jour. Research*. 2:233-248.

USDA-SCS. 1980. Hydrology Manual for North Dakota. USDA-NRCS. Bismarck, ND. 163 p.

USDA-SCS. 1981. Soil Survey of Grand Forks County North Dakota. USDA-NRCS, Bismarck ND. 190 p.

USDA-SCS. 1980. Hydrology Manual for North Dakota. USDA-NRCS. Bismarck, ND. 163 p.

Van Beek, C.G.E.M., F.A.M. Hettinga, and R. Staatman. 1989. The effects of manure spreading and acid deposition upon groundwater quality in Vierlingsbeek, the Netherlands. *IAHS Publication 185*. p. 155-162.

Van Genuchten, M. Th. 1980. A closed-form equation for predicting hydraulic conductivity of unsaturated soils: *Soil Sci. Soc. America Jour.* 44:5:892-897.

Vany'sek, P. 1997. Ionic conductivity and diffusion at infinite dilution. In (Ed.) Lide, D.R.. *CRC Handbook of Chemistry and Physics*. CRC Press, New York. p. 5-93, 5-94.

Vinogradov, A.P., V.A. Grinenko, and V.I. Uistinov. 1962. Isotopic composition of sulfur compounds in the Black Sea. *Geochemistry*. 10:851-873.

Wellman, R.P., F.D. Cook, and H.R. Krouse. 1968. Nitrogen-15: Microbial Alteration of Abundance. *Science*. 161:269-270.

Wisotzky, F. 1998. Chemical reactions in aquifers influenced by sulfide oxidation and in sulfide oxidation zones. In (Ed.) W. Geller, H. Klapper and W. Salomons: *Acidic Mining Lakes*. Berlin. Springer-Verlag. p. 223-236.

APPENDIX

9. APPENDIX

9.1: Sulfate-Redistribution Model Structure

Sulfate redistribution from a source layer was examined under varying long-term recharge and discharge regimes using semi-generic transient-flow applications of a two-dimensional (vertical-longitudinal or vertical-radial) advection-dispersion model. We used VS2DT software (Healy 1990). Governing equations are discussed by Healy (1990, pp. 3-7). Semi-generic model structures were designed to evaluate plausible sulfate changes in the silt and till aquitard layers under a specified range of hydrologic regimes similar to modern local flow conditions. All hydraulic properties are applied to appropriate (EVA, silt, till, and shale) layers according to locally determined stratigraphy. Required hydraulic parameters are longitudinal (x) and vertical (z) hydraulic conductivity ($K_{x,z}$), diffusion coefficient ($D_{x,z}$), and vertical and longitudinal dispersivity ($a_{x,z}$).

9.1.1 Model Structure

Two model formats were employed. These are: (1) a flow-through model, labeled FTM; and (2) a closed-depression model labeled CDM. The same hydrologic parameters were used for both models, with the exception of additional unsaturated soil-hydraulic parameters used in the CDM model.

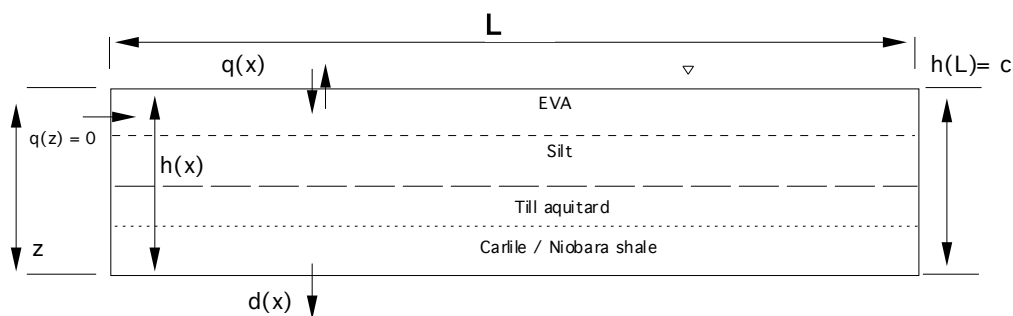


Figure A.1.1. Schematic description of the FTM model.

9.1.1.1 FTM Model Structure

The FTM (Fig. A.1.1) simulates a flow-through hydrologic regime from a barrier (zero-flux vertical boundary) to a constant-head boundary at the outflow, over a total path length, L_x . The bottom boundary is zero-flux. The surface boundary is constant-flux, q_x , for all x on L_x . Relative water-level elevations in the southern EVA, from the seepage-discharge zone on the eastern boundary to the transition to local closed-depression recharge and discharge about half the distance westward to the PE (Fig. 4), can be

simulated using a Dupuit-Forchheimer equation for discharge to a line-sink (Fig. A.1.2) using a constant net recharge, q_x , of $0.007 \text{ m}\cdot\text{y}^{-1}$. We therefore applied this value to the upper constant-flux boundary nodes. Hydraulic properties used in each of the model strata are on Table A.1.1. Their derivation is explained below. The vertical nodes vary from 1 m (in most cases) to 0.1 m where larger hydraulic or solute concentration gradients are incurred. Horizontal nodes vary from as little as 8 m to 300 m, depending on the individual case. Mass balance criteria are $< 0.1\%$ for water and $< 2\%$ for solute, although most applications have solute mass balance $< 0.5\%$.

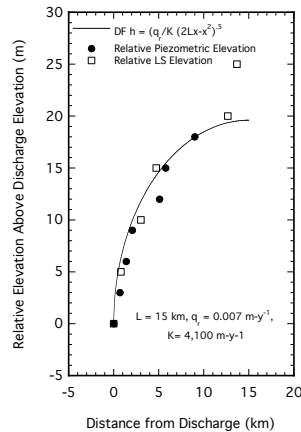


Figure A.1.2. Dupuit-Forchheimer approximation for relative piezometric head in the eastern portion of the South EVA.

Modern measured $[\text{SO}_4^{-2}]$ are used to represent C_o in the shale layer. These are distant from the active (silt and deep EVA) layers and likely have not varied much over the time period simulated. Measured $[\text{SO}_4^{-2}]$ for the deep till on Sites 8 and 9 were identical at $1.46 \text{ mmol}\cdot\text{L}^{-1}$ ($140 \text{ mg}\cdot\text{L}^{-1}$). Because of large depth below the main modern sulfate source in the silt layer, and apparent uniformity, it was assumed that this was likely close to the initial sulfate concentration in the till aquitard after deposition. Constant-concentration nodes having $[\text{SO}_4^{-2}]$ of $9.4 \times 10^{-3} \text{ mmol}\cdot\text{L}^{-1}$ ($0.9 \text{ mg}\cdot\text{L}^{-1}$) were specified for the surface boundary layer. This value was determined from ten years of sulfate measurements in precipitation during the 1990s at Icelandic State Park in NE North Dakota (USGS 1990-1999). Larger surface concentrations were also explored (Section 6.2.1.5). Bottom (zero-flux) boundaries were assigned constant-solute concentrations identical to C_o of the bottom simulated layer. Deep EVA and silt layers are the most active layers and their C_o are specified for each model case.

For most FTM applications, $L_x \sim 3.600$ m were used. The simulated outcomes for the FTM are examined for x on L_x where the horizontal gradient, ∇_x , corresponds to the measured ∇_x of the experiment site being tested. Local EVA ∇_x were estimated using the piezometric map on Fig. 4. These ∇_x are, Site 7 (0.0004), Site 8 (0.00007), Site 9 (0.00024).

Table A.1.1. Hydraulic and solute-transport parameters used for saturated FTM and CDM models.

Layer	K m/y	K_z/K_x	η	D m^2/y	a_z	a_x
EVA	4125	0.1	0.39	0.0055	4	0.006
Silt	90	0.25	0.45	0.0055	4	0.006
Till Aquitard	0.0228	1	0.5	0.00422	-	-
Carlile Shale	0.0063	-	0.2	0.0014	-	-

9.1.1.2 CDM Model Structure

The CDM simulates a closed-depression hydrologic regime, and its long-term effects on sulfate redistribution. The CDM is a 2-D radial model, and is employed in two steps.

Step 1 is an unsaturated-saturated model designed to simulate the intra-annual spatial and temporal distribution of recharge and discharge to an underlying shallow aquifer, under a micro-depression focused recharge and discharge hydrologic system. The model format has been described in detail by Schuh et al. (2003). Vertical nodes ranged from 0.7 to 60 cm, and horizontal nodes ranged from 3 to 800 cm. Mass balance error criteria were $< 1\%$.

In brief summary, the radial model consists of three concentric surface infiltration regimes (Fig. A.1.3). The middle radial interval r_r to r_b is the runoff (and net discharge) area. Infiltration (I_b) for each event = $P-R$, where P is precipitation and R is runoff. The center radial interval (0 to r_r) is the net recharge area. It receives runoff, and $I_r = P + \text{total runoff}/A_r$ where A_r is the area of the net recharge area. The interval r_b to r_{\max} is a "neutral" buffer for the purpose of insulating the micro-depression focused recharge simulation from boundary effects. Infiltration (I_{\max}) for this interval = P . Runoff is estimated using a polynomial transfer function published by Edwards (1982). Its use has been described by (Schuh et al. 2003).

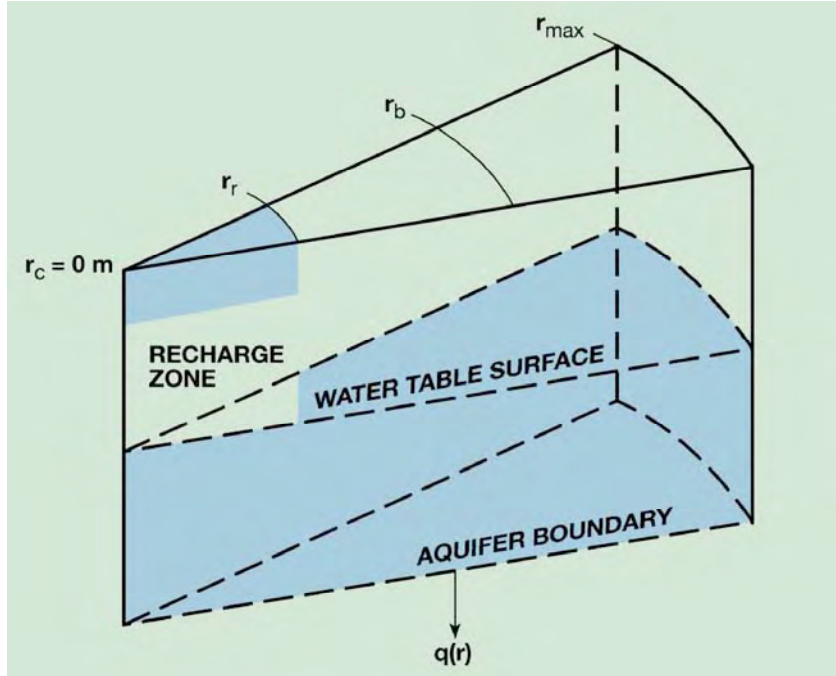


Figure A.1.3. Schematic description of the CDM model.

The unsaturated model is applied in two layers (Table A.1.2) to a depth of 4 m. In-situ unsaturated hydraulic properties and parameters used were measured for a deltaic silt soil (Eckman Loam) similar in texture and composition to the Bearden and Perella soils (Schuh et. al. 1991.) They were applied using the van Genuchten functional format (1980) for the model of Muelem (1976) :

$$K_r = \frac{\left\{1 - (\alpha h)^{n-1} \left[1 + (\alpha h)^n\right]^{-m}\right\}^2}{\left[1 + (\alpha h)^n\right]^{mp}} \quad (\text{A.1})$$

$$m = 1 - \frac{1}{n} \quad (\text{A.2})$$

$$\frac{(\theta - \theta_r)}{(\theta_s - \theta_r)} = \frac{1}{1 + (\alpha h)^n} \quad (\text{A.3})$$

$$K(h) = K_s K_r(h) \quad (\text{A.4})$$

where K_s is saturated conductivity, K_r is relative conductivity, θ is soil volumetric water content and s and r subscripts denote saturated and "residual" values, h is soil-water suction, and a, n, and r are empirical parameters. Parameters are shown on Table A.1.2.

Climatic data used were for 1990 and 1993 from the Carrington Research Extension Center, Foster County, ND. Precipitation was applied in daily increments. Potential Evapotranspiration, calculated using a modified Penman method (Doornboos and Pruitt 1975), and root extension data for sunflowers from Merrill and Tanaka (1998) were applied in 15-day periods. Sunflowers were used because they were native to the warm-season prairie plant community of the EVA. For brevity the reader is referred to Schuh et al. (2001) for a full tabular description of the data used for the model.

Table A.1.2. Hydraulic parameters used for unsaturated (Phase 1) CDM models. Data is for an Eckman Silt Loam (USDA: Haplaboroll), from Schuh et. al. (1991).

Model	Model Layer	Depth (m)	K_s cm-d ⁻¹	q_s	q_r	a cm ⁻¹	n	r
1	1	0-0.66	5.5	0.407	0.078	-0.005	1.5	10.26
1	2	0.66-4	1.54	0.485	0.0	-0.001	1.38	5.46

The differences between the Calciaquoll (net discharge) and Haplaquoll (net recharge) recharge and discharge regimes over the EVA are very subtle. The land surface is very flat so that substantial recharge and discharge occurs through both soils. The local Bearden (Calciaquoll) and Perella (Haplaquoll) landscape composition has been described by the USDA-SCS (1981) as about 65% Bearden and 30% Perella, and they "appear in associations so closely intermingled or so small that mapping them separately is not practical" (USDA-SCS 1980). The seasonal (Spring) high water table was described at 0.46 to 0.76 m below land surface on the Bearden, and near the surface on the Perella. Knuteson et al. (1989) described a Bearden-Lindaas (USDA: Argiaquoll) mapping unit as having a distance of 30 to 50 m from the center of the net recharge area to the divide of the net discharge area. They estimated long-term net evaporative discharge on the Bearden soil to be ~ 3 cm-y⁻¹.

Using the radial model, and treating the runoff area as the net discharge (Calciaquoll) and the runoff receiving area as the net recharge area (Haplaquoll), we were able to match the approximate annual net discharge of 3 cm per year for the following conditions: $r_r = 20$ m, $r_b = 40$ m and $r_{max} = 67$ m; initial high water table 0.4 m below land surface; bottom pressure head 0.8 m above the bottom (4m) boundary; and annual net recharge ~ 5 cm under the net recharge (Haplaquoll) area ($r_r = 0$ to 20 m). The net recharge of the simulated Calciaquoll, the simulated recharge-discharge path length, the relative proportions of net recharge and net discharge area, the initial high water table, and the predominant underlying aquifer piezometric head simulated are close to those

described or measured for the soils and prevailing piezometric head of EVA under the Calciaquoll-Haplaquoll mapping units. The resulting simulated intra-annual distribution of recharge and discharge for the net recharge and net discharge areas using the 1990 data are shown for Fig. A.1.4. Results for the 1993 climate simulations (not shown) are similar.

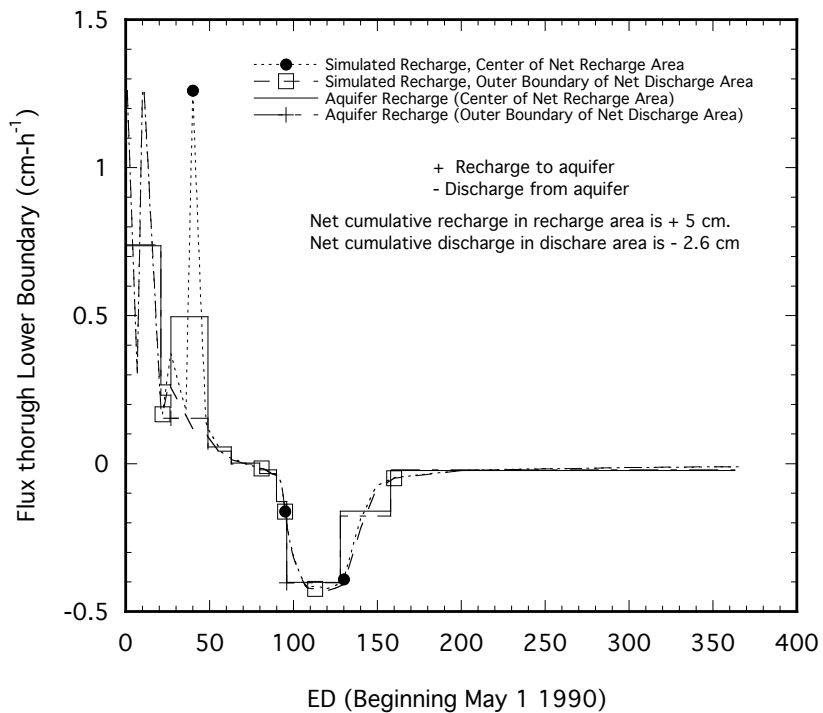


Figure A.1.4. Simulated intra-annual distribution of recharge and discharge to the EVA in 1990, used for application in the CDM.

Step 2 applies the intra-annual radially distributed recharge-discharge regime from step 1 (Fig. A.1.4) to the surface of the aquifer serially for 8 ky. The intra-annual temporal distribution is applied in ten averaged recharge-intervals (Fig. A.1.4). A 67-m (corresponding to step 1) radial 2-D saturated model is employed using the same boundary conditions, strata and hydraulic properties as the FTM model. Vertical discretization and mass balance criteria are the same as the FTM. Horizontal nodes are 8 m except where otherwise specified.

Table A.1.3. Hydraulic conductivity values for the EVA and sub strata.

Location	Grain Matrix	Method	Source	Measured K Values (and related information)
McCanna	coarse and medium sand	pump test	Kelly and Paulson (1970)	$K = 7 \times 10^{-4} \text{ m-s}^{-1}$, ($T = 795 \text{ m}^2\text{-d}^{-1}$, $L = 13 \text{ m}$, $S_c = 0.19$)
Larimore	medium and fine sand	slug test	Kelly and Paulson (1970)	$K = 1.2 \times 10^{-4} \text{ m-s}^{-1}$ to $1.4 \times 10^{-4} \text{ m-s}^{-1}$ (range for six slug tests)
Inkster Aquifer	fine shaley sand	lab - standing head (Klute 1965)	Schuh (unpublished data)	median $K = 1.5 \times 10^{-5} \text{ m-s}^{-1}$ 1.1×10^{-5} to $2.8 \times 10^{-5} \text{ m-s}^{-1}$ (range for three tests)
Inkster Aquifer	silt	lab - standing head (Klute 1965)	Schuh (unpublished data)	median $K = 2.8 \times 10^{-6} \text{ m-s}^{-1}$, range = $8.8 \times 10^{-7} \text{ m-s}^{-1}$ to $4.3 \times 10^{-6} \text{ m-s}^{-1}$, five samples.
Elk Valley Aquifer (aquitard)	clay unoxidized till	slug test (Bouwer and Rice, 1976)	This Experiment	$1.1 \times 10^{-9} \text{ m-s}^{-1}$ (Site 8, 30 m) $5.4 \times 10^{-10} \text{ m-s}^{-1}$ (Site 8, 64 m) $9.3 \times 10^{-10} \text{ m-s}^{-1}$ (Site 8, 81 m)
Elk Valley Aquifer (aquitard)	Carlile shale	slug test (Bouwer and Rice, 1976)	This Experiment	$2.1 \times 10^{-11} \text{ m-s}^{-1}$ (Site 7, 63 m) $2.3 \times 10^{-11} \text{ m-s}^{-1}$ (Site 9, 93 m)

9.1.2 Model Parameters

Hydraulic parameters for each of the modeled stratigraphic units are shown on Table A.1.1 and Table A.1.2. Hydraulic conductivity data from which they were derived are summarized on Table A.1.3. Comparison of vertical K_z measured in the laboratory using core samples [standing-head method, Klute (1986)] from similar materials taken from the nearby Inkster aquifer (about 5 km NE of the Elk Valley aquifer) indicates an approximate vertical to horizontal anisotropy factor of about 0.1. Deltaic silt K_z was measured on undisturbed core samples taken from the Inkster aquifer. An anisotropy of 0.25 was used for silt. For the diffusion coefficient, the diffusivity of calcium, magnesium and sodium sulfate salts was calculated using the ion activity equation (Vany'sek 1997) using common salt concentrations and water temperatures for the EVA. We used a mean value of $8 \times 10^{-5} \text{ cm}^2 \text{ s}^{-1}$. Calculated D were then adjusted for porosity (n) by scaling $D_{\text{SO}_4}^*$ to $D_{\text{Cl}^-}^*$ using an empirical $D_{\text{Cl}^-}^*$ vs. n curve developed by Manheim (1970). The matching $D_{\text{Cl}^-}^*$ was scaled at $h = 0.86$, which is the porosity at which the extrapolated $D_{\text{Cl}^-}^*$ from the Manheim curve matched published $D_{\text{Cl}^-}^*$ for NaCl (Vany'sek 1997). Results are on Table A.1.4. We used $\eta = 0.2$ for the Carlile shale based on the mean porosity of 0.208 for all marine shales from Schultz et al. (1980, Table 22); 0.35 for unoxidized till based on the mean of a summary of h from deep unoxidized tills in North Dakota using data from 112 missile sites compiled by Shaver (1998) from Porter and O'Brien (1962); 0.5 for silt, calculated from bulk densities of 1.2 that we measured on silt

core samples taken from the nearby Inkster aquifer; and 0.39 for sand, based on common η values for fine sands in North Dakota from Schuh et al. (1988, 1991).

Table A.1.4. Estimated in-situ diffusion coefficients for chloride ($D_{Cl^-}^*$) and sulfate ($D_{SO_4^{2-}}^*$).

η	$D_{Cl^-}^*$ cm^2-s^{-1} $\times 10^{-6}$	$D_{SO_4}^*$ cm^2-s^{-1} $\times 10^{-6}$
0.2	1	0.4
0.3	2	1
0.35	2	1
0.4	3	2
0.5	4	3
0.6	6	4
0.7	10	5
0.86	21	8

These compare with $D_{SO_4^{2-}}^* = 3 \times 10^{-6} cm^2 - s^{-1}$ measured by Duursma (1966) for $D_{SO_4^{2-}}^*$ in clean fine sand at 20° C. Berner (1974) used a combined biological, diffusion and advective model for sea-bottom sediments to derive $D_{SO_4^{2-}}^* = 2 \times 10^{-6} cm^2 - s^{-1}$, and reported that the result was "in good agreement with laboratory measurements made by Li" (*Personal Communication cited by Duursma*). The tensor of the mechanical dispersion coefficient is derived as a function [$f(a_{L,T}, v_{ij})$] of the lateral (a_L) and transverse (a_T) dispersivities and the velocity vector (v_{ij}) of the porous medium (Healy 1990). We selected sets of $a_{L,T}$ described as "highly reliable" by Gelhar et al. (1992) for sediments of similar composition and geological history. From these we used the published a_L value of 4 m, and scaled a_T as 0.0063 m. Because of low velocities, mechanical dispersivity should have little effect on solute movement in the till or shale.

9.1.3 General Model Application

The purpose is to examine the initial sulfate concentrations, and redistribution times following a proposed oxidizing event required to match a modern sulfate profile in the EVA-silt-till-bedrock system. Initial sulfate concentrations in the silt and EVA, or in some cases surface sulfate influx, are specified to test assigned event locations. The redistribution is then simulated using FTM and CDM flow scenarios. The key matching layers are the silt and till aquitard underlying the EVA. They are used because both are

more hydraulically conservative than the EVA, and therefore less sensitive to hydraulic parameter and flow-system variability. Because sulfate concentrations are inverse (decreasing in the silt and increasing in the till) over time, we are able to identify unique required C_0 and redistribution times for each simulated scenario, as shown on Fig. 23.

9.2: Transect B-B' Piezometric Data

9.2.1 Piezometric Data For Site 7

On Site 7 the EVA well had been placed previously on May 30, 1991. Three additional wells were constructed in the Carlile shale, the shallow till and the silt layer on October 17, 2001. All holes were drilled with a forward-rotary drill using EVA formation water and without drilling fluid amendments. Wells were developed immediately using air-lift. Shale and till wells were bailed in early December 2001 in preparation for sampling. Wells were evacuated by bailing and sampled in the well-screen using a point-source bailer on January 14, 2002. Multiple evacuations were possible only on the silt and EVA. Piezometric response was measured for > 1,500 days following evacuation as shown on Figure A.2.1. The well elevation was surveyed on October 7, 2002. Piezometric measurements are still being made as of the writing of this report (2/2006) and are available on the SWC database. Hydraulic conductivities for the shale and till were estimated using the method of Bouwer and Rice (1977) and are on Table A.1.3. The close piezometric response of the silt to fluctuating water levels in the EVA indicates strong hydraulic connectivity. The piezometric response of the shallow till (beneath the silt) corresponds closely to the EVA as well. There is little evidence of short-term covariance with EVA response in the underlying shale. Piezometric data are on Table A.2.1.

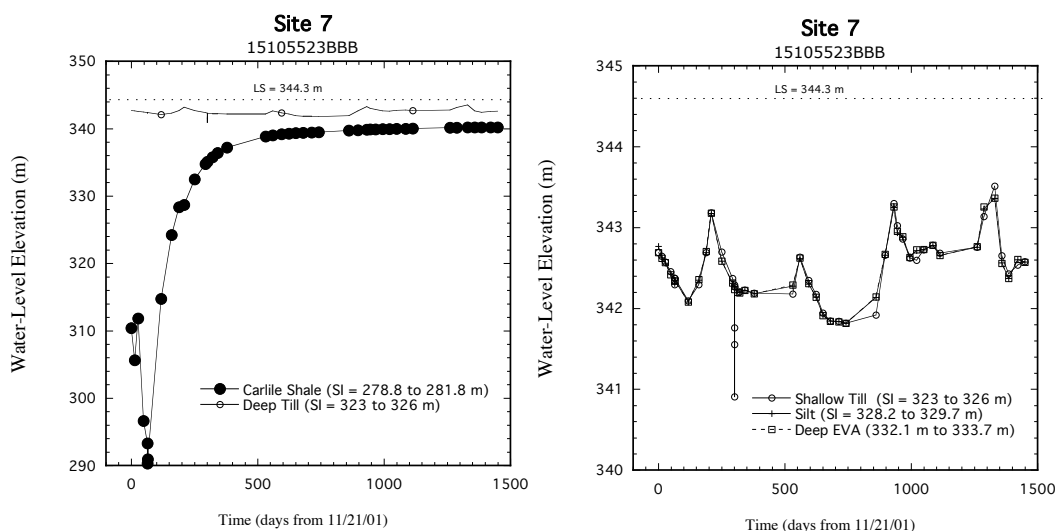


Figure A.2.1. Piezometric response of the Carlile shale and shallow till to well evacuation (left), and comparison of long-term piezometric variation in the shallow till, silt and EVA (right).

Table A.2.1 Piezometric data for the Carlile shale, shallow till, silt, and deep EVA on Site 7.

Carlile Shale			Shallow Till			Silt			Deep EVA		
Date	Days after 11/21/01	WL EL. m	Date	Days after 11/21/01	WL EL. m	Date	Days after 11/21/01	WL EL. m	Date	Days after 11/21/01	WL EL. m
11/9/2005	1449.0	340.19	11/9/2005	1449.0	342.58	11/9/2005	1449.0	342.57	11/9/2005	1449.0	342.57
10/12/2005	1421.0	340.19	10/12/2005	1421.0	342.53	10/12/2005	1421.0	342.60	10/12/2005	1421.0	342.61
9/7/2005	1386.0	340.19	9/7/2005	1386.0	342.43	9/7/2005	1386.0	342.37	9/7/2005	1386.0	342.37
8/10/2005	1358.0	340.20	8/10/2005	1358.0	342.65	8/10/2005	1358.0	342.57	8/10/2005	1358.0	342.56
7/13/2005	1330.0	340.21	7/13/2005	1330.0	343.51	7/13/2005	1330.0	343.36	7/13/2005	1330.0	343.36
6/1/2005	1288.0	340.17	6/1/2005	1288.0	343.14	6/1/2005	1288.0	343.23	6/1/2005	1288.0	343.26
5/4/2005	1260.0	340.15	5/4/2005	1260.0	342.76	5/4/2005	1260.0	342.76	5/4/2005	1260.0	342.76
12/8/2004	1113.0	340.04	12/8/2004	1113.0	342.68	12/8/2004	1113.0	342.66	12/8/2004	1113.0	342.66
11/10/2004	1085.0	340.01	11/10/2004	1085.0	342.78	11/10/2004	1085.0	342.78	11/10/2004	1085.0	342.78
10/5/2004	1049.0	339.98	10/5/2004	1049.0	342.73	10/5/2004	1049.0	342.73	10/5/2004	1049.0	342.73
9/8/2004	1022.0	339.95	9/8/2004	1022.0	342.60	9/8/2004	1022.0	342.71	9/8/2004	1022.0	342.73
8/11/2004	994.00	339.93	8/11/2004	994.00	342.63	8/11/2004	994.00	342.64	8/11/2004	994.00	342.63
7/14/2004	966.00	339.91	7/14/2004	966.00	342.86	7/14/2004	966.00	342.88	7/14/2004	966.00	342.89
6/23/2004	945.00	339.88	6/23/2004	945.00	343.03	6/23/2004	945.00	342.94	6/23/2004	945.00	342.96
6/9/2004	931.00	339.87	6/9/2004	931.00	343.30	6/9/2004	931.00	343.25	6/9/2004	931.00	343.26
5/5/2004	896.00	339.79	5/5/2004	896.00	342.66	5/5/2004	896.00	342.66	5/5/2004	896.00	342.67
3/31/2004	861.00	339.71	3/31/2004	861.00	341.92	3/31/2004	861.00	342.14	3/31/2004	861.00	342.14
12/3/2003	742.00	339.49	12/3/2003	742.00	341.82	12/3/2003	742.00	341.82	12/3/2003	742.00	341.82
11/4/2003	713.00	339.43	11/4/2003	713.00	341.84	11/4/2003	713.00	341.84	11/4/2003	713.00	341.83
10/1/2003	679.00	339.38	10/1/2003	679.00	341.85	10/1/2003	679.00	341.85	10/1/2003	679.00	341.84
9/3/2003	651.00	339.34	9/3/2003	651.00	341.94	9/3/2003	651.00	341.92	9/3/2003	651.00	341.91
8/6/2003	623.00	339.28	8/6/2003	623.00	342.17	8/6/2003	623.00	342.14	8/6/2003	623.00	342.14
7/8/2003	594.00	339.19	7/8/2003	594.00	342.35	7/8/2003	594.00	342.30	7/8/2003	594.00	342.31
6/3/2003	559.00	339.03	6/3/2003	559.00	342.64	6/3/2003	559.00	342.62	6/3/2003	559.00	342.62
5/6/2003	531.00	338.88	5/6/2003	531.00	342.18	5/6/2003	531.00	342.28	5/6/2003	531.00	342.29
12/4/2002	378.00	337.21	12/4/2002	378.00	342.19	12/4/2002	378.00	342.18	12/4/2002	378.00	342.18
10/29/2002	342.00	336.41	10/29/2002	342.00	342.23	10/29/2002	342.00	342.22	10/29/2002	342.00	342.22
10/8/2002	321.00	335.78	10/8/2002	321.00	342.21	10/8/2002	321.00	342.20	10/8/2002	321.00	342.19
9/18/2002	301.00	335.08	9/18/2002	302.00	342.27	9/18/2002	301.00	342.24	10/1/2002	314.00	342.20
9/10/2002	293.00	334.78	9/18/2002	301.00	341.76	9/10/2002	293.00	342.31	9/18/2002	301.00	342.23
7/30/2002	251.00	332.50	9/18/2002	301.00	341.55	7/30/2002	251.00	342.59	9/10/2002	293.00	342.32
6/18/2002	209.00	328.70	9/18/2002	301.00	340.91	6/18/2002	209.00	343.17	7/30/2002	251.00	342.59
5/29/2002	189.00	328.35	9/18/2002	301.00	342.29	5/29/2002	189.00	342.69	6/18/2002	209.00	343.18
4/30/2002	160.00	324.24	9/10/2002	293.00	342.37	4/30/2002	160.00	342.35	5/29/2002	189.00	342.71
3/19/2002	118.00	314.77	7/30/2002	251.00	342.70	3/19/2002	118.00	342.08	4/30/2002	160.00	342.36
1/25/2002	65.000	290.96	6/18/2002	209.00	343.18	1/25/2002	65.000	342.35	3/19/2002	118.00	342.08
1/24/2002	64.000	290.32	5/29/2002	189.00	342.69	1/24/2002	64.000	342.31	1/25/2002	65.000	342.34
1/24/2002	64.000	293.31	4/30/2002	160.00	342.29	1/24/2002	64.000	342.35	1/24/2002	64.000	342.34
1/8/2002	48.000	296.63	3/19/2002	118.00	342.10	1/8/2002	48.000	342.43	1/24/2002	64.000	342.34
12/18/2001	27.000	311.84	1/25/2002	65.000	342.37	12/18/2001	27.000	342.56	1/8/2002	48.000	342.42
12/4/2001	13.000	305.66	1/24/2002	64.000	342.29	12/4/2001	13.000	342.63	12/18/2001	27.000	342.57
11/21/2001	0.0000	310.40	1/24/2002	64.000	342.38	11/21/2001	0.0000	342.77	12/4/2001	13.000	342.62
			1/8/2002	48.000	342.46				11/21/2001	0.0000	342.69
			12/18/2001	27.000	342.57						
			12/4/2001	13.000	342.64						
			11/21/2001	0.0000	342.69						

9.2.2. Piezometric Data For Site 8

On Site 8 the EVA well had been placed previously on September 6, 1989. Four additional wells in the Niobrara shale, the deep till, the shallow till and the silt layer were constructed on October 16, 2001. Wells were drilled and developed in the same manner as Site 7. Shale and till wells were bailed in early December 2001 in preparation for sampling. Well elevations were surveyed on October 7, 2002. Wells were evacuated and sampled by bailing on January 24, 2002, and evacuated again on September 18, 2002. A water sample was collected on January 24, 2002 using a point-source bailer, and piezometric response was measured for > 1,400 days following evacuation as shown on Figure A.2.2. Piezometric measurements are still being made as of the writing of this report (2/2006) and are available on the SWC database. Hydraulic conductivities for the shale and till were estimated using the method of Bouwer and Rice (1977) and are on Table A.1.3. The Niobrara Formation, which is calcareous, is of silty texture on Site 8, and is highly permeable. The close piezometric response of the silt to fluctuating water levels in the EVA indicates strong hydraulic connectivity. The piezometric response of the shallow till (beneath the silt) correspond to the EVA as well, but is dampened and somewhat delayed. There is little evidence of short-term piezometric covariance with EVA response in the underlying deep till or shale. Piezometric data are on Table A.2.2.

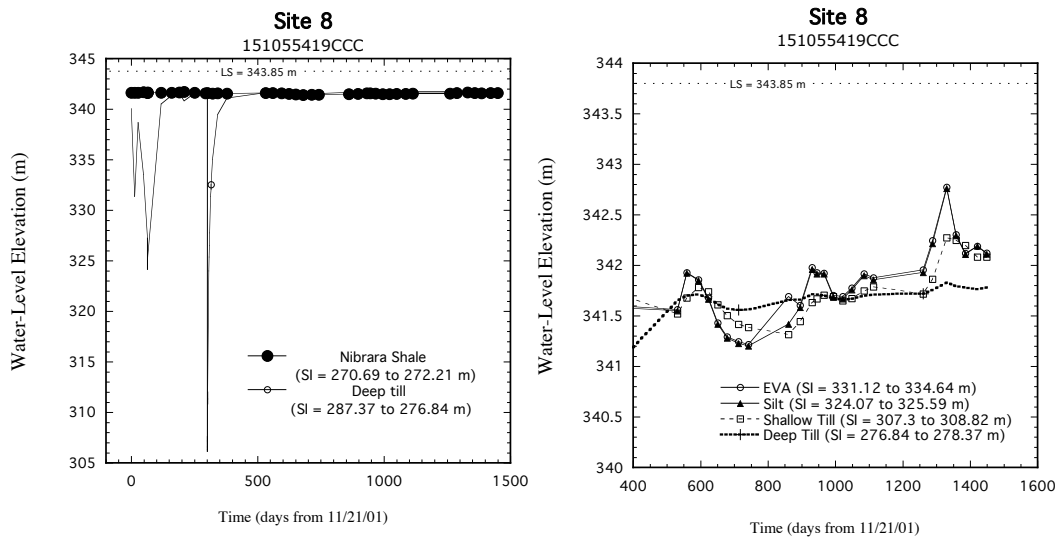


Figure A.2.2. Piezometric response of the Niobrara shale and deep till aquitard to well evacuation (left), and comparison of long-term piezometric variation in the deep till, shallow till, silt and EVA (right).

Table A.2.2a. Piezometric data for the Niobrara shale, shallow till, and deep till on Site 8.

Niobrara Shale			Deep Till			Shallow Till		
Date	Days after 11/21/01	WL EL. m	Date	Days after 11/21/01	WL EL. m	Date	Days after 11/21/01	WL EL. m
11/9/2005	1449.0	341.60	11/9/2005	1449.0	341.78	11/9/2005	1449.0	342.08
10/12/2005	1421.0	341.61	10/12/2005	1421.0	341.77	10/12/2005	1421.0	342.08
9/7/2005	1386.0	341.57	9/7/2005	1386.0	341.78	9/7/2005	1386.0	342.20
8/10/2005	1358.0	341.61	8/10/2005	1358.0	341.79	8/10/2005	1358.0	342.25
7/13/2005	1330.0	341.67	7/13/2005	1330.0	341.83	7/13/2005	1330.0	342.27
6/1/2005	1288.0	341.62	6/1/2005	1288.0	341.76	6/1/2005	1288.0	341.86
5/4/2005	1260.0	341.55	5/4/2005	1260.0	341.72	5/4/2005	1260.0	341.72
12/8/2004	1113.0	341.55	12/8/2004	1113.0	341.71	12/8/2004	1113.0	341.79
11/10/2004	1085.0	341.53	11/10/2004	1085.0	341.70	11/10/2004	1085.0	341.75
10/5/2004	1049.0	341.52	10/5/2004	1049.0	341.67	10/5/2004	1049.0	341.67
9/8/2004	1022.0	341.51	9/8/2004	1022.0	341.66	9/8/2004	1022.0	341.65
8/11/2004	994.0	341.50	8/11/2004	994.0	341.67	8/11/2004	994.0	341.69
7/14/2004	966.0	341.56	7/14/2004	966.0	341.70	7/14/2004	966.0	341.71
6/23/2004	945.0	341.57	6/23/2004	945.0	341.71	6/23/2004	945.0	341.67
6/9/2004	931.0	341.58	6/9/2004	931.0	341.71	6/9/2004	931.0	341.63
5/5/2004	896.0	341.53	5/5/2004	896.0	341.66	5/5/2004	896.0	341.45
3/31/2004	861.0	341.51	3/31/2004	861.0	341.66	3/31/2004	861.0	341.32
12/3/2003	742.0	341.44	12/3/2003	742.0	341.56	12/3/2003	742.0	341.39
11/4/2003	713.0	341.44	11/4/2003	713.0	341.56	11/4/2003	713.0	341.42
10/1/2003	679.0	341.42	10/1/2003	679.0	341.57	10/1/2003	679.0	341.50
9/3/2003	651.0	341.46	9/3/2003	651.0	341.61	9/3/2003	651.0	341.61
8/6/2003	623.0	341.54	8/6/2003	623.0	341.68	8/6/2003	623.0	341.74
7/8/2003	594.0	341.59	7/8/2003	594.0	341.71	7/8/2003	594.0	341.78
6/3/2003	559.0	341.63	6/3/2003	559.0	341.70	6/3/2003	559.0	341.68
5/6/2003	531.0	341.61	5/6/2003	531.0	341.65	5/6/2003	531.0	341.52
12/4/2002	378.0	341.55	12/4/2002	378.0	341.11	12/4/2002	378.0	341.69
10/29/2002	342.0	341.58	10/29/2002	342.0	339.49	10/29/2002	342.0	341.69
10/8/2002	321.0	341.56	10/8/2002	321.0	335.04	10/8/2002	321.0	341.41
9/18/2002	301.0	341.61	10/3/2002	316.0	332.53	10/3/2002	316.0	341.02
9/10/2002	293.0	341.59	10/2/2002	315.0	332.08	10/2/2002	315.0	340.92
7/30/2002	251.0	341.64	10/1/2002	314.0	331.35	10/1/2002	314.0	340.77
6/18/2002	209.0	341.73	9/27/2002	310.0	327.75	9/27/2002	310.0	339.71
5/30/2002	190.0	341.68	9/26/2002	309.0	326.51	9/26/2002	309.0	339.25
4/30/2002	160.0	341.65	9/25/2002	308.0	325.39	9/25/2002	308.0	338.76
3/19/2002	118.0	341.64	9/24/2002	307.0	324.00	9/24/2002	307.0	338.13
1/25/2002	65.000	341.67	9/19/2002	302.0	312.04	9/19/2002	302.0	329.04
1/24/2002	64.000	341.62	9/19/2002	302.0	311.34	9/19/2002	302.0	328.25
1/24/2002	64.000	341.65	9/19/2002	302.0	310.82	9/19/2002	302.0	327.64
1/8/2002	48.000	341.70	9/18/2002	301.0	307.63	9/18/2002	301.0	322.99
12/18/2001	27.000	341.64	9/18/2002	301.0	307.16	9/18/2002	301.0	322.10
12/4/2001	13.000	341.64	9/18/2002	301.0	306.58	9/18/2002	301.0	320.64
11/21/2001	0.0000	341.65	9/18/2002	301.0	306.36	9/18/2002	301.0	320.08
			9/18/2002	301.0	306.13	9/18/2002	301.0	319.52
			9/18/2002	301.0	341.67	9/18/2002	301.0	341.87
			9/10/2002	293.0	341.66	9/10/2002	293.0	341.90
			7/30/2002	251.0	341.58	7/30/2002	251.0	342.03
			6/18/2002	209.0	340.82	6/18/2002	209.0	341.87
			5/30/2002	190.0	341.55	5/30/2002	190.0	341.81
			4/30/2002	160.0	341.36	4/30/2002	160.0	341.73
			3/19/2002	118.0	340.53	3/19/2002	118.0	341.73
			1/25/2002	65.000	325.44	1/25/2002	65.000	339.07
			1/24/2002	64.000	324.14	1/24/2002	64.000	337.91
			1/24/2002	64.000	327.25	1/24/2002	64.000	340.88
			1/8/2002	48.000	333.54	1/8/2002	48.000	340.45
			12/18/2001	27.000	338.68	12/18/2001	27.000	340.68
			12/4/2001	13.000	331.35	12/4/2001	13.000	339.25
			11/21/2001	0.0000	340.06	11/21/2001	0.0000	339.97

Table A.2.2b. Piezometric data for the silt and EVA on Site 8.

Silt			Deep EVA		
Date	Days after 11/21/01	LS. EL. = 343.88 m WL EL. m	Date	Days after 11/21/01	LS. EL. = 343.78 m WL EL. m
11/9/2005	1449.0	342.11	11/9/2005	1449.0	342.12
10/12/2005	1421.0	342.19	10/12/2005	1421.0	342.19
9/7/2005	1386.0	342.11	9/7/2005	1386.0	342.12
8/10/2005	1358.0	342.30	8/10/2005	1358.0	342.31
7/13/2005	1330.0	342.76	7/13/2005	1330.0	342.77
6/1/2005	1288.0	342.22	6/1/2005	1288.0	342.24
5/4/2005	1260.0	341.93	5/4/2005	1260.0	341.96
12/8/2004	1113.0	341.86	12/8/2004	1113.0	341.88
11/10/2004	1085.0	341.90	11/10/2004	1085.0	341.92
10/5/2004	1049.0	341.76	10/5/2004	1049.0	341.78
9/8/2004	1022.0	341.67	9/8/2004	1022.0	341.69
8/11/2004	994.0	341.69	8/11/2004	994.0	341.70
7/14/2004	966.0	341.92	7/14/2004	966.0	341.92
6/23/2004	945.0	341.92	6/23/2004	945.0	341.93
6/9/2004	931.0	341.96	6/9/2004	931.0	341.98
5/5/2004	896.0	341.59	5/5/2004	896.0	341.60
3/31/2004	861.0	341.42	3/31/2004	861.0	341.69
12/3/2003	742.0	341.20	12/3/2003	742.0	341.22
11/4/2003	713.0	341.23	11/4/2003	713.0	341.25
10/1/2003	679.0	341.28	10/1/2003	679.0	341.29
9/3/2003	651.0	341.42	9/3/2003	651.0	341.43
8/6/2003	623.0	341.67	8/6/2003	623.0	341.68
7/8/2003	594.0	341.85	7/8/2003	594.0	341.86
6/3/2003	559.0	341.92	6/3/2003	559.0	341.93
5/6/2003	531.0	341.55	5/6/2003	531.0	341.56
12/4/2002	378.0	341.58	12/4/2002	378.0	341.60
10/29/2002	342.0	341.61	10/29/2002	342.0	341.62
10/8/2002	321.0	341.62	10/8/2002	321.0	341.62
9/18/2002	301.0	341.71	10/1/2002	314.0	341.63
9/10/2002	293.0	341.77	9/10/2002	293.0	341.76
7/30/2002	251.0	342.00	7/30/2002	251.0	341.99
6/18/2002	209.0	342.47	6/18/2002	209.0	342.48
5/30/2002	190.0	342.01	5/30/2002	190.0	342.02
4/30/2002	160.0	341.69	4/30/2002	160.0	341.71
3/19/2002	118.0	341.56	3/19/2002	118.0	341.57
1/25/2002	65.000	341.76	1/25/2002	65.000	341.78
1/25/2002	65.000	341.76	1/25/2002	65.000	341.78
1/8/2002	48.000	341.82	1/8/2002	48.000	341.83
12/18/2001	27.000	341.91	12/18/2001	27.000	341.92
12/4/2001	13.000	341.98	12/4/2001	13.000	341.98
11/20/2001		341.99	11/21/2001	0.0000	342.00
11/9/2005	1449.0	342.11	11/9/2005	1449.0	342.12
10/12/2005	1421.0	342.19	10/12/2005	1421.0	342.19
9/7/2005	1386.0	342.11	9/7/2005	1386.0	342.12
8/10/2005	1358.0	342.30	8/10/2005	1358.0	342.31
7/13/2005	1330.0	342.76	7/13/2005	1330.0	342.77
6/1/2005	1288.0	342.22	6/1/2005	1288.0	342.24
5/4/2005	1260.0	341.93	5/4/2005	1260.0	341.96
12/8/2004	1113.0	341.86	12/8/2004	1113.0	341.88
11/10/2004	1085.0	341.90	11/10/2004	1085.0	341.92
10/5/2004	1049.0	341.76	10/5/2004	1049.0	341.78
9/8/2004	1022.0	341.67	9/8/2004	1022.0	341.69
8/11/2004	994.0	341.69	8/11/2004	994.0	341.70
7/14/2004	966.0	341.92	7/14/2004	966.0	341.92
6/23/2004	945.0	341.92	6/23/2004	945.0	341.93
6/9/2004	931.0	341.96	6/9/2004	931.0	341.98
5/5/2004	896.0	341.59	5/5/2004	896.0	341.60

9.2.3. Piezometric Data For Site 9

On Site 9 five wells were constructed in the Carlile shale, the deep till, the shallow till, the silt layer and the EVA on October 15, 2001. Wells were drilled and developed in the same manner as Site 7. Shale and till wells were bailed in early December 2001 in preparation for sampling. Well elevations were surveyed on October 7, 2002. Wells were evacuated by bailing and sampled in the well-screen using a point-source bailer on January 14, 2002. Multiple evacuations were possible only on the silt and EVA. Piezometric response was measured for > 1,500 days as shown on Figure A.2.3. Piezometric measurements are still being made as of the writing of this report (2/2006) and are available on the SWC database. Hydraulic conductivities for the shale and till were estimated using the method of Bouwer and Rice (1977) and are on Table A.1.3. After 1,500 days the Carlile shale water level was still recovering. The close piezometric response of the silt to fluctuating water levels in the EVA indicates strong hydraulic connectivity. The piezometric response of the shallow till (beneath the silt) corresponds to the EVA as well, but is dampened and somewhat delayed. Pressure response to the EVA in the deep till and shale is strongly dampened. There is little evidence of short-term piezometric covariance with EVA response in the underlying deep till or shale. Piezometric data are on Table A.2.3.

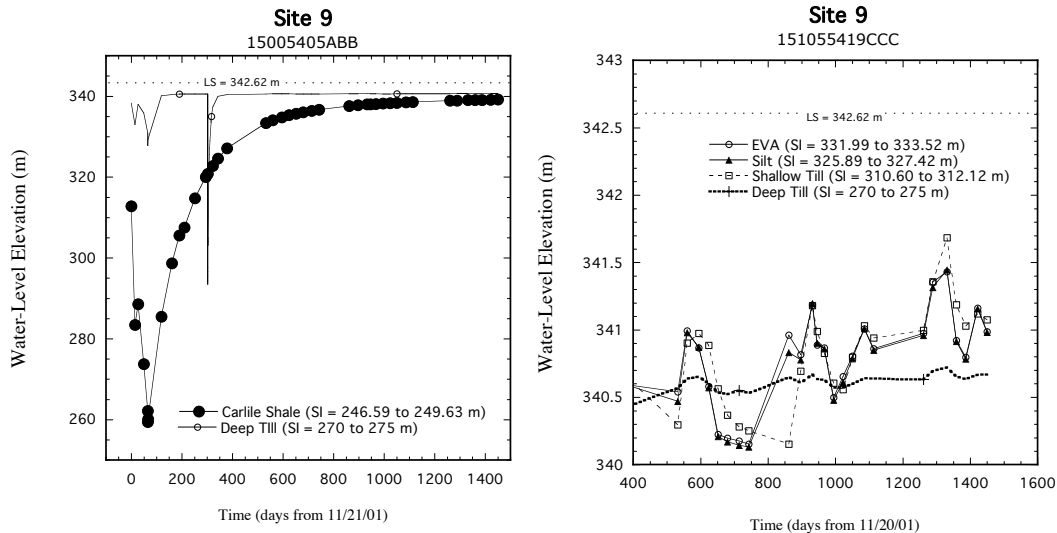


Figure A.2.3. Piezometric response of the Carlile shale and deep till aquitard to well evacuation (left figure), and comparison of long-term piezometric variation in the deep till, shallow till, silt and EVA (right).

Table A.2.3a. Piezometric data for the Carlile Shale, shallow till, and deep till on Site 9.

Carlile Shale			Deep Till			Shallow Till		
Date	Days after 11/21/01	LS. EL. = 342.62 m WL EL. m	Date	Days after 11/21/01	LS. EL. = 342.55 m WL EL. m	Date	Days after 11/21/01	LS. EL. = 342.61 m WL EL. m
11/9/2005	1450.0	339.17	11/9/2005	1450.0	340.67	11/9/2005	1450.0	341.07
10/12/2005	1422.0	339.14	10/12/2005	1422.0	340.67	10/12/2005	1422.0	341.12
9/7/2005	1387.0	339.10	9/7/2005	1387.0	340.64	9/7/2005	1387.0	341.03
8/10/2005	1359.0	339.08	8/10/2005	1359.0	340.65	8/10/2005	1359.0	341.19
7/13/2005	1331.0	339.05	7/13/2005	1331.0	340.72	7/13/2005	1331.0	341.68
6/1/2005	1289.0	338.96	6/1/2005	1289.0	340.69	6/1/2005	1289.0	341.36
5/4/2005	1261.0	338.91	5/4/2005	1261.0	340.63	5/4/2005	1261.0	341.00
12/8/2004	1114.0	338.58	12/8/2004	1114.0	340.64	12/8/2004	1114.0	340.94
11/10/2004	1086.0	338.50	11/10/2004	1086.0	340.64	11/10/2004	1086.0	341.03
10/5/2004	1050.0	338.39	10/5/2004	1050.0	340.60	10/5/2004	1050.0	340.80
9/8/2004	1023.0	338.31	9/8/2004	1023.0	340.57	9/8/2004	1023.0	340.56
8/11/2004	995.00	338.22	8/11/2004	995.00	340.57	8/11/2004	995.00	340.60
7/14/2004	967.00	338.13	7/14/2004	967.00	340.63	7/14/2004	967.00	340.83
6/23/2004	946.00	338.03	6/23/2004	946.00	340.64	6/23/2004	946.00	340.99
6/9/2004	932.00	337.98	6/9/2004	932.00	340.67	6/9/2004	932.00	341.18
5/5/2004	897.00	337.81	5/5/2004	897.00	340.61	5/5/2004	897.00	340.69
3/31/2004	862.00	337.60	3/31/2004	862.00	340.65	3/31/2004	862.00	340.15
12/3/2003	743.00	336.71	12/3/2003	743.00	340.53	12/3/2003	743.00	340.25
11/4/2003	714.00	336.44	11/4/2003	714.00	340.55	11/4/2003	714.00	340.28
10/1/2003	680.00	336.06	10/1/2003	680.00	340.52	10/1/2003	680.00	340.37
9/3/2003	652.00	335.71	9/3/2003	652.00	340.53	9/3/2003	652.00	340.56
8/6/2003	624.00	335.31	8/6/2003	624.00	340.60	8/6/2003	624.00	340.89
7/8/2003	595.00	334.81	7/8/2003	595.00	340.65	7/8/2003	595.00	340.97
6/3/2003	560.00	334.09	6/3/2003	560.00	340.64	6/3/2003	560.00	340.90
5/6/2003	532.00	333.41	5/6/2003	532.00	340.57	5/6/2003	532.00	340.30
12/4/2002	379.00	327.11	12/4/2002	379.00	340.42	12/4/2002	379.00	340.65
10/29/2002	343.00	324.59	10/29/2002	343.00	339.97	10/29/2002	343.00	340.66
10/8/2002	322.00	322.79	10/8/2002	322.00	337.30	10/8/2002	322.00	340.66
9/18/2002	302.00	320.84	10/3/2002	317.00	334.98	10/3/2002	317.00	340.67
9/10/2002	294.00	320.05	10/2/2002	316.00	334.42	10/2/2002	316.00	340.67
7/30/2002	252.00	314.75	10/1/2002	315.00	333.50	10/1/2002	315.00	340.67
6/18/2002	210.00	307.57	9/27/2002	311.00	328.95	10/1/2002	315.00	340.67
5/29/2002	190.00	305.59	9/26/2002	310.00	327.22	9/27/2002	311.00	340.66
4/30/2002	161.00	298.66	9/25/2002	309.00	325.61	9/26/2002	310.00	340.66
3/19/2002	119.00	285.49	9/24/2002	308.00	323.57	9/25/2002	309.00	340.66
1/25/2002	66.000	260.16	9/19/2002	303.00	305.12	9/24/2002	308.00	340.66
1/24/2002	65.000	259.47	9/19/2002	303.00	303.99	9/19/2002	303.00	340.22
1/24/2002	65.000	262.21	9/19/2002	303.00	303.15	9/19/2002	303.00	340.00
1/8/2002	49.000	273.78	9/18/2002	302.00	340.57	9/19/2002	303.00	339.74
12/17/2001	27.000	288.60	9/18/2002	302.00	297.60	9/18/2002	302.00	327.12
12/4/2001	14.000	283.44	9/18/2002	302.00	296.68	9/18/2002	302.00	340.93
11/20/2001	0.0000	312.84	9/18/2002	302.00	295.49	9/18/2002	302.00	333.24
			9/18/2002	302.00	294.29	9/18/2002	302.00	331.03
			9/18/2002	302.00	293.50	9/18/2002	302.00	327.12
			9/18/2002	302.00	340.57	9/18/2002	302.00	323.14
			9/10/2002	294.00	340.57	9/18/2002	302.00	321.51
			7/30/2002	252.00	340.57	9/18/2002	302.00	340.93
			6/18/2002	210.00	340.53	9/10/2002	294.00	340.95
			5/29/2002	190.00	340.53	7/30/2002	252.00	341.16
			4/30/2002	161.00	340.41	6/18/2002	210.00	341.33
			3/19/2002	119.00	340.12	5/29/2002	190.00	340.77
			1/25/2002	66.000	329.40	4/30/2002	161.00	340.38
			1/24/2002	65.000	327.77	3/19/2002	119.00	340.36
			1/24/2002	65.000	330.90	1/25/2002	66.000	340.48
			1/8/2002	49.000	335.87	1/24/2002	65.000	339.87
			12/17/2001	27.000	338.02	1/24/2002	65.000	340.54
			12/4/2001	14.000	332.95	1/8/2002	49.000	340.63
			11/20/2001	0.0000	338.28	12/17/2001	27.000	340.70
						12/4/2001	14.000	340.69
						11/20/2001	0.0000	340.39

Table A.2.3b. Piezometric data for the silt and EVA on Site 9.

Silt			Deep EVA		
Date	Days after 11/20/01	LS. EL. = 342.66 m WL EL. m	Date	Days after 11/20/01	LS. EL. = 342.66 m WL EL. m
11/9/2005	1450.0	340.98	11/9/2005	1450.0	340.99
10/12/2005	1422.0	341.16	10/12/2005	1422.0	341.16
9/7/2005	1387.0	340.78	9/7/2005	1387.0	340.80
8/10/2005	1359.0	340.92	8/10/2005	1359.0	340.92
7/13/2005	1331.0	341.45	7/13/2005	1331.0	341.43
6/1/2005	1289.0	341.32	6/1/2005	1289.0	341.35
5/4/2005	1261.0	340.96	5/4/2005	1261.0	340.97
12/8/2004	1114.0	340.85	12/8/2004	1114.0	340.86
11/10/2004	1086.0	341.01	11/10/2004	1086.0	341.01
10/5/2004	1050.0	340.79	10/5/2004	1050.0	340.81
9/8/2004	1023.0	340.61	9/8/2004	1023.0	340.65
8/11/2004	995.00	340.48	8/11/2004	995.00	340.50
7/14/2004	967.00	340.86	7/14/2004	967.00	340.87
6/23/2004	946.00	340.90	6/23/2004	946.00	340.89
6/9/2004	932.00	341.20	6/9/2004	932.00	341.18
5/5/2004	897.00	340.78	5/5/2004	897.00	340.82
3/31/2004	862.00	340.83	3/31/2004	862.00	340.96
12/3/2003	743.00	340.13	12/3/2003	743.00	340.15
11/4/2003	714.00	340.14	11/4/2003	714.00	340.17
10/1/2003	680.00	340.17	10/1/2003	680.00	340.20
9/3/2003	652.00	340.21	9/3/2003	652.00	340.22
8/6/2003	624.00	340.57	8/6/2003	624.00	340.58
7/8/2003	595.00	340.87	7/8/2003	595.00	340.87
6/3/2003	560.00	340.98	6/3/2003	560.00	340.99
5/6/2003	532.00	340.47	5/6/2003	532.00	340.54
12/4/2002	379.00	340.60	12/4/2002	379.00	340.60
10/29/2002	343.00	340.67	10/29/2002	343.00	340.68
10/8/2002	322.00	340.67	10/8/2002	322.00	340.66
9/18/2002	302.00	340.69	9/18/2002	302.00	340.68
9/10/2002	294.00	340.76	9/10/2002	294.00	340.75
7/30/2002	252.00	340.75	7/30/2002	252.00	340.71
6/18/2002	210.00	341.32	6/18/2002	210.00	341.28
5/29/2002	190.00	340.91	5/29/2002	190.00	340.91
4/30/2002	161.00	340.51	4/30/2002	161.00	340.55
3/19/2002	119.00	340.28	3/19/2002	119.00	340.28
1/25/2002	66.000	340.34	1/25/2002	66.000	340.55
1/25/2002	66.000	340.59	1/25/2002	66.000	340.55
1/8/2002	49.000	340.66	1/8/2002	49.000	340.63
12/17/2001	27.000	340.78	12/17/2001	27.000	340.78
12/4/2001	14.000	340.79	12/4/2001	14.000	340.79
11/20/2001	0.0000	340.82	11/20/2001	0.0000	340.82
11/9/2005	1450.0	340.98	11/9/2005	1450.0	340.99
10/12/2005	1422.0	341.16	10/12/2005	1422.0	341.16
9/7/2005	1387.0	340.78	9/7/2005	1387.0	340.80
8/10/2005	1359.0	340.92	8/10/2005	1359.0	340.92
7/13/2005	1331.0	341.45	7/13/2005	1331.0	341.43
6/1/2005	1289.0	341.32	6/1/2005	1289.0	341.35
5/4/2005	1261.0	340.96	5/4/2005	1261.0	340.97
12/8/2004	1114.0	340.85	12/8/2004	1114.0	340.86
11/10/2004	1086.0	341.01	11/10/2004	1086.0	341.01
10/5/2004	1050.0	340.79	10/5/2004	1050.0	340.81
9/8/2004	1023.0	340.61	9/8/2004	1023.0	340.65
8/11/2004	995.00	340.48	8/11/2004	995.00	340.50
7/14/2004	967.00	340.86	7/14/2004	967.00	340.87
6/23/2004	946.00	340.90	6/23/2004	946.00	340.89
6/9/2004	932.00	341.20	6/9/2004	932.00	341.18
5/5/2004	897.00	340.78	5/5/2004	897.00	340.82

9.3: Transect A-A' (Site 5) Silt-Layer Mineral Analysis

(ANALYSIS BY THE UNIVERSITY OF NORTH DAKOTA ENERGY AND ENVIRONMENTAL RESEARCH CENTER)

Text italicized in brackets is added by the authors: ex. [xxx]

This sample was analyzed using SEM to determine if any gypsum ($\text{CaSO}_4 \cdot 2 \text{H}_2\text{O}$) was present. An x-ray map was made showing the relationship between the Ca and S as well as several point analyses.

Figures 1 and 2 are x-ray maps of Ca and S respectively, and [these elements] do not correspond with the same pixel location in any of the occurrences measured.

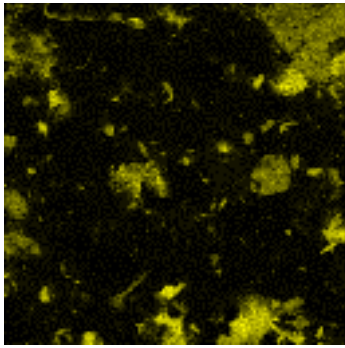


*Figure A.3.1.**
Figure 1. Ca x-ray map.

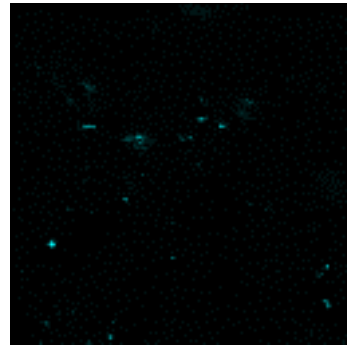


*Figure A.3.2.**
Figure 2. S x-ray map.

Several points were analyzed as well as the x-ray map. Figure 3 shows a backscattered image of the area where the analyses were taken and the numbers correspond to the points where the analyses were taken.

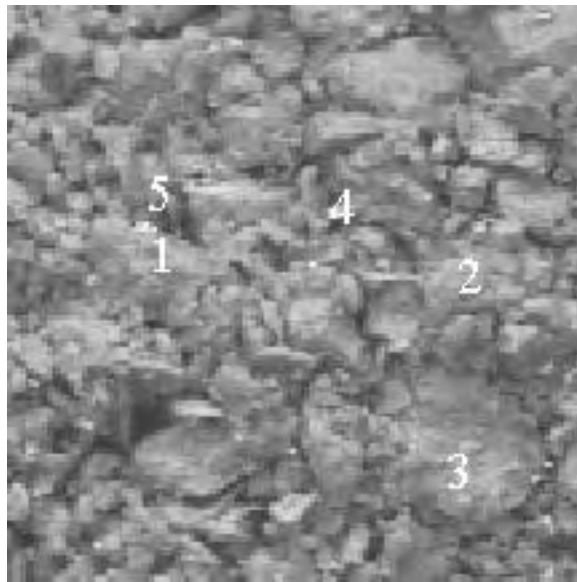


*Figure A.3.3** Backscattered Image

[Table A.3.1]*. chemical analyses at points 1 through 5.

	Point 1	Point 2	Point 3	Point 4	Point 5
Na	0.35	0	5.24	0.13	0.27
Mg	1.29	21.44	0.59	0.56	0.77
Al	10.3	6.61	18.37	5.92	6.16
Si	72.35	20.23	64.68	49.94	68.86
P	0.28	0.08	0.12	0	0.25
S	0	0.29	0.01	19.97	10.44
Cl	0.05	0.19	0.03	0	0.18
K	3.1	1.46	1.25	1.7	3.16
Ca	3.21	46.9	1.65	3.13	2.31
Ti	0	0	0.17	0.25	0
Cr	0	0	0.09	0.19	0
Fe	8.49	2.79	7.79	18.15	7.29
Ba	0.57	0	0	0.06	0.32
O-counts	5694	4995	5215	3296	5039
C-counts	2251	3213	1346	1668	2814

The chemical analyses are in weight % except for the bottom 2 rows labeled O-counts and C-counts. These are the raw x-ray counts for oxygen and carbon. Since there are no reliable standards for those elements, we simply keep track of x-ray counts rather than try to quantify them.

This is likely a mix of alumino-silicate minerals and carbonate minerals. There appears to be quartz grains and clays for the most part, but likely include some type of carbonate material as either discrete particles, the cementing agent, or both. Point 1 is mostly a silt-sized quartz particle with clays adhering to the surface. The high O and C counts indicate that it is likely associated with carbonates. Point 2 is likely a dolomite and clay mix and Point 3 is mostly clays. Points 4 and 5 both have relatively large amount of sulfur associated with them with iron being elevated as well. With the O counts being high, it is unlikely that this represents pyrite but rather FeSO_4 or FeCO_3 . It is possible that a small amount of Ca may be in the form of CaSO_4 in a few cases although most data points high in S were low in Ca.

*Text italicized in brackets is added by the authors: ex. [xxx] to conform to report format.